

AD-A032 552

TECHNION - ISRAEL INST OF TECH HAIFA DEPT OF AERONAU--ETC F/G 20/4
INVESTIGATIONS OF THE ROLLING-UP OF THE VORTEX WAKE AND CALCULA--ETC(U)
JUN 76 J ROM, H PORTNOY, C ZOREA

UNCLASSIFIED

TAE-277

AFOSR-TR-76-1146

NL

1 OF 2
AD
A032552



AFOSR 71-2145

FINAL REPORT

June, 1976

FC
Technion Research &
Development Foundation Ltd.
Haifa, Israel

AFOSR - TR - 76 - 1146

AD A032552

FINAL REPORT

**INVESTIGATIONS OF THE ROLLING-UP OF THE VORTEX WAKE
AND CALCULATION OF NON-LINEAR AERODYNAMIC
CHARACTERISTICS OF WINGS**

BY

J. ROM, H. PORTNOY and C. ZOREA

Department of Aeronautical Engineering
Technion — Israel Institute of Technology
Haifa, Israel

Approved for public release;
distribution unlimited.

T.A.E. REPORT No. 277

DDC
RECEIVED
NOV 24 1976
C

AIR FORCE OFFICE OF SCIENTIFIC RESEARCH (AFSC)
NOTICE OF TRANSMITTAL TO DDC
This technical report has been reviewed and is
approved for public release IAW AFR 190-12 (7b).
Distribution is unlimited.
A. D. BLOSE
Technical Information Officer

This document has been approved for public release and sale; its distribution is unlimited

Qualified requestors may obtain additional copies from the Defense Documentation Center;
all others should apply to the Clearinghouse for Federal Scientific and Technical Information.

SECURITY CLASSIFICATION OF THIS PAGE (When Data Entered)

14 REPORT DOCUMENTATION PAGE		READ INSTRUCTIONS BEFORE COMPLETING FORM	
1. REPORT NUMBER AFOSR - TR - 76 - 1146	2. GOVT ACCESSION NO.	3. RECIPIENT'S CATALOG NUMBER	
4. TITLE (and Subtitle) INVESTIGATIONS OF THE ROLLING-UP OF THE VORTEX WAKE AND CALCULATION OF NON-LINEAR AERODYNAMIC CHARACTERISTICS OF WINGS		5. TYPE OF REPORT & PERIOD COVERED FINAL Rept 1 Jan 71 - 31 Dec 75	
6. AUTHOR(s) J. ROM, H. PORTNOY C. ZOREA		7. PERFORMING ORGANIZATION REPORT NUMBER TAE Report No-277	
8. CONTRACT OR GRANT NUMBER(s) AFOSR 71-2145-71		9. PROGRAM ELEMENT, PROJECT, TASK AREA & WORK UNIT NUMBERS 681307 9781-01 61102F	
10. CONTROLLING OFFICE NAME AND ADDRESS TECHNION - ISRAEL INSTITUTE OF TECHNOLOGY DEPT OF AERONAUTICAL ENGINEERING HAIFA, ISRAEL		11. REPORT DATE June 1976	
11. CONTROLLING OFFICE NAME AND ADDRESS AIR FORCE OFFICE OF SCIENTIFIC RESEARCH/NA BLDG 410 BOLLING AIR FORCE BASE, D C 20332		12. NUMBER OF PAGES 96	
14. MONITORING AGENCY NAME & ADDRESS (if different from Controlling Office)		15. SECURITY CLASS. (of this report) UNCLASSIFIED	
15a. DECLASSIFICATION/DOWNGRADING SCHEDULE			
16. DISTRIBUTION STATEMENT (of this Report) Approved for public release; distribution unlimited.			
17. DISTRIBUTION STATEMENT (of the abstract entered in Block 20, if different from Report)			
18. SUPPLEMENTARY NOTES			
19. KEY WORDS (Continue on reverse side if necessary and identify by block number) VORTEX WAKE ROLL-UP OF VORTICES NON-LINEAR AERODYNAMICS WINGS <i>THIS REPORT INVESTIGATES</i>			
20. ABSTRACT (Continue on reverse side if necessary and identify by block number) This report summarizes the research programs conducted under Grant AFOSR 71-2145 during the period 1971-1975. The main research program was aimed at the investigation of the rolling-up of vortices over and behind wings of low and high aspect ratios, and simultaneously the evaluation of the aerodynamic characteristics including the spanwise and chordwise pressure distributions on the wings. The present method is based on the extension of the Vortex Lattice concepts also to low aspect ratio wings and the rolled-up vortex which is established over as well as behind the wings. The computer program, which was developed, is capable			

DD FORM 1 JAN 73 1473

EDITION OF 1 NOV 65 IS OBSOLETE

UNCLASSIFIED

SECURITY CLASSIFICATION OF THIS PAGE (When Data Entered)

343 875
608

of reproducing the results of the Vortex Lattice Method (VLM) for linear aerodynamic coefficients for high aspect ratio wings. The wake effect is included in the modified VLM program. This wake calculation showed that the center of the tip vortex is very near the wings' tip for the high aspect ratios wings. The non-linear aerodynamic characteristics are evaluated when the vortices are shed over the wing and begin the rolling-up process from the leading edges. This effect is particularly important for wings of low aspect ratios. The calculation program includes options for the evaluation of the trajectories of the vortices shed from the side edges, leading edges and from each cell on the planform. The non-linear aerodynamic characteristics as well as the pressure distributions are computed. The results are in good agreement with measured data. Numerical problems and limitations of the present method are discussed. The finite thickness of the vortex wake is being studied by using a two-dimensional method and assuming that the wake cross section contains vorticity in an otherwise irrotational field. The wake development under its own induced field is calculated, ignoring viscous dissipation. A finite spiral wake structure is observed to develop. The research program included also some investigations of viscous-inviscid interactions, particularly problems which are important for wing-body aerodynamics. Calculation programs based on various iterative processes between the solution of the viscous flow regions and the essentially inviscid regions have been studied.

UNCLASSIFIED

AF OSR 71-2145.

JUNE 1976

FINAL REPORT

INVESTIGATIONS OF THE ROLLING-UP OF THE VORTEX
WAKE AND CALCULATION OF NON-LINEAR AERODYNAMIC
CHARACTERISTICS OF WINGS.

by

J. ROM, H. PORTNOY and C. ZOREA,
Department of Aeronautical Engineering,
Technion - Israel Institute of Technology,
Haifa, Israel.

TAE REPORT No. 277

ADDITIONAL: for	When Section	<input checked="" type="checkbox"/>
NTIS	Both Section	<input type="checkbox"/>
D.S.		
CHART GUIDED		
JUSTIFICATION		
BY DISTRIBUTION/AVAILABILITY CODES		
Dist.	AVAIL. CODE	SPECIAL
A		

D D C
RECEIVED
NOV 24 1976
C

ABSTRACT

This report summarizes the research programs conducted under Grant AF CSR 71-2145 during the period 1971-1975.

The main research program was aimed at the investigation of the rolling up of vortices over and behind wings of low and high aspect ratios, and simultaneously the evaluation of the aerodynamic characteristics including the spanwise and chordwise pressure distributions on the wings. The present method is based on the extension of the Vortex Lattice concepts also to low aspect ratio wings and the rolled-up vortex which is established over as well as behind the wings. The computer program, which was developed, is capable of reproducing the results of the Vortex Lattice Method (VLM) for linear aerodynamic coefficients for high aspect ratio wings. The wake effect is included in the Modified VLM program. This wake calculation showed that the center of the tip vortex is very near the wings' tip for the high aspect ratios wings.

The non-linear aerodynamic characteristics are evaluated when the vortices are shed over the wing and begin the rolling up process from the leading edges. This effect is particularly important for wings of low aspect ratios. The calculation program includes options for the evaluation of the trajectories of the vortices shed from the side edges, leading edges and from each cell on the planform. The non-linear aerodynamic characteristics as well as the pressure distributions are computed. The results are in good agreement with

measured data.

Numerical problems and limitations of the present method are discussed. The finite thickness of the vortex wake is being studied by using a two-dimensional method and assuming that the wake cross section contains vorticity in an otherwise irrotational field. The wake development under its own induced field is calculated, ignoring viscous dissipation. A finite spiral wake structure is observed to develop.

The research program included also some investigations of viscous-inviscid interactions, particularly problems which are important for wing-body aerodynamics. Calculation programs based on various iterative processes between the solutions of the viscous flow regions and the essentially inviscid regions have been studied.

TABLE OF CONTENTS

	<u>PAGE No.</u>
ABSTRACT	I - II
TABLE OF CONTENTS	III - IV
LIST OF SYMBOLS	V - VII
LIST OF FIGURES	VIII - XI
I. INTRODUCTION	1 - 6
II. THE GENERALIZED VORTEX-LATTICE TECHNIQUE - METHODS OF CALCULATION OF THE TRAJECTORIES OF THE VORTICES AND THE AERODYNAMIC CHARACTERISTICS OF THE WING	7 - 10
2.1. Geometrical Division of the Planform into Cells	7 - 8
2.2. Selection of Appropriate Initial Vortex Distribution	8 - 9
2.3. Calculation of the Induced Velocity Field	9
2.4. Calculation of the Vortex Trajectories	9
2.5. Evaluation of the Aerodynamic Parameters	10
III. THE ROLLING UP OF THE WAKE BEHIND WINGS	11 - 24
3.1. The Thick Vortex Layer Model	17 - 24
IV. THE METHOD OF CALCULATION OF THE NONLINEAR AERO- DYNAMIC CHARACTERISTICS OF WINGS	25 - 33
a. Definition of the Model for the Wing Planform (Steps 1 and 2)	25
b. Establishment of the Initial Conditions and the Strength of the Vortices (Step 3)	25 - 26
c. Calculation of the Velocity Field (Step 4)	26
d. Calculation of the Vortex Trajectories (Step 5)	27

	<u>PAGE No.</u>
e. Calculation of the Strength of the Vortices (Step 6)	27
g. Calculation of the Aerodynamic Coefficients and the Wake Characteristics (Step 7)	27 - 28
(1) RECTANGULAR WINGS	28 - 31
(2) DELTA WINGS	31 - 32
(3) SECONDARY VORTEX SEPARATION	32 - 33
(4) COMPUTER PERIODS	33
V. DISCUSSION OF RESULTS	34 - 36
REFERENCES	37 - 42
FIGURES	43 - 93

LIST OF SYMBOLS

A	wake cross-section at any station x .
A'	initial wake cross-section at $x = 0$.
AR	aspect ratio of wing.
a	side of triangular element, opposite corner A, divided by s .
b	side of triangular element, opposite corner B, divided by s ; wing span.
b'	the distance between the vorticity centers of the tip vortices.
C	boundary of cross-section A.
C'	boundary of cross-section A'.
C_D	wing drag coefficient.
C_{D_i}	wing induced drag coefficient.
C_L	wing lift coefficient.
C_M	wing pitching moment coefficient.
c	side of triangular element, opposite corner C, divided by s .
K_i, K_j	influence coefficients
K_n	$= \xi_n^* \Delta A_n^*$
M	total number of triangular elements in wake cross-section.
N	number of different values of ξ_n^* .
N_c	divisions in the chordwise directions.
N_s	divisions in the spanwise directions.
n	number denoting a typical triangular element.
P	perimeter of S.
r_A	$= \zeta - \zeta_A /s$.
r_B	$= \zeta - \zeta_B /s$.

r_C	$= \zeta - \zeta_C /s.$
R_O	the core diameter of the wings' vortex.
S	closed region with constant vorticity distribution.
s	wing semi-span.
t^*	dimensionless time. See Equation (4).
U	free stream velocity.
u	velocity component in the x direction.
V_n	element influence function. See Equation (14).
v	velocity component in the y direction.
v^*	non-dimensional form of v . See Equation (3).
W_n	element influence function. See Equation (15).
w	velocity component in the z direction.
w^*	non-dimensional form of w . See Equation (3).
W_I^*	$- W_I^*$ is the usual downwash calculated in the Trefftz plane for an unrolled wake.
x	streamwise coordinate.
y	spanwise coordinate positive to the right.
y^*	$= y/s.$
z	third coordinate of the right-handed set x, y, z .
z^*	$= z/s.$
α	angle of attack.
α	$= \arg (\zeta - \zeta_A).$
α_B	$= \arg (\zeta_B - \zeta_A).$
α_C	$= \arg (\zeta_C - \zeta_A).$
β	$= \arg (\zeta - \zeta_B).$

β_A	$= \arg (\zeta_A - \zeta_B)$.
β_C	$= \arg (\zeta_C - \zeta_B)$.
γ	$= \arg \zeta - \zeta_C$.
γ_A	$= \arg (\zeta_A - \zeta_C)$.
γ_B	$= \arg (\zeta_B - \zeta_C)$.
ΔA_n	area of nth triangular element.
ΔA_n^*	$= \Delta A_n / s^2$.
Δt^*	dimensionless time step in numerical integration.
Δv_n^*	contribution to v^* from nth triangular element.
Δw_n^*	contribution to w^* from nth triangular element.
ϵ	thickness ratio of elliptic wake cross-section.
ζ	$= y + iz$.
ζ_A	ζ at corner A of nth element.
ζ_B	ζ at corner B of nth element.
ζ_C	ζ at corner C of nth element.
θ	$= \cos^{-1} y^*$.
λ	$= \tan^{-1} (dz^*/dy^*)_C$.
$\xi(x,y,z)$	vorticity distribution within A.
$\xi^*(t^*, t^*, z^*)$	non-dimensional form of ξ . See Equation (5).
ξ_n	constant value of ξ in nth triangle.
ξ_n^*	non-dimensional form of ξ_n .
ξ_s	constant value of ξ inside S.
$\omega(y)$	vorticity distribution within A'.
$\omega^*(y^*)$	non-dimensional form of ω . See Equation (5).

LIST OF FIGURES

FIGURE No.

- 1 Flow Chart of Calculation Method.
- 2 The Cell Arrangements and the Associated Vortices and Control Points for Rectangular and Delta Wings.
- 3 Vortex Wake Calculations for Elliptic Lift Distribution.
- 4 VLM Vortex Wake Calculations.
- 5 Nonlinear Vortex Wake Calculations.
- 6 Nonlinear Finite Core Rolled Up Wake Calculations.
- 7 Schematic Diagram for the Calculation of Cores Diameters.
- 8 Problems in the Calculations of the Vortex Sheet Roll-up-"Escape" of the "Tip" Vortex.
- 9 Problems in the Calculations of the Vortex Sheet Roll-up-Cross-Over of Vortex Lines.
10. Problems in the Calculations of the Vortex Sheet Roll-Up-Too Many Subdivisions.
11. Two and Three Dimensional Rolled up Wake Shapes Calculated by Elliptic Lift Distribution Procedure. (Axes are Given by Half Span Units).
12. The Rolled-Up Wake Shapes Calculated by the VLM Procedure with Step Sizes $M = 16$ and $M = 32$.
13. The Rolled-up Wake Shapes Calculated by the MVLM Procedure with Step Size $M = 16$ and $M = 32$.
14. The Rolled up Wake Shape Calculated by the VLM Procedure with Finite Core Vortices. Rectangular Wing of $AR = 1$ at $\alpha = 10^\circ$ and $N = 41$, $M = 32$.

FIGURE No.

15. Wake Cross-Sections and System of Axes.
16. Notation for a Triangular Element and a Field Point.
17. Layout of Elements in an Elliptic Wake.
18. The Initial Roll up at the Tip of a 4% Thick Elliptic Wake.
19. The Initial Roll up at the Tip of a 5% Thick Elliptic Wake.
20. The Initial Roll up at the Tip of a 6% Thick Elliptic Wake.
21. Example of a Complete Half wake.
22. Vorticity within Core as a Function of t^* .
23. Mean Core Diameter as a Function of t^* .
24. The Height to Width Ratio of the Core as a Function of t^* .
25. Number of Turns of the Tip Spiral as a Function of t^* .
26. Maltby's Model [34].
27. Comparison of the Vortex Sheet at The Trailing Edge from a Rectangular Wing $AR = 5.33$ Obtained from Different Models ($\alpha = 12^\circ$)
28. Comparison of the Measured Core Size with the Calculated Results for a Rectangular Wing of $AR = 5.33$ at the Trailing Edge Plane.
29. The Lift Coefficient of a Rectangular Wing of $AR = 1$.
30. The Pitching Moment Coefficient of a Rectangular Wing of $AR = 1$.
31. The Induced Drag Coefficient of a Rectangular Wing of $AR = 1$.
32. ΔC_p of a Rectangular Wing of $AR = 1$ at $\alpha = 20^\circ$; Experimental Results of Scholtz [40].
33. The ΔC_p Calculated by the Proposed Method for a Rectangular Wing of $AR = 1$ at $\alpha = 20^\circ$.

FIGURE No.

34. ΔC_p of a Rectangular Wing of AR = 1 at $\alpha = 10^\circ$, Experimental Results of Scholtz [40].
35. The ΔC_p Calculated by the Proposed Method for a Rectangular Wing of AR = 1, at $\alpha = 10^\circ$.
36. The Influence of the Profile Shape on the Pressure Distribution of a Rectangular Wing of AR = 1. [30].
37. The Rolling Up of the Vortex Sheet at the Trailing Edge Plane of a Rectangular Wing of AR = 1 as a Function of Incidence.
38. The Near Wake Development Behind a Rectangular Wing of AR = 1, at $\alpha = 20^\circ$.
39. The Rolling up of the Vortices Shed from Side and Trailing Edge over a Rectangular Wing of AR = 1 at $\alpha = 10^\circ$.
40. Comparison of the Aerodynamic Coefficients C_L , C_M , C_{D_i} for a Rectangular Wing of AR = 0.25.
41. ΔC_p of a Rectangular Wing of AR = 0.25 at $\alpha = 20^\circ$ Following the Experimental Results of Wickens [42].
42. ΔC_p calculated by the Proposed Method for a Rectangular Wing of AR = 0.25 at $\alpha = 20^\circ$.
43. Rolling up of the Vortices Shed From Sides and Trailing Edges of a Rectangular Wing of AR=0.25 at Incidence $\alpha = 20^\circ$.
44. Comparison of Experimental and Computed Lift Coefficient C_L as a Function of α for Delta Wing of AR = 1.
45. Comparison of Experimental and Computed Lift Coefficient C_L as a Function of α for Delta Wing of AR = 1.5.

FIGURE No.

46. Comparison of Experimental and Computed Lift Coefficient C_L as a Function of α for Delta Wing of $AR = 2$.
47. Center of Pressure of a Delta Wing of $AR = 1$ as a Function of Incidence.
48. ΔC_p of a Delta Wing of $AR = 1.46$ at $\alpha = 19.1^\circ$; Experimental Results from Ref. [47].
49. The ΔC_p Calculated by the Proposed Method for Delta Wing of $AR = 1.46$ at $\alpha = 20^\circ$.
50. ΔC_p of a Delta Wing of $AR = 1.46$ at $\alpha = 14^\circ$; Experimental Results from Ref. [47].
51. The ΔC_p Calculated by the Proposed Method for a Delta Wing of $AR = 1.46$ at $\alpha = 15^\circ$.
52. Lift Coefficient C_L Induced Drag Coefficient C_{D_i} ($AR = 1.46$).
53. Vortex Lines on a Delta Wing of $AR = 1$ at $\alpha = 20^\circ$ (6 x 6 Sub-Divisions).

I. INTRODUCTION

The present report summarizes the research program conducted under Grant AF OSR 71-2145 during the period 1971-1975. Results of this research program are presented in the reports and papers listed in References 1 to 10.

The research program was aimed at the investigation of the rolling up of vortices over and behind wings of various planforms, and the simultaneous evaluation of the spanwise and chordwise loadings. This unified analysis is the main feature of the calculation method presently developed. On one hand this method is based on the representation of the vortex distribution over the wing planforms by a vortex lattice similar in some respects to the method developed by Falkner (Refs. 11, 12, 13); on the other hand, the effects of the vortices from each cell which are shed into the flow field are also considered, in the present investigation. These vortices are first allowed to leave the wing planform from its trailing edges, as in the investigations of Westwater [14], Hacket and Evans [15] and Hancock and Butter [16], Rom and Zorea [2]. In further steps the three-dimensional geometry, the shedding of vortices from the side and leading edges and from every cell in the planform and the combined calculation of the vortex wake and the wing lift are developed.

Since the present work makes no assumptions concerning the trailing vortex behaviour once it has left the wing - assumption which would limit the calculation to a particular range of aspect ratios -

and since separation of the vortices is permitted at all edges or over the whole wing, the present approach will cover all the range of aspect ratios in an unified manner provided it can be shown that separation is automatically suppressed when it is inappropriate, as for example, in the case of the leading-edge and surface of a high-aspect-ratio wing. The calculations of Reference 5 show this to be effectively done.

Various relevant investigations are presented in Refs. 17 to 23, and in the publications under the present Grant in References 2, 4, 5. Another important aspect of the vortex wake investigation is the process of rolling up of the vortex sheet. This process was first investigated by Kaden [24] and by Spreiter and Sacks [25]. The effects on the process of rolling up of the finite thickness of the wing and its wake was investigated as part of our program. The effects of wing thickness on the flow field are presented in Refs. 1 and 7 and an investigation of the initial rolling up of a thick vortex layer is presented in Ref. 10.

An additional topic, investigated by both lifting-line theory and vortex-lattice calculations, is the manner of the effect of a number of vortex suppressing devices, which have been tried, on the overall aerodynamic properties of the wings to which they are attached [6],[8]. The results for a Boeing 747 wing fitted with eighteen pairs of triangular vanes for vortex suppression, which were calculated, as reported in Reference 8, are compared there with experimental results given in Ref. 33. Good agreement is obtained for the reduction of C_L at cruise condition but ΔC_D is much larger than that given by experiment. Most of

the C_D increment found in the calculation is due to the vane drag and not to the change of wing induced drag.

An important result of the new method of References 2, 4 and 5 is the evaluation of the non-linear aerodynamic coefficients. There are a number of methods proposed for the evaluation of the non-linear lift of wings. Some of the investigations that form the basis for methods of calculation of non-linear aerodynamic lift coefficient were presented by Brown and Michael [26], Mangler and Smith [27, 28, 29], Gersten [30] and Polhamus [31]. The method developed in the present research make the evaluation of the non-linear characteristics of wings possible as summarized in Ref. 5.

The computer programs developed in References 2, 4 and 5 follow the procedure by which the wing is first divided into cells. Then a bound vortex element is placed at the "quarter chord" of each cell and a control point is placed at the middle of its "three quarter chord". The trailing vortices can be taken to be shed away from the edges of each bound vortex and to continue in the wing plane to the trailing edges. In this case the variation of the aerodynamic characteristics vary essentially linearly with the angle of attack [2]. On the other hand these vortices can be taken to leave the wing plane from only the side and trailing edges or from each cell. When the trailing vortices are allowed to leave from the side and trailing edges only the trajectories of these trailing vortices are determined by an iterative calculation which results in the evaluation of non-linear aerodynamic characteristics. In the case when the trailing vortices are allowed to leave the wing plane at each cell at an arbitrary

local angle (similar to Gersten's model) these vortices can be either straight lines (as in Gersten's model) or free to roll up above and behind the wing planform non-linear aerodynamic wing characteristics are also obtained [2].

The numerical problems involved in approximating the circulation distribution by discrete ideal vortices have been investigated, The numerical difficulties associated with using discrete ideal vortices become even more difficult when the vortices are shed from the cells in the wings' planform or from its side edges. In order to eliminate some of these difficulties it was proposed in Ref. 5 to use the finite core vortex model. As a first approximation the core size is related to the local vortex strength by the method proposed by Sprieter and Sacks [25].

An additional subject of investigation dealt with the improving the linearized solution for the flow near the tips and wake edges of a lifting wing in incompressible flow, mainly with a view to its more effective utilization in the calculation of the rolling up of the trailing vortex wake (Ref. 1). The linearized solution always exhibits singularities of velocity at the wing leading edge and the wake edge due to the replacement of these actually or effectively radiused edges by sharp ones in the linearisation process. The present treatment takes account of the actual or, in the case of the wake, effective radius of the edge by the method of matched asymptotic expansions and so eliminate this unrealistic feature.

The result takes the form of an integral for the perturbation potential which is uniformly valid to first approximation in all parts of the flow field about the wing and wake. The calculation by this method of the potential function, the velocity and the pressure distributions on ellipsoidal wings at zero incidence is presented in Ref. 7.

Investigations of wing wake roll up have assumed the wake to be a vortex sheet of zero thickness. We have initiated a study assuming that the wake cross-section has a finite thickness and some plausible shape. A two-dimensional method, analogous to that of Westwater, is developed, assuming that the wake cross-section contains vorticity in an otherwise irrotational field.

The wake is divided into triangular elements and the vorticity in these is determined by assuming a linear transverse velocity profile in the wake and that the initial unrolled wake moves downwards as determined by the wing spanwise loading through ordinary wing-wake theory. Euler time step integration is then used to calculate the wake development under its own induced velocity field, ignoring viscous dissipation. A finite spiral wake structure is observed to develop. Some preliminary results are presented in Ref. 10.

The research effort started under Grant AF OSR 71-2145 included also an investigation of viscous-inviscid interaction; particularly emphasizing areas and problems which are important for wing aerodynamics. The interactive flow analysis is based on dividing the flow field to regions where the flow is essentially inviscid and regions where the flow is dominated by

viscous effects. In each region the appropriate flow equations are applied. The solutions are then matched by properly defined compatibility relations on a boundary surface. However, neither the position of the boundary surface nor the conditions on this boundary are known beforehand. These are to be determined by the complete solution. Therefore problems of this type are generally solved by an iteration procedure. In these cases the interactive process between the viscous flow and the essentially inviscid external flow is the dominating process in the flow field. This means that the hierarchical procedures, which form the basis for the boundary layer methods are not valid for flow with strong interaction. Some of the important characteristics of such flows as well as some possible methods for analysis are discussed in a paper presented at the Goldstein Symposium, (Ref. 9).

II. THE GENERALIZED VORTEX-LATTICE TECHNIQUE - METHODS OF CALCULATION OF THE TRAJECTORIES OF THE VORTICES AND THE AERODYNAMIC CHARACTERISTICS OF THE WING.

The methods of calculation are based on a unified procedure for calculation of vortices distributed on the wing planform and the vortices shed from the wing into the flow over and behind the wing. The results of this calculation give on one hand the loading distribution on the wing planform which makes possible the evaluation of the aerodynamic characteristics (such as lift, induced drag, aerodynamic moments etc.) and on the other hand this calculation is used for the determination of the flow field over the wing and the trailing vortex flow field behind the wing, so that the wake geometry may be iteratively relaxed into the proper form.

The calculation procedure follows the following steps (shown schematically in Fig. 1).

2.1. Geometrical Division of the Planform into Cells

The wing planform is first divided into cells by proper spanwise and chordwise divisions. This division is similar in many respects to that used in the standard vortex lattice method. One has to select a reasonable number of divisions. A small number of divisions (large cells) will result in insufficient accuracy while an excessive number of divisions will cause numerical problems (as discussed in (Ref.2)). Each cell is then represented by a separate horseshow vortex with the bound vortex positioned at the cell's $1/4$ chord line and the trailing vortices are either embedded in the wing planform and leave the wing at the trailing line or are free to leave the wing planform right at the edges of the bound vortex. It is also possible

to allow only the vortices from the leading and side edges to be free to leave into the flow while all other trailing vortices are embedded in the wing planform and leave the wing at its trailing edge.

The vortex strengths are calculated to be compatible with the boundary conditions applied at control points positioned at the middle of the $3/4$ chord lines of each cell. For rectangular wings the number of chordwise and spanwise divisions can be selected as required, whereas in the case of delta wings, it is found that we must use equal number of spanwise and chordwise division lines. The bound vortex lines and the control points are positioned as shown in Fig. 2, where examples of the divisions of rectangular and delta wings are shown.

2.2. Selection of Appropriate Initial Vortex Distribution

The initial vortex distribution is determined by the physical model used for the flow field. These models can be:

- (1) All vortices embedded in the wing planform and leaving the wing at the trailing edges into the wake and rolling up behind the wing.
- (2) Trailing vortices leaving the $1/4$ chord line of each cell on the leading and side edges only (rectangular planform) or from leading edges only (delta planforms). The other vortices are embedded in the wing planform and leave at the trailing edges only. The rolling-up starts at the side edges or leading edges for rectangular and delta wings respectively.

- (3) All vortices leaving each cell into the free stream above the wing and rolling up into the trailing vortex formation. In this case it is found that a good starting condition is obtained by allowing the vortices to leave the wing at a local angle equal to half the angle of attack, as used by Bollay [35] and Gersten [36]. The correct final vortices trajectories are obtained after few iterations.

2.3. Calculation of the Induced Velocity Field.

The induced velocity field is calculated using the Biot-Savart law. The position of the downstream edge of each segment in the wake flow field is calculated taking into account the induced velocities at the upstream edge. The effect of self-induced velocities on each vortex is accounted by using the concept of a cut off radius [32].

2.4. Calculation of the Vortex Trajectories

The local position of the vortices can be assumed to coincide with the path of the streamline. Therefore, the position of the vortices can be evaluated from the calculated flow velocities:

$$\frac{dy}{dx} = \frac{v}{u + U} ; \quad \frac{dz}{dx} = \frac{w}{u + U} \quad (1)$$

The accuracy of this calculation depends on the numerical method for integration. In the present program either the Euler integration method or the second order Runge-Kutta technique are used.

2.5. Evaluation of the Aerodynamic Parameters

At the end of each iteration the local vortex strengths are evaluated by the solution of a system of linear equations. The number of equations is equal to the number of cells. This system of equations can be solved by matrix calculations. By proper integration of the strengths of the vortices over the planform, it is possible to evaluate any desired aerodynamic parameter. In this program the calculated parameters are : C_L , C_{D_i} , C_M , $x_{c.p.}$, $y_{c.p.}$, the coordinates of the centroid of the vortex core b' ; z' and the size of the vortex core far downstream.

III. THE ROLLING UP OF THE WAKE BEHIND WINGS

The vortex wake behind a wing of high aspect ratio has been approximated by a zero thickness vortex sheet. The calculation of the roll-up of this vortex sheet can be done if the vortex sheet is represented by a finite number of discrete line vortices.

The method of calculation of this vortex flow is presented in previous reports (Ref. 2,5), and is shown schematically in Figs. 3,4,5,6 and 7.

The first calculation is based on the simplified model of a two-dimensional wake with an elliptic spanwise circulation distribution. This program reproduces the early work of Westwater [14] in which the flow in a fixed stationary plane far behind a moving wing with elliptic circulation distribution is identified with the problem of the motion of a two-dimensional array of point vortices moving under their own mutual influences (see (a) in Fig. 3).

The basic program enables us to investigate many of the practical problems which occur in all discrete vortex models: whether to use equal-strength or equally-spaced vortices, the problem of "cross-over" of the vortex trajectories, "escape" of the tip vortex and the development of an irregular shape of the sheet (see Figs. 8,9,10).

The problems are basically due to the use of the concentrated point vortex model with its associated velocity singularities, plus accumulative effects of rounding-off errors etc. In spite of these difficulties reasonable numerical solutions, were found to be possible by a proper choice of the number and spacing of the vortices and the size of the time intervals (corresponding to the downstream separating of the planes at which the

vortex pattern is calculated step by step). The correct combinations were found by a series of numerical experiments. It is important to note that due to the causes mentioned, too many vortices or stations can lead to the deterioration of the results rather than convergence to a limiting form.

In the next stage of the work a wing with an elliptic circulation distribution is dealt with, employing a single bound vortex on the wing quarter-chord line (see (b) in Fig. 3). The trailing vortices are continued straight from this line to the trailing edge and, from the trailing edge downstream. Their rolling-up is taken, as a first approximation, to be given by the results of Section (a). The corrections necessary to this wake shape to conform with the lifting-line vortex pattern are then calculated by a series of iterations, assuming the elliptic spanwise circulation distribution unchanged throughout. The experience gained in stage (a) is utilized to select the number of vortices etc. At a later stage the finite-core concept is incorporated here too.

A practical point worth mentioning is as follows: The rolling-up calculations only carried as far as ten semi-spans downstream of the trailing edge. However, a correction for the influence of the portion of the wake downstream of this station was incorporated. At the ninth and tenth stations the center of gravity of the vortex-wake cross-section (in the half-span domain) was found and a line through these two points was taken to define the position and direction of a single replacement trailing vortex from each half wing, starting from the tenth station extending to infinity and having the appropriate ultimate strength (i.e. equal to the value of the mid-span circulation - similar to that used

in [15]). The induced velocity due to this pair of semi-infinite vortices was taken as an appropriate correction for the influence of the portion of wake downstream of the tenth station on the flow upstream of it. This method was employed in all subsequent stages.

The result of calculation of the wake shape behind a rectangular wing of $AR = 3$ is shown in Fig. 10. A comparison of this result with that of the infinite vortex (Westwater) model is indicated as the 2-D curve in this Figure.

At this stage a lifting-surface theory was introduced to enable us to deal with general wing shapes with some accuracy (Fig. 4).

The standard vortex-lattice technique is employed [5 - 10] to start with. The wing is divided into cells by a number of equally spaced streamwise lines and by either equally-spaced constant-percentage-chord lines or by lines perpendicular to the stream. A bound vortex element is placed at the "quarter-chord" of each box and a control point is established at the middle of its "three-quarter-chord" line. The usual trailing vortices are taken to spring from each bound vortex element and to continue straight downstream in the wing plane, and the unknown vortex strengths are found, in the usual way, by evaluating the downwash at each point, equating it to the value given by the boundary condition, and solving the resultant system of linear equations. The wing aerodynamic coefficients are then found from the results, to a linear approximation.

A first approximation to the rolling up is now found by taking the actual spanwise distribution of the circulation (which will generally not be elliptic and performing a two-dimensional calculation of rolling up, as was

done in Section (a) for the elliptic case. This now taken as the first approximation to the rolled up wake shape starting from the trailing edge. As in Section (b), the first approximation to the wake shape is improved iteratively using the calculated vortex strengths. During these iterations the vortex strengths on the wing are kept constant. Using the new wake shape the vortex distribution on the wing and the aerodynamic coefficients are recalculated. We then return to the recalculation of a new vortex wake shape by iterations; keeping the vortex strengths fixed, and so on. Some wake shapes calculated by these procedures are shown in Figs. 11 and 12.

In the program of investigation of the wing with vortices leaving the planform, the calculation starts with the free vortices leaving at an angle of $\alpha/2$ to the wing planform and then extending in straight lines into the wake. The system of bound-vortex elements is set up exactly as in the previous section and the vortex strengths and wing properties are found by a similar process. The rolling up of the vortex wake can now be obtained by calculating the induced motion of the individual vortex lines due to mutual interactions. The final shape is determined by an iteration procedure described in Fig. 5, involving the recalculation of the vortex strengths and the corresponding wake shape. This calculation cannot be done using the ideal line vortices because of the difficulties of intersection and "escape" of the vortices discussed previously. Therefore, this model is used only to determine the non-linear aerodynamic coefficients with straight trailing vortices. The use of finite core vortices may

eliminate some of the problems and enable the calculation of this rolled-up vortex wake to be carried out. This calculation is now underway. However a simpler calculation is possible when it is assumed that vortices are shed only from the planform edges. In this case the new vortex wake shape can be recalculated by the iterative procedure indicated in Fig. 6 step 1.

The numerical problem associated with the use of ideal line vortices lead us to look for a solution by the use of finite core vortices. Since the actual wake has thickness and is not an infinitesimally thin sheet, this is also a better approximation to the real wake. We assume a core diameter which is determined by the condition of constant vorticity per unit cross-sectional area of the core. The density of the vorticity in the core can then be calculated, for instance, by using the core size calculated by Spreiter and Sacks [19].

We impose the condition that as soon as two cores touch the two vortices are replaced by a single one at the center of gravity of the pair. The new core diameter is determined by the condition of conservation of vorticity at the same vortex density. This procedure overcomes the difficulties caused by the approach of ideal vortices, i.e., "intersection" and "escape". This procedure limits the number of vortices automatically, thus helping to eliminate also other irregularities. Furthermore, this method ensures that, when all the vortices are amalgamated far downstream, we end up with a pair of vortices with the correct diameter and strength matching the expected vortex pair in the far field.

Under these assumptions the core radius is determined by the relation,

$$R_i^2 = \frac{K_i}{\sum_{j=1}^n K_j} \cdot R_o^2 \quad (2)$$

R_o being the final core diameter.

The vortex core diameter is evaluated at present by using the method presented by Spreiter and Sacks [19]. Accordingly the core diameter is

$$\frac{R_o}{b'} = 2 \left\{ 1 + \exp \left[- \frac{4\pi \cdot AR \cdot C_{D_i}}{C_L^2} \left(\frac{b'}{b} \right)^2 - \frac{1}{4} \right] \right\}^{-1} \quad (3)$$

when the wing loading is elliptical, $C_{D_i} = C_L^2 / \pi AR$ and $b'/b = \pi/4$. In this case the core radius of the vortex in the far field is $R_o = 0.197b' = 0.155b$.

The vortex-wake shape obtained when 41 finite-core vortices are initially placed with equal spacing on the trailing edge of a rectangular wing is shown in Fig. 14. It should be pointed out that during the wake development calculations a number of vortices combine and we find less vortices in the wake than the initial number.

The procedure for the calculation of the wake characteristics associated with the finite-core vortices is outlined in Fig. 6. The detailed procedure for the calculation of the vortex core diameter is outlined in Fig. 7.

3.1. The Thick Vortex Layer Model

This investigation is an attempt to remove the unrealistic features of the earlier models, namely zero wake thickness and vorticity concentrated on lines, by assuming that the wake vorticity is contained in a layer of finite thickness with some plausible cross-sectional shape. The wake flow is assumed to be two-dimensional and the rolling-up is studied via the time-dependent development of this model, exactly as in Westwater's work, so that we deal with a slow rolling-up taking place far behind the wing, once more. The introduction of vorticity distributed continuously throughout the wake cross-section enables us to obtain a more acceptable picture of the initial rolling up phase than the infinite spiral of Kaden.

Having selected an appropriate wake cross-section its area is divided into triangular elements within each of which the vorticity is assumed constant, and for which simple expressions giving the velocity field have been derived (Ref. 10). The strength of the vorticity within each triangle is determined using two assumptions:

- (1) The vorticity is constant through the wake thickness. This corresponds to an assumption that the transverse velocity profile within the wake is linear.
- (2) The periphery of the wake is moving downwards with a velocity determined by spanwise position and wing spanwise loading, exactly as in ordinary wing-wake theory.

Assumption (1) can evidently be removed at the cost of increasing the number of triangular elements used.

Once the triangle strengths are found, the network of points defining the wake is allowed to distort with time under its self-induced velocity field, using Euler integration. During this process viscous dissipation is neglected, so that the vorticity inside each triangle remains constant, as will its area (due to continuity), even though the shape changes.

The mathematical model of the wake and the notation are illustrated in Fig. 15.

The unrolled wake cross-section A' , whose boundary is denoted by C' , stretches between $y = -s$ and $y = +s$ in the plane $x = 0$. At subsequent stations $x = x$, the boundary is denoted by C and the wake has a rolled up form of cross Section A with vorticity distribution $\xi(x, y, z)$ determined by the original configuration of the wake cross-section, the original vorticity distribution with it, $\xi(0, y, z)$, and the elapsed time x/U . It is assumed that

$$\xi(0, y, z) = \omega(y), \quad (4)$$

corresponding to a linear variation with z of the velocity, v , within the initial wake section, if the wake is assumed thin.

We define dimensionless coordinates

$$y^* = \frac{y}{s} ; \quad z^* = \frac{z}{s} \quad (5)$$

and since a typical velocity of the flow in the wake cross-sectional plane is $2UC_L/\pi \cdot AR$, we also define dimensionless velocity components, time and vorticity by

$$v^* = \frac{\pi AR.v}{2UC_L} ; \quad w^* = \frac{\pi AR.w}{2UC_L} \quad (6)$$

$$t^* = \frac{2C_L x}{\pi AR.s} \quad (7)$$

$$\omega^*(y^*) = \frac{\omega \pi AR.s}{2UC_L} ; \quad \xi^*(t^*, y^*, z^*) = \frac{\xi \pi AR.s}{2UC_L} \quad (8)$$

We assume that ω or ω^* is determined by the boundary conditions:

$$(a) \quad w^* \cos \lambda - v^* \sin \lambda = w_I^*(y^*) \cos \lambda \quad (9)$$

on C'

where $(dz^*/dy^*)_{C'} = \tan \lambda$, and

$$(b) \quad \sqrt{v^{*2} + w^{*2}} \rightarrow 0 \quad \text{as} \quad \sqrt{y^{*2} + z^{*2}} \rightarrow \infty. \quad (10)$$

$w_I^*(y^*)$ is the non-dimensionalised downwash distribution in the Trefftz plane as calculated from the usual unrolled thin-wake theory. For example, $w_I^* = -1$ for elliptic spanwise load distribution. It is readily shown that, in the general form, w_I^* is dependent on the form of the spanwise loading and y^* only (c.f. Reference 3).

It now follows that for a given initial wake cross-section and spanwise loading, the velocities v^* and w^* of a given fluid particle are functions of t^* only, so that the subsequent non-dimensional coordinates of the particles constituting the rolled wake are functions of t^* only, determined by the differential equations

$$\frac{dy^*}{dt^*} = v^* ; \quad \frac{dz^*}{dt^*} = w^* . \quad (11)$$

The equations (8) are integrated numerically step by step, starting from the initial configuration, using Euler integration.

It remains to determine the velocity field (v^*, w^*) due to the distribution ξ^* within C .

At any value of x , the two-dimensional velocity field, (v, w) , is determined by integrating the effects of point vortices of strengths $\xi(x, y, z) dy dz$ over the area of the wake cross-section, A .

To facilitate the numerical calculations, A is divided into a finite number of small triangular elements within each of which the value of ξ is assumed constant. We now find expressions for Δv_n^* and Δw_n^* due to a typical element of this kind for points outside its boundary, or approaching the boundary in a limiting sense. This enables us to calculate v^* and w^* for the assemblage of triangles at all the node points of the triangular mesh, including internal nodes of A , since such points may be regarded as being inside infinitesimal cavities excluded from all the adjacent triangles, and we calculate, in effect, the principal value of the velocity integral - which is precisely the required definition of this integral inside the vorticity distribution.

The velocity field outside any area S containing a constant vorticity distribution, ξ_s , may be written

$$v - iw = \frac{-i\xi_s}{2\pi} \int \int_S \frac{dy_1 dz_1}{y + iz - y_1 - iz_1} \quad (12)$$

Using Green's theorem, this may be converted to a line integral around P , the perimeter of S :

$$v - iw = \frac{i\xi_s}{2\pi} \int_P \ln(\zeta - y_1 - iz_1) dy_1 \quad (13)$$

where $\zeta = y + iz$.

If (10) is applied to a typical triangle of A , of area ΔA_n , vorticity distribution strength ξ_n and vortices defined by $\zeta_A, \zeta_B, \zeta_C$ (Fig. 2), we obtain

$$\begin{aligned} \Delta v_n - i\Delta w_n = & \frac{-i\xi_n \Delta A_n}{\pi} \left\{ \frac{\zeta - \zeta_A}{(\zeta_C - \zeta_A)(\zeta_B - \zeta_A)} \ln(\zeta - \zeta_A) + \right. \\ & \left. + \frac{\zeta - \zeta_B}{(\zeta_C - \zeta_B)(\zeta_A - \zeta_B)} \ln(\zeta - \zeta_B) + \frac{\zeta - \zeta_C}{(\zeta_A - \zeta_C)(\zeta_B - \zeta_C)} \ln(\zeta - \zeta_C) \right\}. \end{aligned} \quad (14)$$

ξ_n and ΔA_n are both invariant with the motion for an infinitesimal triangle in incompressible flow, the product $\xi_n \Delta A_n$ being the circulation around the element.

If we now write $s^2 \Delta A_n^* = \Delta A_n$, then

$$\xi_n \Delta A_n = \frac{2UsC_L}{\pi AR} \xi_n^* \Delta A_n^* = \frac{2UsC_L}{\pi AR} K_n \quad (15)$$

and if (see Fig. 2)

$$\begin{aligned} \zeta - \zeta_A &= sr_A e^{i\alpha}; & \zeta - \zeta_B &= sr_B e^{i\beta}; & \zeta - \zeta_C &= sr_C e^{i\gamma} \\ \zeta_B - \zeta_A &= sce^{i\alpha\beta}; & \zeta_C - \zeta_A &= sbe^{i\alpha\gamma} \\ \zeta_C - \zeta_B &= sae^{i\beta\gamma}; & \zeta_A - \zeta_B &= sce^{i\beta\alpha} \\ \zeta_A - \zeta_C &= sbe^{i\gamma\alpha}; & \zeta_B - \zeta_C &= sae^{i\gamma\beta} \end{aligned} \quad (16)$$

we obtain from (11)

$$\begin{aligned}
 \Delta v_n^* &= \frac{K_n}{\pi} \left\{ \frac{r_A}{bc} [\sin(\alpha - \alpha_C - \alpha_B) \ln r_A + \alpha \cos(\alpha - \alpha_C - \alpha_B)] + \right. \\
 &\quad + \frac{r_B}{ca} [\sin(\beta - \beta_C - \beta_A) \ln r_B + \beta \cos(\beta - \beta_C - \beta_A)] + \\
 &\quad \left. + \frac{r_C}{ab} [\sin(\gamma - \gamma_A - \gamma_B) \ln r_C + \gamma \cos(\gamma - \gamma_A - \gamma_B)] \right\} = \\
 &= K_n V_n(y^*, z^*) \tag{17}
 \end{aligned}$$

$$\begin{aligned}
 \Delta w_n^* &= \frac{K_n}{\pi} \left\{ \frac{r_A}{bc} [\cos(\alpha - \alpha_C - \alpha_B) \ln r_A - \alpha \sin(\alpha - \alpha_C - \alpha_B)] + \right. \\
 &\quad + \frac{r_B}{ca} [\cos(\beta - \beta_C - \beta_A) \ln r_B - \beta \sin(\beta - \beta_C - \beta_A)] + \\
 &\quad \left. + \frac{r_C}{ab} [\cos(\gamma - \gamma_A - \gamma_B) \ln r_C - \gamma \sin(\gamma - \gamma_A - \gamma_B)] \right\} = \\
 &= K_n W_n(y^*, z^*) \tag{18}
 \end{aligned}$$

Hence we have the approximations

$$v^* \approx \sum_{n=1}^M K_n V_n(y^*, z^*) \tag{19}$$

$$w^* \approx \sum_{n=1}^M K_n W_n(y^*, z^*) . \tag{20}$$

The details of the numerical calculation procedure and results for the wake of elliptic cross-section are presented in Ref. 10. The notation for the triangular elements is shown in Fig. 16. Some results showing the appearance of the tip region for various stages of the initial roll-up are shown in Figs. 18, 19 and 20 for $\epsilon = 0.4, 0.5$ and 0.6 , respectively

and in Fig. 21 one example of a complete half-wake is shown. It should be noted that to clarify the inner detail of the spiral, the vertical scale has been exaggerated in these figures and this vertical scale is not uniform throughout all the pictures. The results of this calculation and the significant features of the model used are also discussed in detail in Ref. 10.

The analysis of the results shows that, for the range of thickness ratios covered, for the elliptic cross-sectioned wake:

- (1) Thickness has little effect on the amount of vorticity within the core at a given t^* (Figure 22).
- (2) Thickness has almost no effect on the size of the core at a given t^* (Figure 23).
- (3) Except in the very initial stages of roll-up, the core is of approximately elliptic shape with height/width ratio about 0.8 for all three thickness ratios studied (Figure 24).
- (4) The number of turns of the spiral within the core at a given t^* increases with reduction of ϵ , except for very small values of t^* when the spiral is, in any case, ill-defined (Figure 25). About one and three-quarter turns are observed for the $\epsilon = .04$ case at $t^* = .0128$ and for the $\epsilon = .05$ case at $t^* = .0160$, and for the $\epsilon = .06$ case at $t^* = .0192$, just over one and a half turns.
- (5) An interesting result observed in all three cases is that the original tip point of the unrolled wake does not become the

tip point of the spiral; instead it recedes back along the outer edge of the coil. This appears to be true also for subsequent tip points of the spiral - these do not remain at the tip but are dragged back along the outer edge of the spiral in their turn and their place is taken by other points which were originally more inboard along the upper edge of the unrolled wake.

This work is being extended into the more complete stages of rolling-up and also to deal with different spanwise loadings.

IV. THE METHOD OF CALCULATION OF THE NONLINEAR AERODYNAMIC CHARACTERISTICS OF WINGS.

The present method is developed to calculate the aerodynamic characteristics of wings at subsonic speeds. The wings can have various Aspect Ratios from low to high and can be at any angle of attack below that of stall or vortex breakdown. The calculation includes also the evaluation of the shape of the rolled up vortex sheet above and behind the wing as well as the velocity field. A schematic model for the flow over a wing at a high angle of attack as presented by Maltby [34] is shown in Fig. 26. For low aspect ratio wings, the rolling up of the vortex sheet above the wing affects the pressure distribution and results in the non-linear lift variation at increasing angles of attack.

The calculation procedure is described in the flow chart shown in Fig. 1. The calculation is divided into the following:

a. Definition of the Model for the Wing Planform (Steps 1 and 2)

The planform of the wing is divided into cells as shown in Fig.

2. The number of subdivisions has to be limited due to numerical problems as well as the size of computer memory. The bound vortex and the control points positions are clearly indicated in Fig. 2.

b. Establishment of the Initial Conditions and the Strength of the Vortices (Step 3).

The initial conditions for the calculation involve the determination of the values of the strength of the vortices in each cell on the planform and in the wake. This requires the

assertion of an initial shape for the wake. For rectangular and delta wings the initial shape of the vortices is assumed to be straight lines issuing from the bound vortex of each cell and continuing downstream towards $+\infty$. These vortices can be issued from the trailing edge only, so that initially the vortices are embedded in the planform. Other options are to issue the vortices in straight lines at an arbitrary local angle from : (a) each cell, (b) from all edges (sides, leading and trailing edges) or (c) from side and trailing edges only. These options can be selected by the proper computer code. The initial local angle is selected to be half the angle of attack. This trailing vortex configuration which was suggested by Bollay [35] and by Gersten [36] is found to be very suitable as a starting condition. These initial conditions enable the calculation of the corresponding strengths of the vortices.

c. Calculation of the Velocity Field (Step 4).

The induced velocity at each point is calculated by the Biot-Savart law, by adding the influence of all the vortices as well as self induced effects. The effect of curvature on the self induced velocity is dealt by choosing a cutoff radius as suggested by Crow (Ref. 32).

d. Calculations of the Vortex Trajectories (Step 5)

The position of the vortices is calculated from the induced flow field by the numerical integration of the relations presented in Part II, Eq.

1. During the investigation both the Euler integration method and a second order Runge-Kutta method were used.

In order to facilitate the convergence of the calculation the iteration procedure for the determination of the new vortex position is damped by a relaxation factor.

e. Calculation of the Strength of the Vortices (Step 6)

Knowing the shape and position of the vortices in a given iteration the strengths of the vortices are calculated by a solution of the matrix equation

$$\{\tan \alpha\} = [H] \{k\} \quad (21)$$

where $[H]$ is the influence matrix and $\{k\}$ is the strength of the vortices while α is the local angle of attack. The order of the matrix is equal to the number of cells. Each equation is obtained by imposing the zero vertical velocity at the control point of each cell. The matrix equation (21) is solved numerically.

f. Calculation of the Aerodynamic Coefficients and the Wake Characteristics (Step 7)

At the completion of each iteration the vortex strength and the positions of the vortices are determined. These vortex calculations can be used for the evaluation of the aerodynamic loading distributions as well as the integral values for lift, drag and various

aerodynamic moments. In the present investigations the values of C_L , C_M , C_{D_i} and $x_{c.p.}$ and $y_{c.p.}$ and the position of the tip vortex center and the size of the final vortex core diameter are calculated.

The results obtained for rectangular and delta wings by this method and the comparison with results obtained by other methods as well as experimental data is presented in the following Sections.

(1) RECTANGULAR WINGS

The results of the calculation for a rectangular wing of high Aspect Ratio are presented in Figs. 27 and 28. In this case the lift is very nearly linear and therefore it is a good case for comparison of the present method to the conventional linear ones .

The calculation indicate that the vortex core is positioned very near the wing tip. The result is in good agreement with the experimental data (Fig. 27). In the case where the vortices are allowed to leave the wing planform at each cell, the calculations predict the existence of the relatively weak secondary vortex of positive sign. This is in contrast to the linear theory results which have the vortex core center at the $\pi b/4$ and do not predict any secondary vortices.

The value of the size of the vortex core far downstream can be compared with the experimental data of Refs.37 and 38. The present calculation indicate a core size of $a_c/2_b = 2.7\%$ independent of angle of attack. This value is in reasonable agreement with the experimental data presented in Fig. 28.

It is interesting to note in Fig. 27 that the main features of the vortex sheet shape are already obtained when the vortices are allowed to leave the wing at the side edges only. Furthermore, there is practically no difference between the results obtained when vortices were allowed to leave from all cells or from only the leading and side edges.

The interesting effects of non-linear loading variation can be seen from the calculations of the loading on a rectangular wing of $AR = 1$. This wing is selected because of the available experimental data reported in Refs. 39, 40 and 41.

The results of the calculations using the present method and the comparison with the experimental data for C_L , C_M and C_{D_i} are shown in Figs. 29, 30 and 31 respectively. The planform divisions used are: $N_C = 2$, $N_S = 10$; $N_C = 2$, $N_S = 20$; $N_C = 4$, $N_S = 10$. For all of these divisions the results are very good. The value of C_{D_i} increases slightly for larger N_S , improving the agreement with the experimental data. In Fig. 31, the calculated values of C_{D_i} are shifted by the experimentally measured C_{D_o} for better comparison with the measured values.

Comparison of the experimental and calculated loading at $\alpha = 20^\circ$ and $\alpha = 10^\circ$ are presented in Figs. 32, 33, 34 and 35.

Here, the agreement is generally good except for the high peaks in ΔC_p near leading and side edges. This is well illustrated in Fig. 36 where the effect of the wings' profile measured in Ref. 40 are presented. It can be seen that the calculated results are in better agreement with the data of the thin wing.

The shape of the trailing vortex wake is shown in Figs. 37, 38 and 39. The roll up of the vortices at the trailing edge plane of the wing is illustrated in Fig. 37. It can be seen that the vortex trajectories are such that there is a large vortex on the wing situated near each of the side edges over the planform. The interaction of the rolled up side vortices with the vortices shed from the trailing edge is shown in Fig. 38. The rolled up vortex contains 42% of the total wing vortex strength. At the distance of $0.8b$ behind the wing this vortex is much larger in size and in strength. The vortices shed from the trailing edge are much weaker. The vortices near the edge are of opposite sign to those at the rolled up side vortex. Therefore, a cusp is obtained at their intersection. The observation of Maltby (Ref. 34), shown in Fig. 26, indeed shows the appearance of this cusp and the existence of a secondary vortex of opposite sign at this intersection position. The overall shape of the vortex over and behind the $AR = 1$ wing up to 10 half spans behind the trailing edge is shown in Fig. 39.

The availability of experimental results for a rectangular wing of $AR = 0.25$ (Ref. 42) make this wing a good test for our method for the very slender rectangular wings. The aerodynamic coefficients are compared in Fig. 40. Excellent agreement is found even at $\alpha = 20^\circ$.

The pressure loading, ΔC_p , on the wing is shown in Figs. 41 and 42, the measured and calculated values are presented respectively. The agreement between these results is very good except at the leading edges.

These calculations are performed with the wing divided into 48 cells ($N_c = 8$, $N_s = 6$). This division was selected in order to facilitate the comparison with the experimental data. The shape of the rolled up vortex can be obtained from the computed trajectories of the side vortices shown in Fig. 43.

(2) DELTA WINGS

The triangular geometry of the delta planform requires special considerations due to the cell shape and therefore to the applicable calculation method.

There are a number of methods proposed in Refs. 17, 22 and 23, however, we are able to obtain good results with the computation method presented in Figs. 1 and 2. The triangular planform is divided into equal number of chordwise and spanwise divisions, $N_c = N_s$. The triangular cells have their bound vortex on a line connecting the $1/4c$ point to the tip. The control point is located on the median line at the $3/4c$ distance from the apex.

The calculated lift coefficients for delta wings of $AR = 1$; 1.5 and 2 are compared with the experimental data as well as with the classical non-linear theories. These are shown in Figs. 44, 45 and 46 respectively. The agreement with the experimental results is reasonable, however, the variance increases as the aspect ratio decreases. The aerodynamic center for the

AR = 1 delta wing is shown in Fig. 47.

The loading in each cell, ΔC_p , is calculated and compared to the experimental data of Ref. 47 in Figs. 48 and 49 at nominally $\alpha = 20^\circ$ and at $\alpha = 14^\circ$ in Figs. 50 and 51. The calculated distributions shown in Figs. 49 and 51 are similar to the measured ones although, there is loss of details in the distribution due to the relatively large cell size and due to the edges effects noted already in the treatment of the rectangular wings.

The induced drag is also evaluated and compared to the experimental results of Ref. 48 in Fig. 52. Here the agreement is very good.

The pattern of the vortices shed from the delta's leading edges is presented in Fig. 53 for a wing of AR = 1 and a 6×6 division ($N_C = N_S = 6$).

Although, the results presented here are encouraging there are difficulties in the calculations of delta planforms, particularly for slender wings with AR less than 1. These difficulties arise because of the very strong induced velocities due to the small distances between the discrete vortices at low AR and large number of cells. If one introduces finite core vortices, the core size limits the number cells. Therefore it is reasonable to expect good results with the present method for delta wings of Aspect Ratios 1, or higher.

(3) SECONDARY VORTEX SEPARATION

The present method includes the option of calculating the trajectories of the vortices when these are shed from each cell. This calculation results in the appearance of additional rolled up vortices. These secondary

vortices are much weaker than those that form the main lift vortex. The existence of these secondary vortices is found in experiments on both rectangular wings and on delta wings (Ref. 34). The calculations of the secondary vortices on delta wings involved some problems due to one of the "secondary" vortices jumping outside of the wing's planform. However, here also the secondary vortex phenomenon is observed.

(4) COMPUTATION PERIODS

The present method requires about 150-800 seconds on the IBM 370/168 computer.

The rectangular wings calculations require about 150-200 seconds, while the delta wing calculation require more iterations so that the computing time is extended to about 300 seconds. The calculations of the full vortex wake trajectories more than doubles these periods, to about 600-800 seconds.

V. DISCUSSION OF RESULTS

The present method is based on the extension of the Vortex Lattice concepts also to low aspect ratio wings and to the vortex sheet which is established over and behind all wings. As part of this investigation a computer program is developed. This program is capable of reproducing the results of the Vortex Lattice Method (VLM) for linear aerodynamic coefficients of high aspect ratio wings. The addition of the effect of the vortex sheet behind the wing (i.e. vortices shed from the trailing edges) is presented in the Modified Vortex Lattice Method (MVLM). The program enables the calculation of the rolled up vortex sheet behind the high aspect ratio wings as well as the correct lift (circulation) distribution on the wing planform. This wake calculation showed that for rectangular wings the center of the tip vortex core is very close to the wings' tip rather than at the $\pi/4(b/2)$ obtained from the elliptic lift distribution. Furthermore, it was found that although the vortex wake behind the wing rolls up into two concentrated vortices practically these do not affect the linear lift of the wing itself. It is therefore clear that the non-linear aerodynamic coefficients are due to the vortices which are shed on and over the wings' planform. This effect is particularly significant for low aspect ratio wings. Therefore the calculation method does include the programs for the evaluation of trajectories of the vortices shed from the side and leading edges and from each cell on the planform. These vortices roll up into the well known leading edge vortices on the delta wing or to the attached side vortex for the low aspect ratio rectangular wing. The resulting non-linear aerodynamic characteristics are computed with good accuracy.

The representation of the vortex sheet by discrete vortices causes problems in the numerical calculations. It was found that the number of divisions has to be limited. In order to allow for a more realistic model the finite core vortex model has been proposed. Some calculations using this model have also been performed.

The results of the method in the evaluation of the aerodynamic characteristics on wing and their wakes are very encouraging. By allowing vortices to be shed from all the cells in the planform the vortex structures that are obtained in these calculations, the secondary vortex separations, are similar to those found in experimental measurements.

The calculations of the pressure distributions for both rectangular and delta wings are generally in good agreement with experimental data. Some differences are due to the local effects of the leading edge shape which affects the results of the experiments. These leading edge shape effects are not accounted for in the present calculation method.

The extremely short distances between the vortices over the low aspect ratio delta wings causes considerable problems. It was found that the present method can be used for the computation of delta wings down to $AR = 1$. Some difficulties appear with the secondary vortex structure, where some of the vortices are "thrown out" of the vortex pattern around the wing. These effects must be further studied.

In conclusion, it seems that the present method is capable in dealing with a large group of wing planforms and present results which are in good

agreement with experimental data. It is planned to extend the computer programs for planforms of general shapes and to include effects of camber and flaps. The method can also be extended to the calculation of several wings in tandem, thus enabling the evaluation of the aerodynamic characteristics of the mutually interactive wings.

REFERENCES

1. Rom, J. and H. Portnoy, The flow near the tips and wake edges of a lifting wing with trailing-edge separation, TAE Report No. 132, July 1971, Department of Aeronautical Engineering, Technion-Israel Inst. of Technology, Haifa, Israel.
2. Rom, J. and Zorea, C., The calculation of the lift distribution and the near vortex wake behind high and low aspect ratio wing in subsonic flow, TAE Report No. 168, December 1972, Department of Aeronautical Engineering, Technion-Israel Inst. of Technology, Haifa, Israel.
3. Rom, J., and Small, D.R. Effects of transverse disturbances on heat transfer in a laminar axisymmetric boundary layer, AIAA Jr. Vol. 11, Nov. 1973, pp. 1503-1508.
4. Rom, J., Portnoy, H. and Zorea, C, Investigation into the formation of wing tip vortices, TAE Report No. 199, February 1974, Department of Aeronautical Engineering, Technion-Israel Inst. of Technology, Haifa, Israel.
5. Rom, J. Zorea, C., and Gordon, R, On the calculation of non-linear aerodynamic characteristics and the near vortex wake, Proceedings of the 9th Congress of ICAS, Paper No. 74-27, August 1974, pp. 214-228.
6. Portnoy, H, Aerodynamic effects of vortex suppressors, TAE Report No. 221, July 1974, Department of Aeronautical Engineering, Technion-Israel Inst. of Technology, Haifa, Israel.
7. Costi, S. and H. Portnoy, Incompressible inviscid symmetrical flow about ellipsoids - comparison of an approximate theory with exact results, TAE Report No. 233, November 1974, Department of Aeronautical Engineering, Technion-Israel Inst. of Technology, Haifa, Israel.

8. Portnoy, H., Calculations of the aerodynamic effects on certain vortex supressing devices, TAE Report No. 235, December 1974, Department of Aeronautical Engineering, Technion-Israel Inst. of Technology, Haifa, Israel.
9. Rom, J, Flows with strong interactions between the viscous and inviscid regions, SIAM Jr. of Applied Mathematics, September 1975, pp. 309-327.
10. Portnoy, H, The initial roll-up of a thick, two-dimensional wake behind a wing of finite span, TAE Report No. 262, November 1975, Department of Aeronautical Engineering, Technion-Israel Inst. of Technology, Haifa, Israel.
11. Falkner, V.M, The calculation of aerodynamic loading surface of any shape. British ARC R & M 1910, 1943.
12. Falkner, V.M, The solution of lifting plane problems by vortex lattice theory, British ARC R & M 2591, 1947.
13. Falkner, V.M, Calculated loadings due to incidence of a number of straight and swept back wings, British ARC R & M 2596, London, 1948.
14. Westwater, F.L., Rolling up of the surface of discontinuity behind an aerofoil of finite span, British ARC R & M 1692, 1935.
15. Hacket, J.F, and Evans, M.R, Vortex wakes behind high lift wings, Journal of Aircraft, Vol. 8, No. 5, pp. 334-340, 1971.
16. Hancock, G.J, and Butter, D.J., A numerical method for calculating the trailing vortex system behind a swept wing at low speed. The Aeronautical Journal, Vol. 75, No. 728, pp. 564-568, 1971.
17. Rehbach, C, Numerical Investigation of vortex sheets issued along a separation line near the leading edge of a wing. EUROMECH 41. Colloquim. Concentrate Vortices. Norwich (G.B.) 18-21 Sept. 1973.

18. Maskew, B, The calculation of potential flow aerodynamics characteristics of combined lifting surfaces with relaxed wakes, Hawker-Siddeley Aviation, Ltd., (Brough) Aerodynamics Design Dept., Note YAD 3192, 1973.
19. Labrujere, Th. E, A numerical method for the determination of the vortex sheet location behind a wing in incompressible flow, NLR TR 72091U, July 1972.
20. Hedman, S.G, Computation of vortex models for wings at high angles of attack in incompressible flow, FFA Tech., Note No. FFA-AU-653, Feb. 1973.
21. Lind, I.A, A nonlinear vortex lattice method applicable to three-dimensional wing systems with rolled up vortex wakes in low subsonic flow, Forces & Moments on some Flat and a high lift wing, KTH Aero Report FI 43, May 1973.
22. Mandril, O.A., Mook, D.T., and Nayfeh, A.H, Non-linear prediction of aerodynamic loads on lifting surfaces. AIAA Preprint 74-503, June 1974.
23. Johnson, F.T. and Rubbert, P.E, Advanced panel type influence coefficient methods applied to subsonic flows, AIAA Preprint 75-50, January 1975.
24. Kaden, H, Aufwönglung eines unstabilen Unstetigkeitsfahsche, Ing. Archiv. Bd. II, Heft 2, May 1931, pp. 140-168.
25. Spreiter, J.R. and Sacks, A.G, The rolling up of the trailing vortex sheet and its effects on the downwash behind wings. J. of the Aero. Sciences, Vol. 18, No. 1, January 1951, pp. 21-32.
26. Brown C, and Michael, W., Jr., On slender wings with leading edge separation, NACA TN 3430, April 1955.
27. Mangler, K.W, and Smith, J.H.B, A theory for slender delta wings with leading edge separation, RAE Tech. Note No. Aero 2442, April 1956.

28. Mangler, K.W, and Smith, J.H.B, Calculation of the flow past slender delta wings with leading edge separation, RAE Report No. Aero 2593, May 1957.
29. Mangler, K.W, and Smith, J.H.B, A theory of slender wings with leading edge separation, Proc. Royal Soc., London, Series A, Vol. 251, 1959, pp. 200-217.
30. Gersten, K, A non-linear lifting surface theory especially for low aspect ratio wings, AIAA J. Vol. 1, No. 4, 1963, pp. 924-925.
31. Polhamus, E.C, A concept of the vortex lift of sharp-edge delta wings based on a leading edge suction analogy, NASA TND-3767, December 1966.
32. Crow, S.C, Stability theory for a pair of trailing vortices, AIAA Paper 71-53, the Aerospace Meeting, New York, January 1970.
33. Kirkeman, K.L, Brown, C.E. and Goodman, A., Evaluation of effectiveness of various devices for attenuation of trailing vortices based on model tests in a large towing basin, NASA CR-2202, December 1973.
34. Maltby R.L, A visualization technique for flows separating from highly swept edges, J.A.S. 1958.
35. Bollay, W, A contribution to the theory of planing surfaces, J.A. Sci. 4, 1937, p.294-296.
36. Gersten, K, A non linear lifting surface theory specially for low aspect ratio wings, AIAA Journal, Vol. 1, No. 4, 1963, pp. 924-925.
37. Chigier, N.A, and Corsiglia, V.R, Wind tunnel studies of wing wake turbulence. AIAA, 10th Aerospace Sciences Meeting, San Diego, Calif. January 17-19, 1972, Paper 72-41.

38. Chigier, N.A, and Corsiglia, V.R, Tip vortices-velocity distributions
NASA TMX 62.087, September 1971.
39. Garner, H.C, and Lehrian, D.E, Non-linear theory of steady forces on
wings with leading edge flow separation, R & M 3375, 1964.
40. Scholtz, N, Kraft-und Druckverteilungsmessungen an Tragflächen kleiner
streckung, Forschung Ing. Wes. 16 Bd. Heft 3, 1945-1950, pp.85-91.
41. Quick, A.W, Möglichkeiten der Luft-und Raumfahrtforschung in der
Bundesrepublik Deutschland, Zeitschrift für Flugwissenschaften, 10,
1961, pp. 307-333.
42. Wickens, R.H, The vortex wake and aerodynamic load distribution of
slender rectangular wings. Canadian Aeronautics & Space Journal, Vol.
13, 1967, pp. 247-260.
43. Bartlett, G.E, and Vidal, R.J, Experimental investigation of influence
of edge shape on the aerodynamic characteristics of low aspect ratio wings
at low speeds. J.A.S. Vol. 22, No. 8, August 1955, pp. 517-533.
44. Tosti, L.P, Low speed static stability and damping in roll characteristics
of some swept and unswept low aspect ratio wings, NACA TN 1468, 1947.
45. Peckhman, D.H, Low speed wind tunnel tests on a series of uncambered
slender pointed wings with sharp edges. R & M No. 3186, Brit. A.R.C.1961.
46. Sacks, A.H, A theoretical investigation of the aerodynamics of slender
wing body combinations exhibiting leading edge separation. NASA CR-719,
March 1967.
47. Marsden, D.J, Simpson, R.W, and Rainbird, W.J, An investigation into the
flow over delta wings at low speeds with leading edge separation. The
College of Aeronautics, Cranfield, Rep. N. 114, February 1958.

48. Wentz, W.H, and Kohlman, D.L, Vortex breakdown on slender sharp-edged wings. AIAA Aircraft Design and Operation Meeting, Los Angeles, California, AIAA Paper No. 69-778, July 1969.

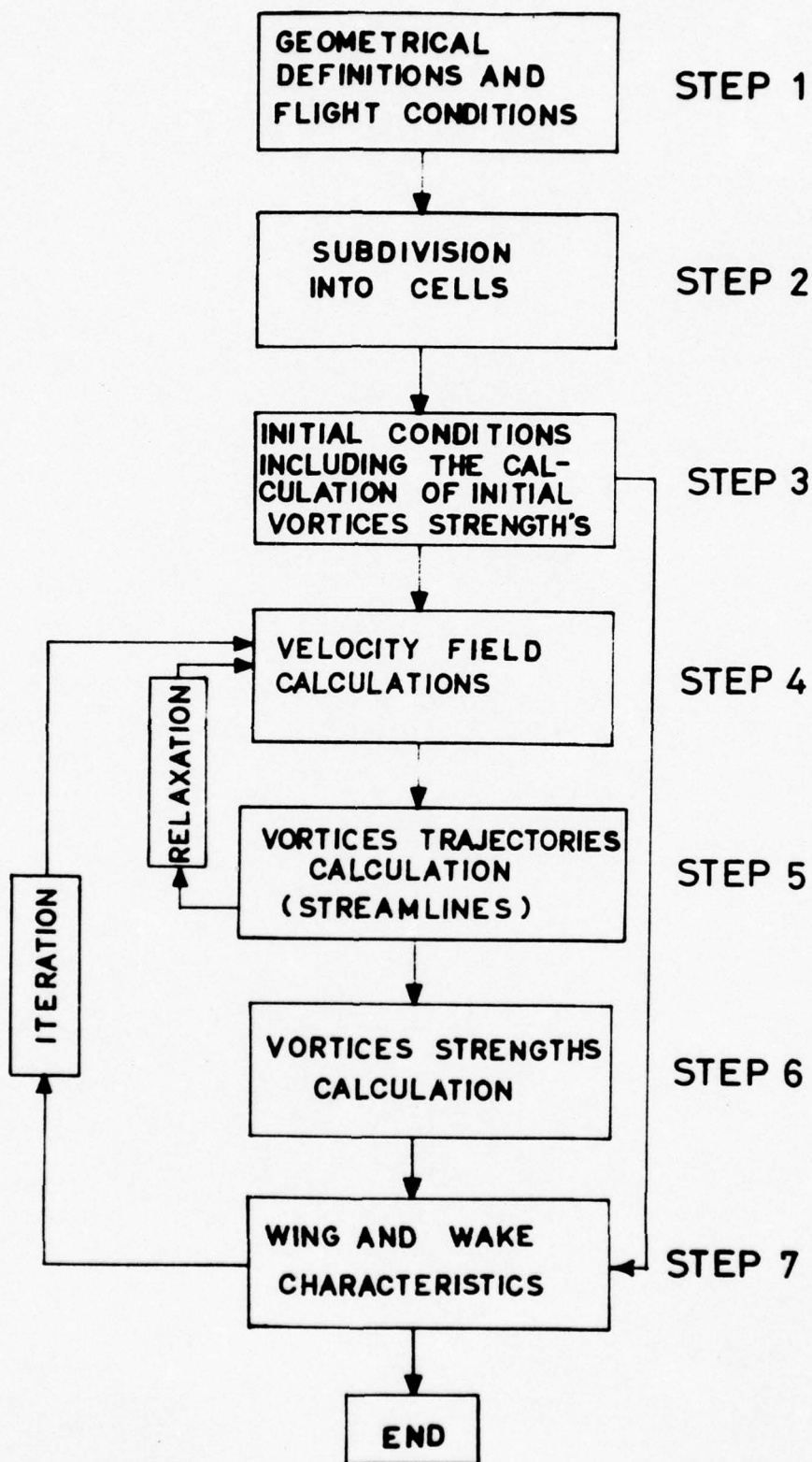


FIG. 1 -FLOW CHART OF CALCULATION METHOD.

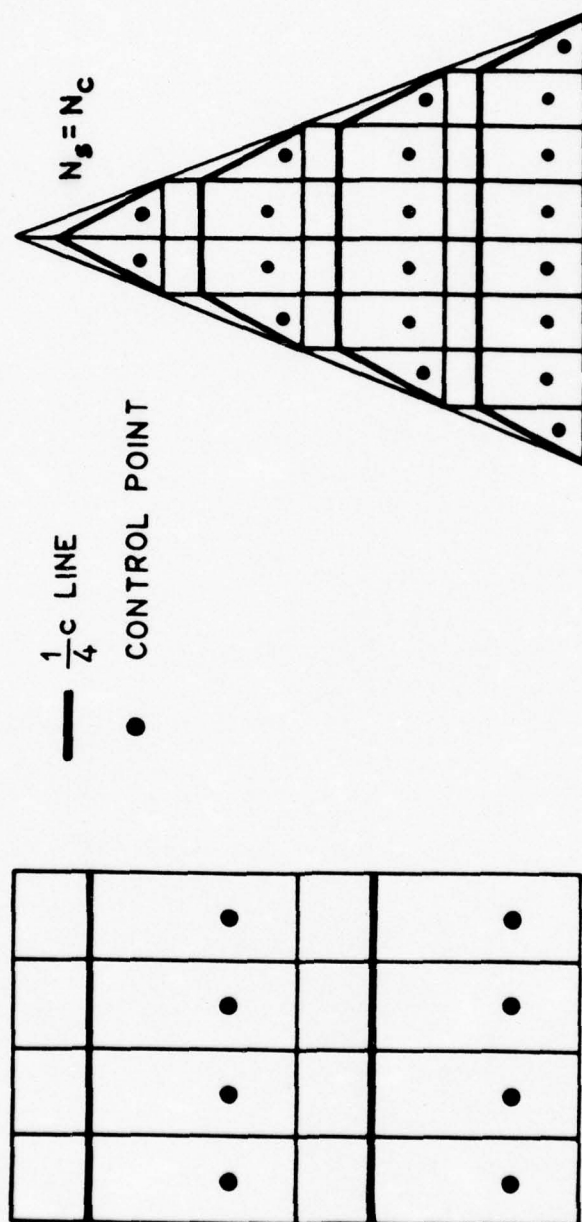


FIG. 2 -THE CELL ARRANGEMENTS AND THE ASSOCIATED VORTICES AND CONTROL POINTS FOR RECTANGULAR AND DELTA WINGS.

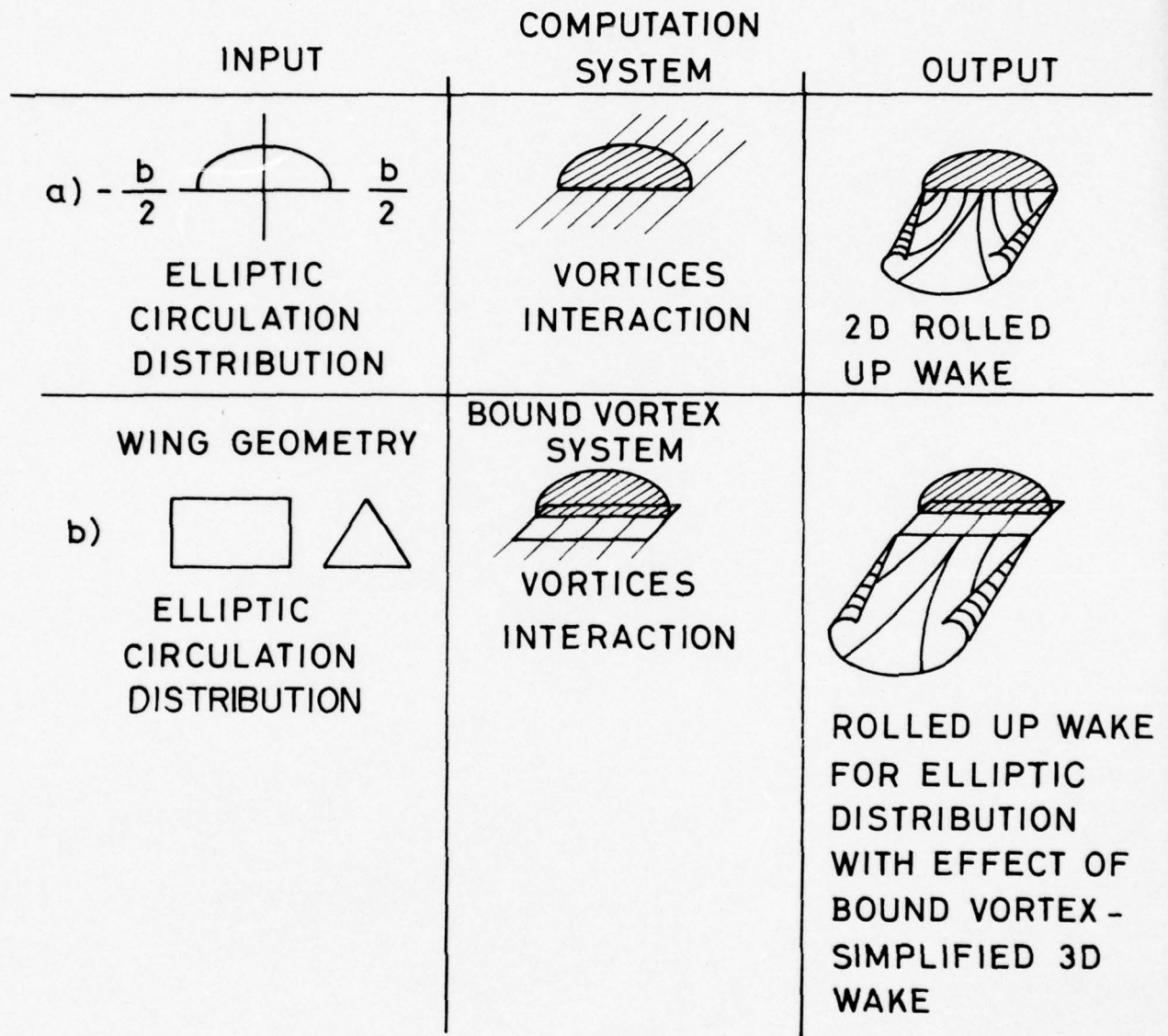


FIGURE 3 - VORTEX WAKE CALCULATIONS FOR ELLIPTIC LIFT DISTRIBUTION .

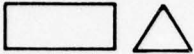




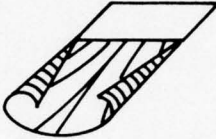
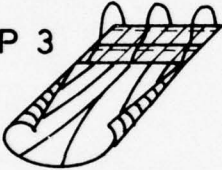

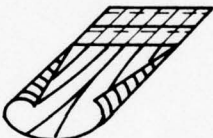
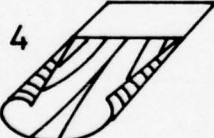
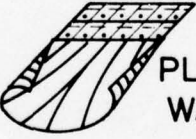

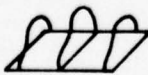

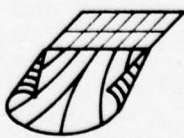
INPUT	COMPUTATION SYSTEM	OUTPUT
STEP 1  WING GEOMETRY	 PLANAR WAKE	 CIRCULATION DISTRIBUTION
STEP 2  CIRCULATION DISTRIBUTION ON T.E.	 2D VORTICES INTERACTION	 VLM - 2D ROLLED UP WAKE
STEP 3  CIRCULATION AND 2D ROLLED UP WAKE	 VORTICES INTERACTION	 VLM - 3D ROLLED UP WAKE
STEP 4  3D ROLLED UP WAKE	 NON PLANAR WAKE MODIFIED VLM CALCULATION	 "LINEAR" CIRCULATION MODIFIED BY ROLLED- UP VORTEX WAKE
STEP 5  NEW "LINEAR" CIRCULATION DISTRIBUTION	 3D ROLLED UP WAKE NEW 3D VORTICES INTERACTION	 MVLM 3D ROLLED UP WAKE

FIGURE 4 - VLM VORTEX WAKE CALCULATIONS.

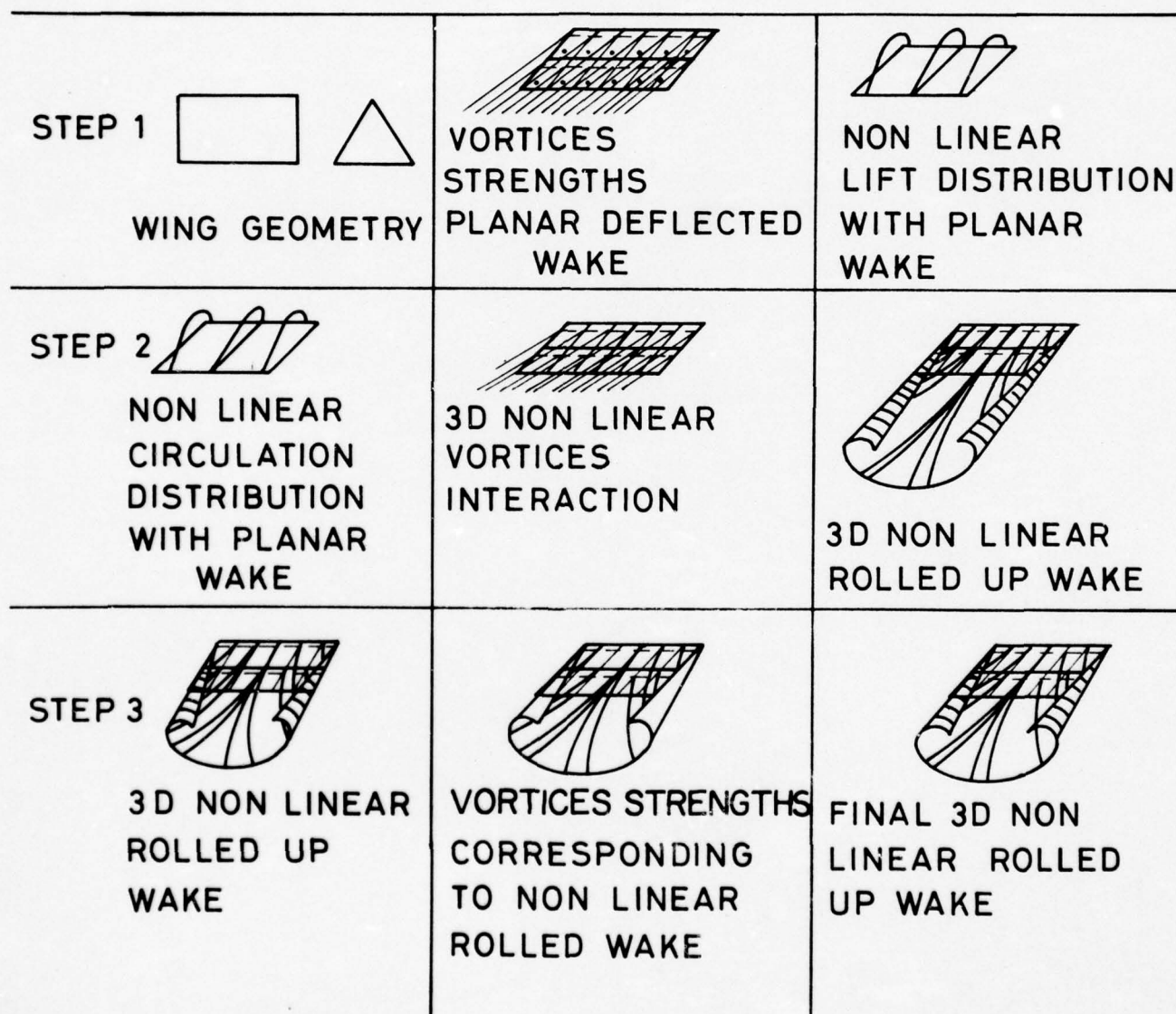


FIGURE 5 - NONLINEAR VORTEX WAKE CALCULATIONS

- 48 -
COMPUTATION
SYSTEM



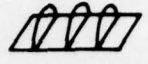
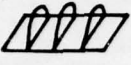
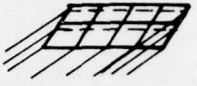
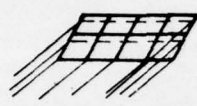
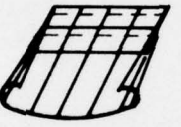
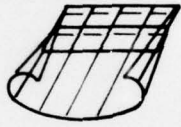
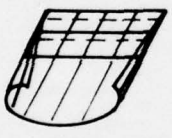
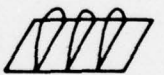
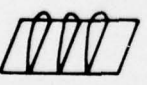
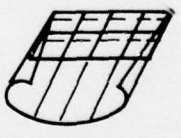
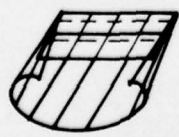
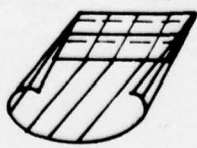
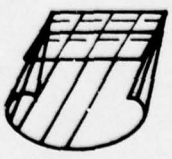
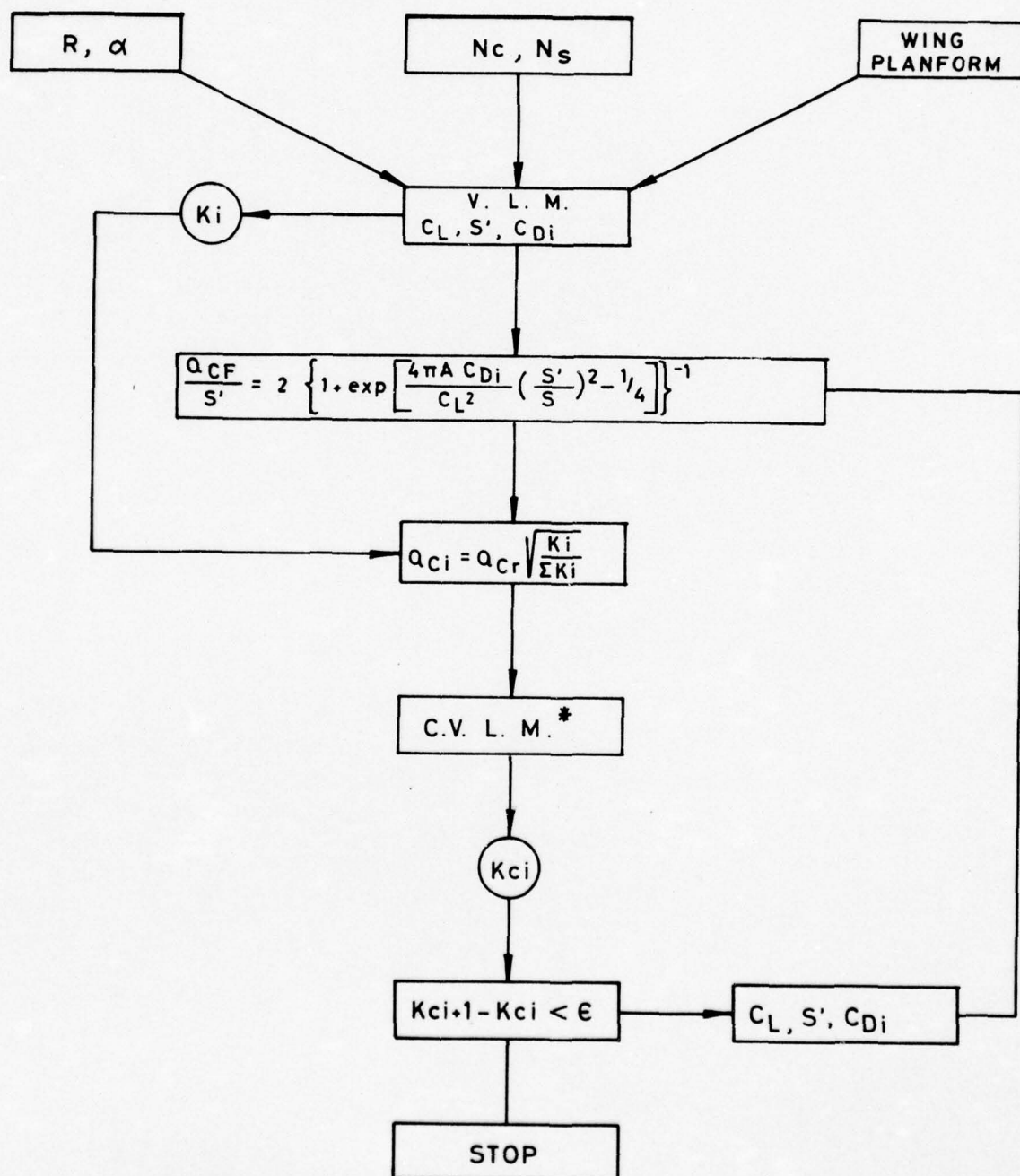
	INPUT	COMPUTATION SYSTEM	OUTPUT
STEP 1	 WING GEOMETRY	 COMPUTE VORTICES STRENGTHS EDGE VORTICES SEPARATION PLANAR WAKE	 NON LINEAR CIRCULATION DISTRIBUTION WITH PLANAR WAKE AND EDGE SEPARATION
STEP 2	 NON LINEAR CIRCULATION DISTRIBUTION	<div style="border: 1px solid black; padding: 5px; text-align: center;"> FLOW CHART (FIG. 7) </div> VORTEX CORES CALCULATION	 PLANAR DEFLECTED WAKE WITH VORTEX CORES
STEP 3	 PLANAR DEFLECTED WAKE WITH VORTEX CORES	 3D NON LINEAR VORTICES INTERACTION	 ROLLED-UP NON LINEAR WAKE
STEP 4	 ROLLED-UP NON LINEAR WAKE	$[\alpha] = [H][K]$ NEW VORTICES STRENGTHS CALCULATION	 NEW NON LINEAR CIRCULATION
STEP 5	 NEW NON LINEAR CIRCULATION	<div style="border: 1px solid black; padding: 5px; text-align: center;"> FLOW CHART (FIG. 7) </div> NEW VORTEX CORES CALCULATION	 ROLLED-UP NON LINEAR WAKE WITH NEW VORTEX CORES
STEP 6 ITERATIVE PROCEDURE STEPS 4,5,6)	 ROLLED-UP NON LINEAR WAKE WITH NEW VORTEX CORES	 VORTICES INTERACTION	 ROLLED-UP NON LINEAR WAKE

FIGURE 6 - NONLINEAR FINITE CORE ROLLED UP WAKE CALCULATIONS.



* CORRECTED V.L.M. METHOD.

FIGURE 7 - SCHEMATIC DIAGRAM FOR THE CALCULATION OF CORES DIAMETERS.

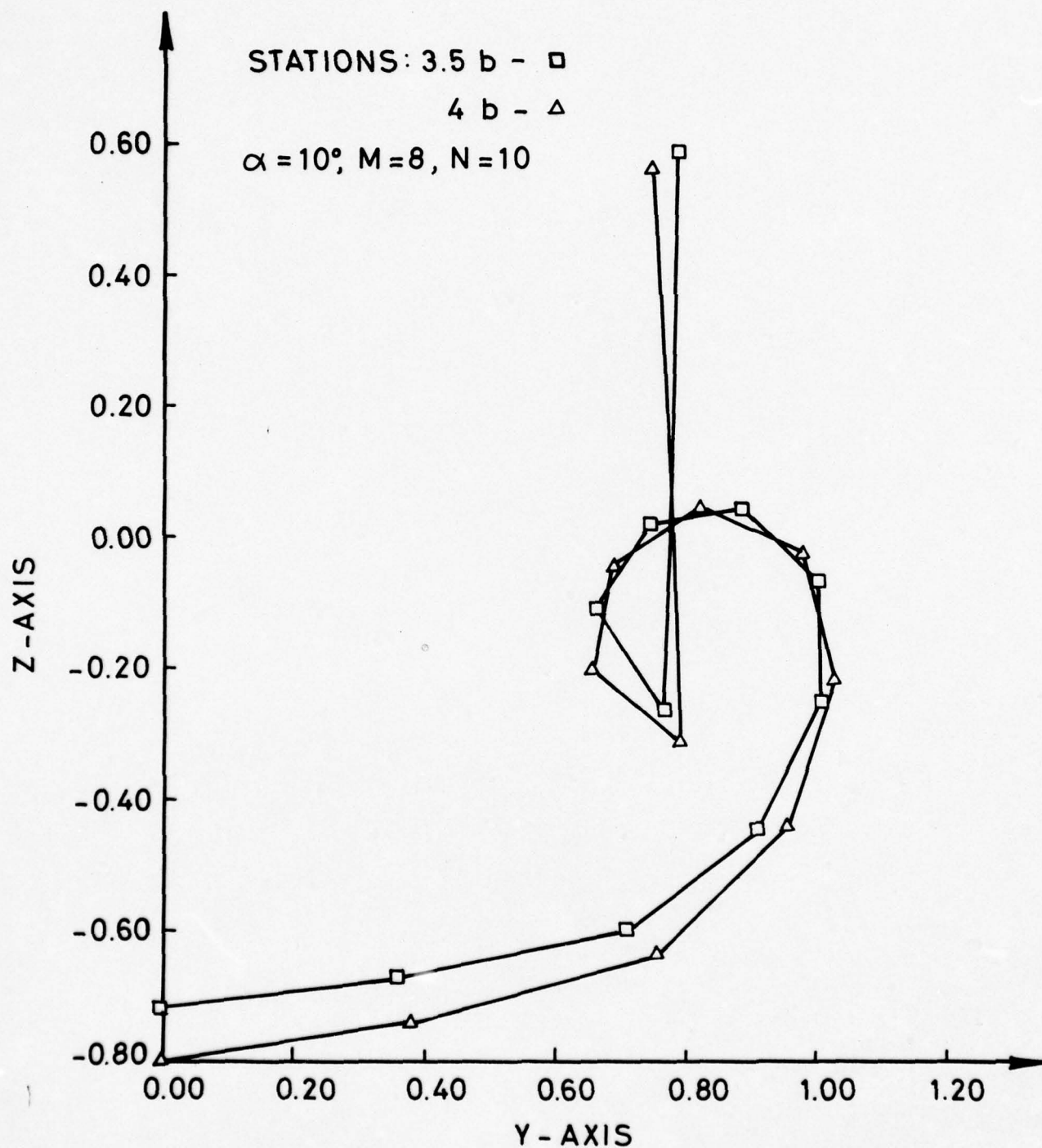


FIGURE 8 - PROBLEMS IN THE CALCULATIONS OF THE VORTEX SHEET ROLL-UP-"ESCAPE" OF THE "TIP" VORTEX.

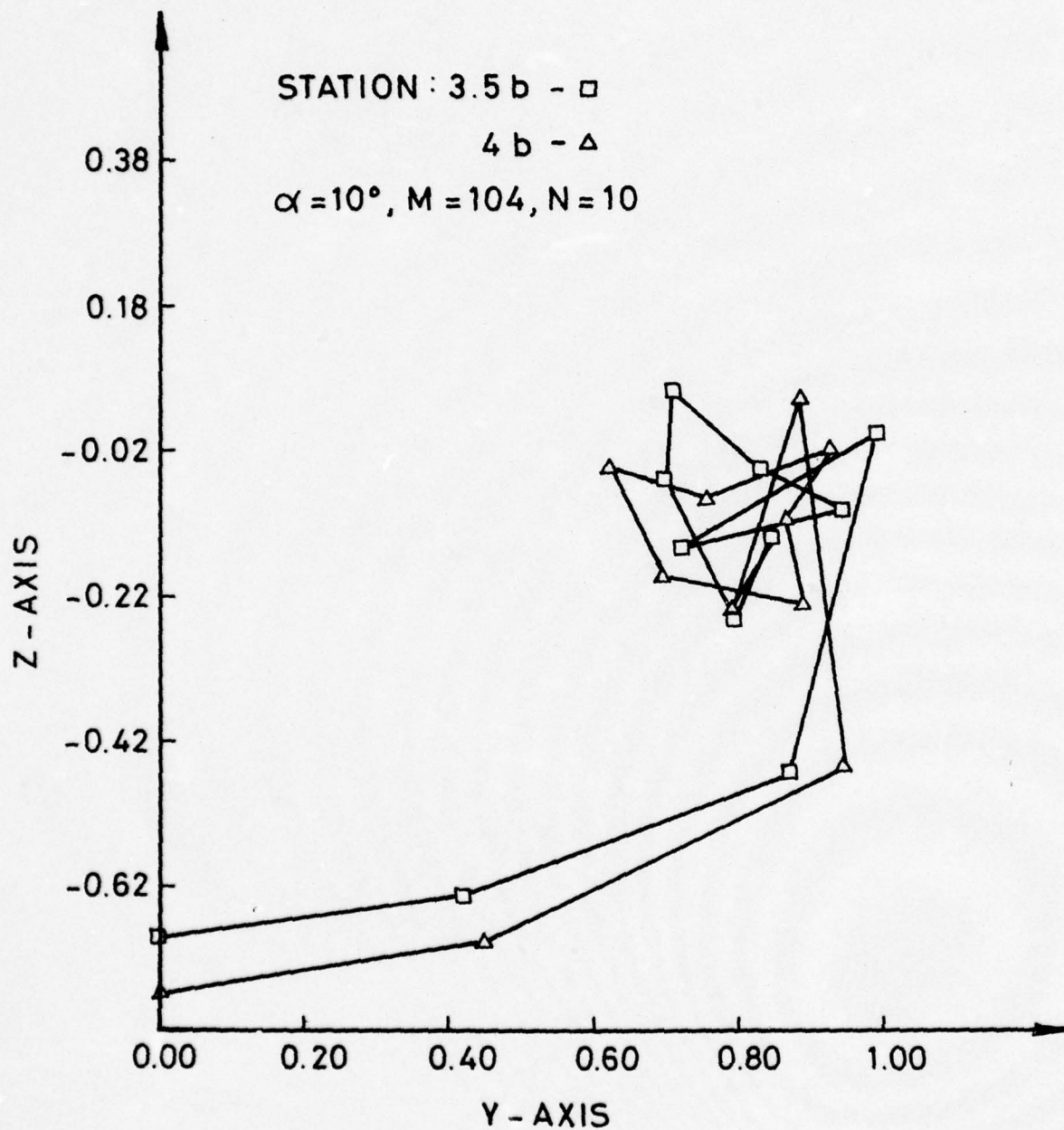


FIGURE 9 - PROBLEMS IN THE CALCULATIONS OF THE VORTEX SHEET ROLL-UP-CROSS-OVER OF VORTEX LINES.

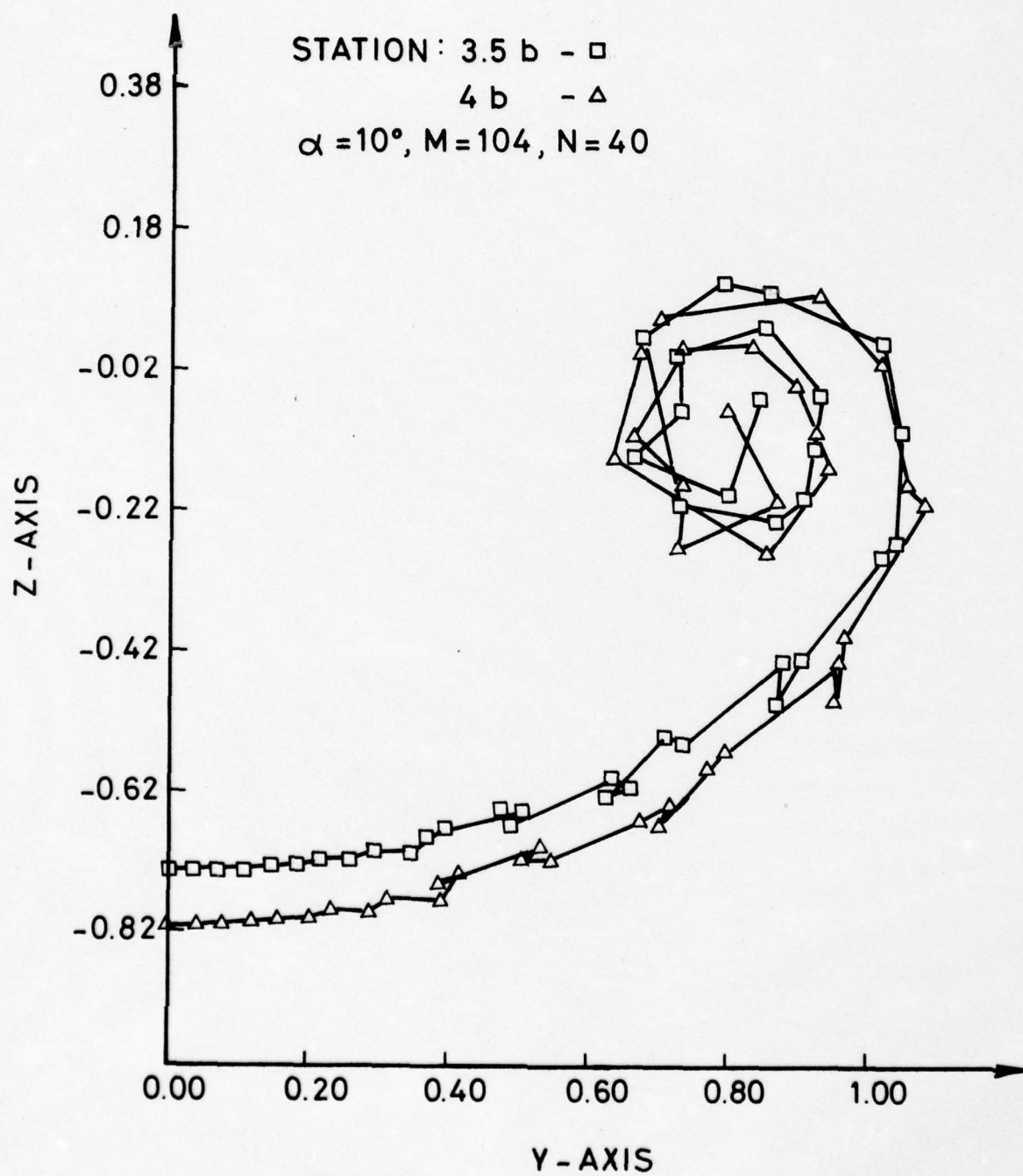


FIGURE 10 - PROBLEMS IN THE CALCULATIONS OF THE VORTEX SHEET ROLL-UP-TOO MANY SUBDIVISIONS.

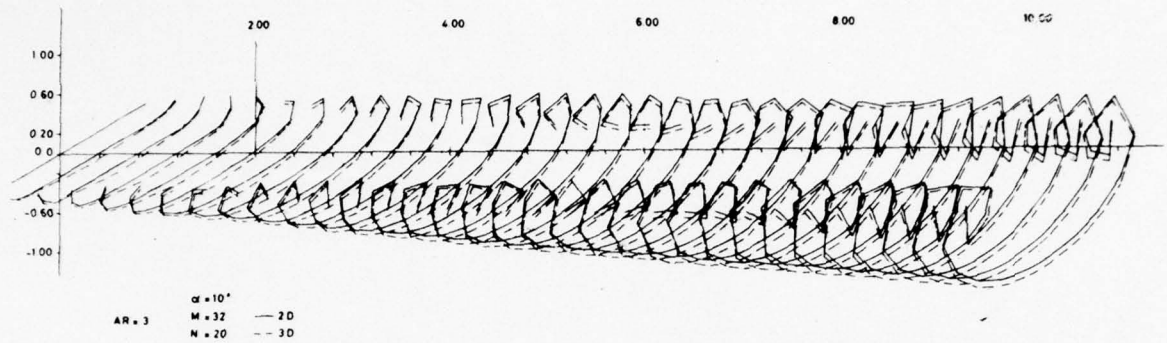


FIGURE 11 - TWO AND THREE DIMENSIONAL ROLLED UP WAKE SHAPES CALCULATED BY ELLIPTIC LIFT DISTRIBUTION PROCEDURE. (AXES ARE GIVEN BY HALF SPAN UNITS).

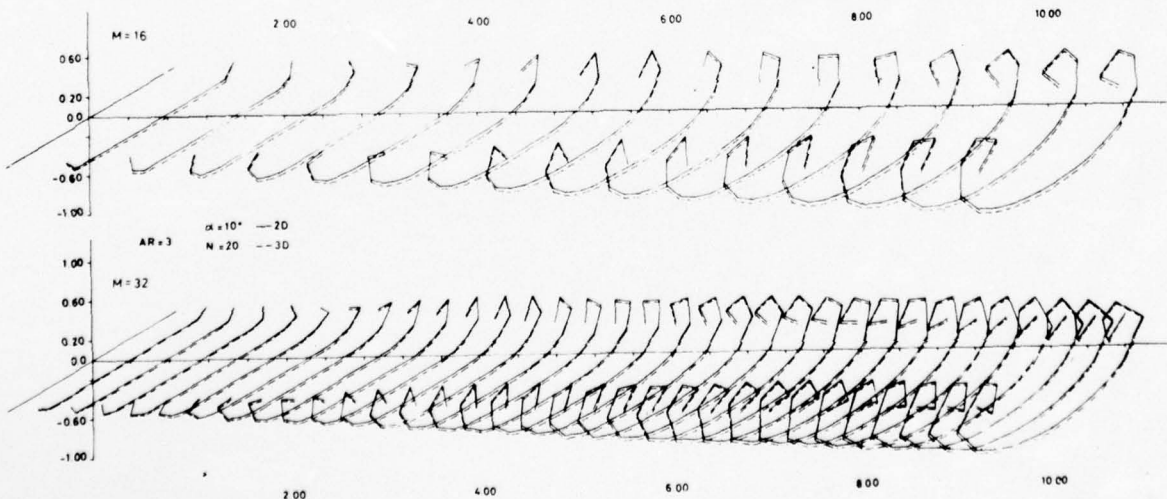


FIGURE 12 - THE ROLLED-UP WAKE SHAPES CALCULATED BY THE VLM PROCEDURE WITH STEP SIZES $M = 16$ and $M = 32$.

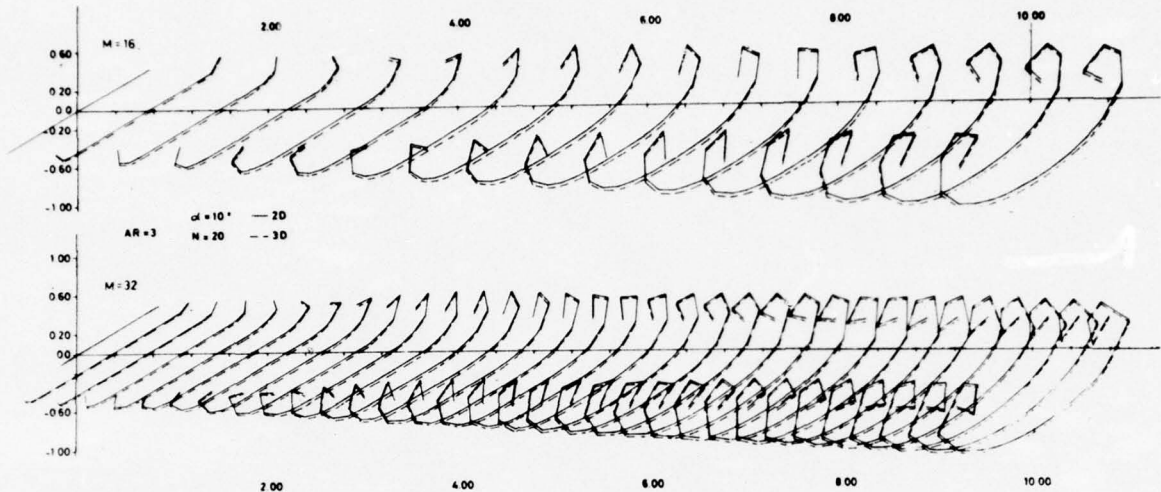


FIGURE 13 - THE ROLLED-UP WAKE SHAPES CALCULATED BY THE MVLM PROCEDURE WITH STEP SIZE $M = 16$ AND $M = 32$.

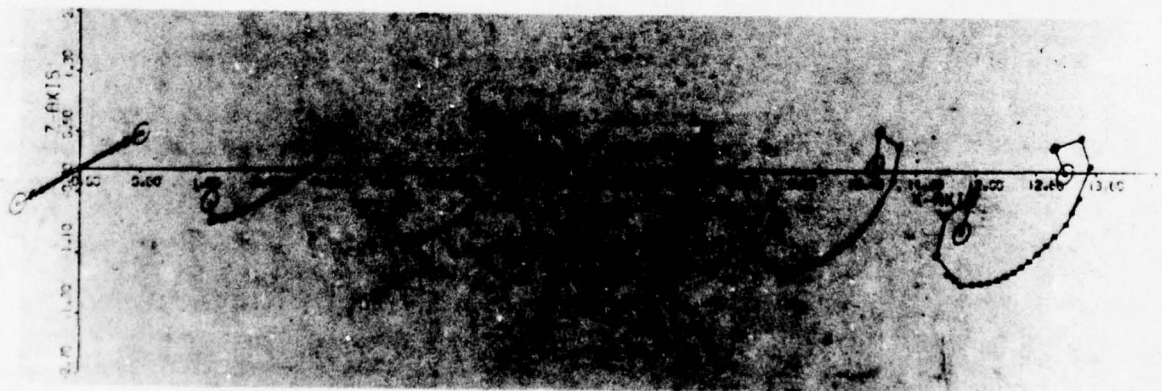


FIGURE 14 - THE ROLLED UP WAKE SHAPE CALCULATED BY THE VLM PROCEDURE WITH FINITE CORE VORTICES. RECTANGULAR WING OF $AR = 1$ at $\alpha = 10^\circ$ and $N = 41$, $M = 32$.

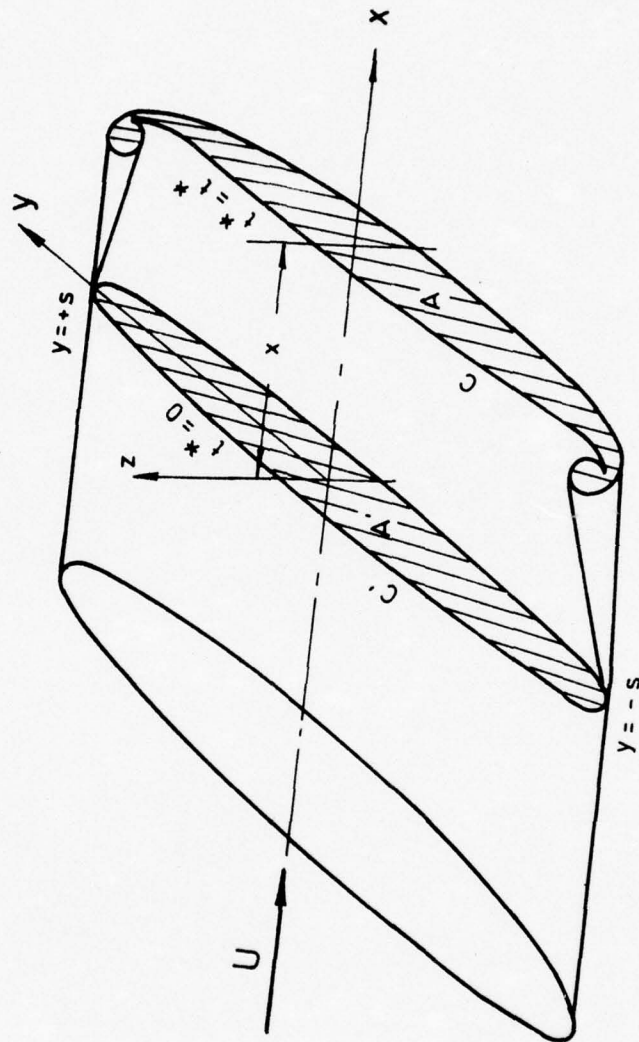


FIG.15 WAKE CROSS - SECTIONS & SYSTEM OF AXES.

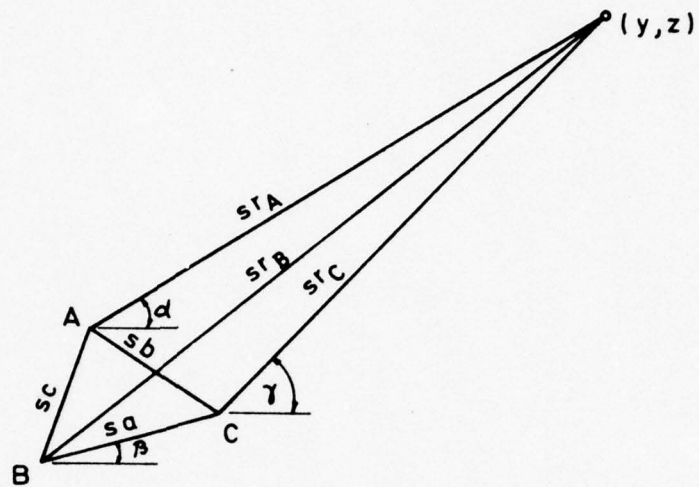


FIG.16 NOTATION FOR A TRIANGULAR ELEMENT & A FIELD POINT

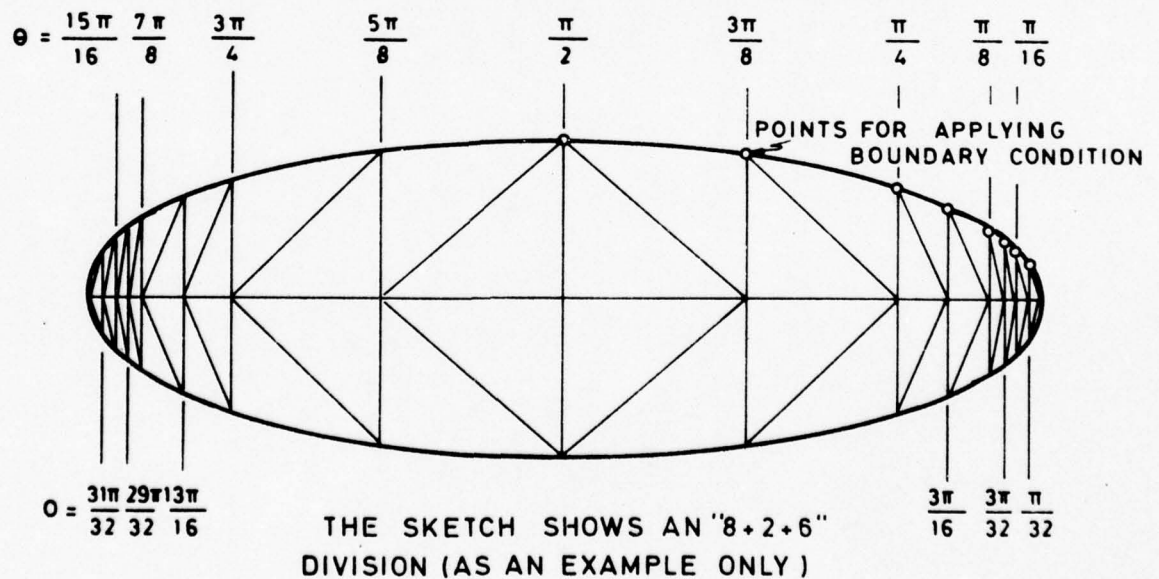


FIG.17 LAYOUT OF ELEMENTS IN AN ELLIPTIC WAKE

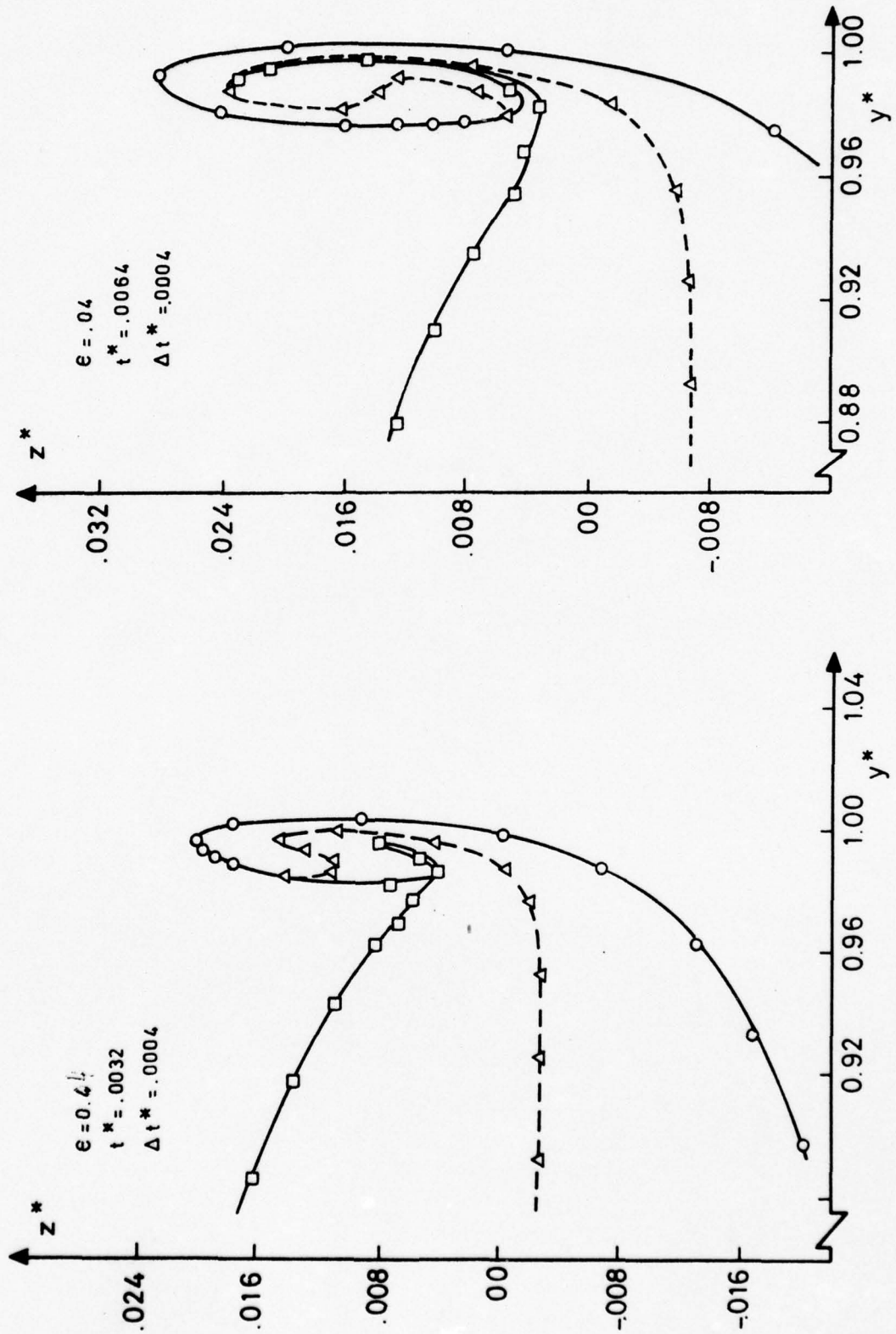


FIGURE 18 - THE INITIAL ROLL UP AT THE TIP OF A 4% THICK ELLIPTIC WAKE.

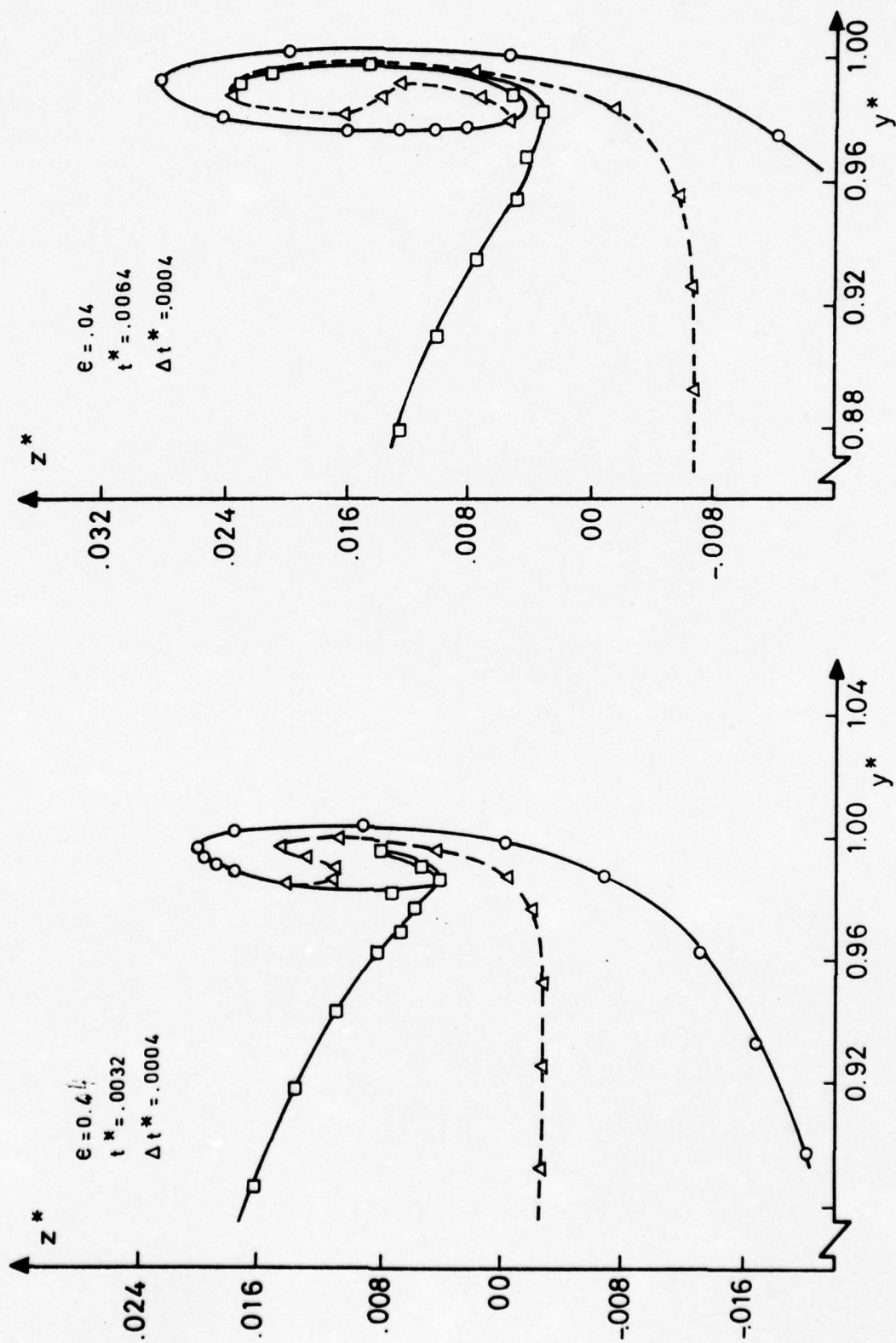


FIGURE 18 - THE INITIAL ROLL UP AT THE TIP OF A 4% THICK ELLIPTIC WAKE.

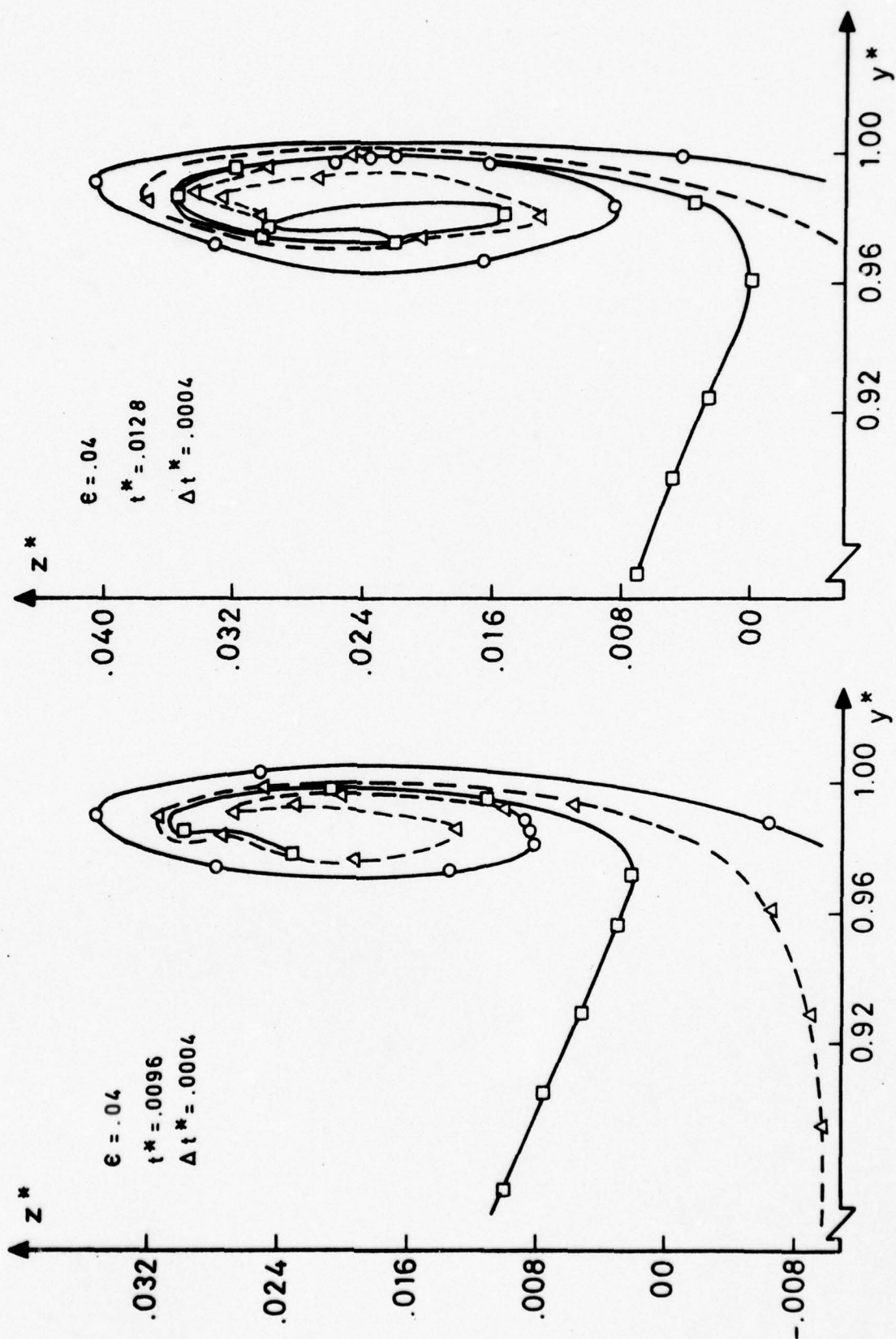


FIG.18 CONT.

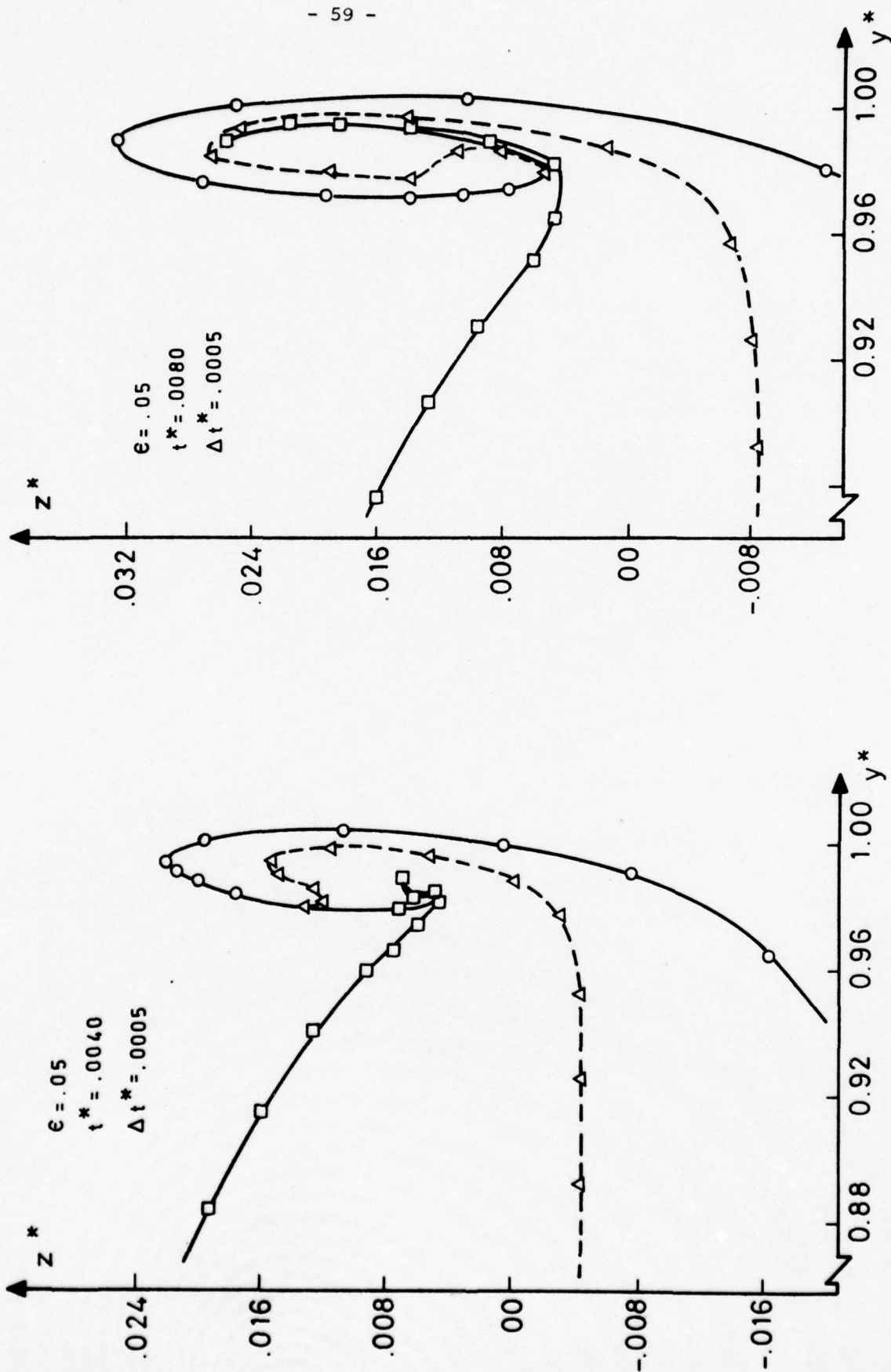


FIGURE 19 - THE INITIAL ROLL UP AT THE TIP OF A 5% THICK ELLIPTIC WAKE.

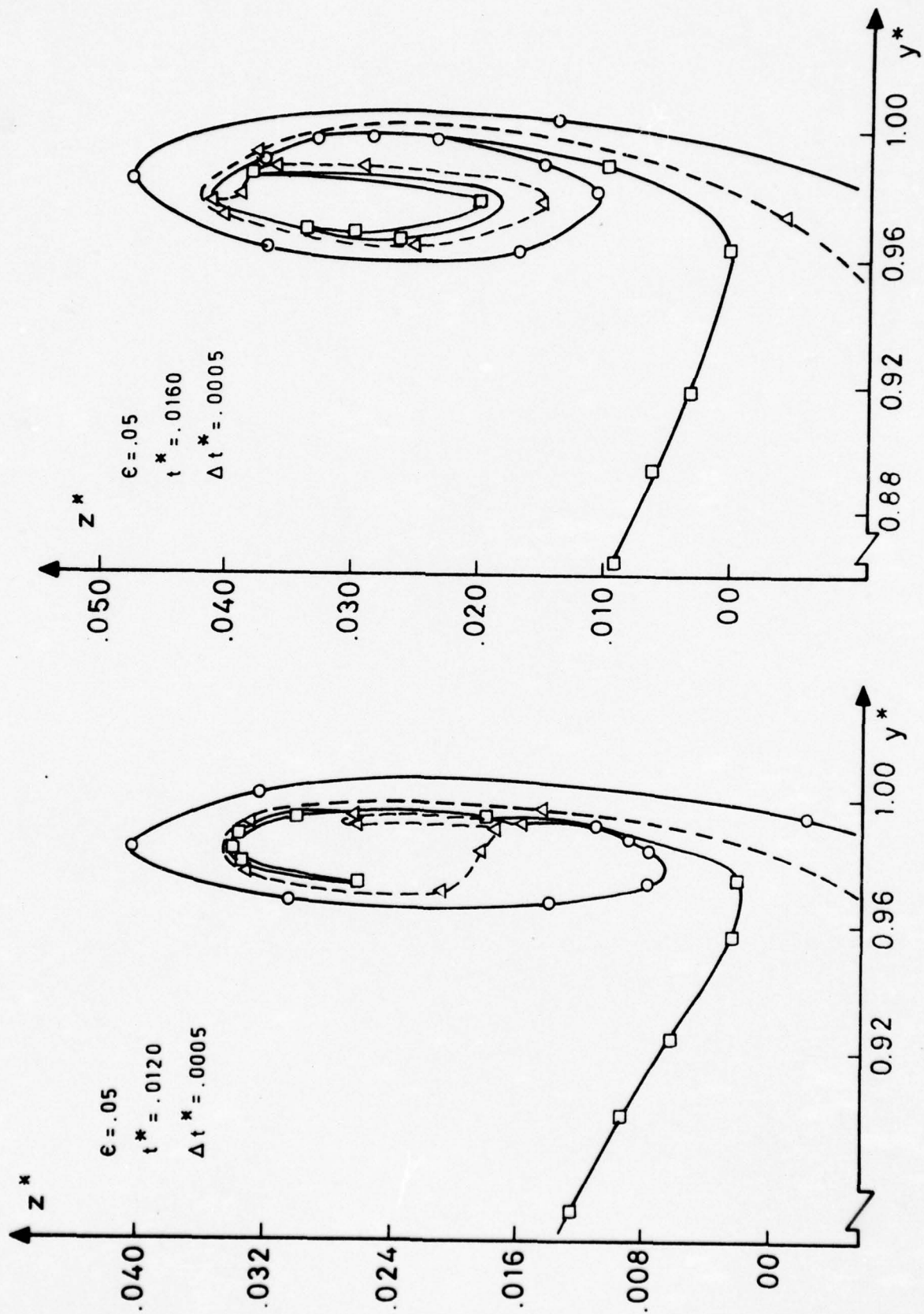


FIG.19 CONT.

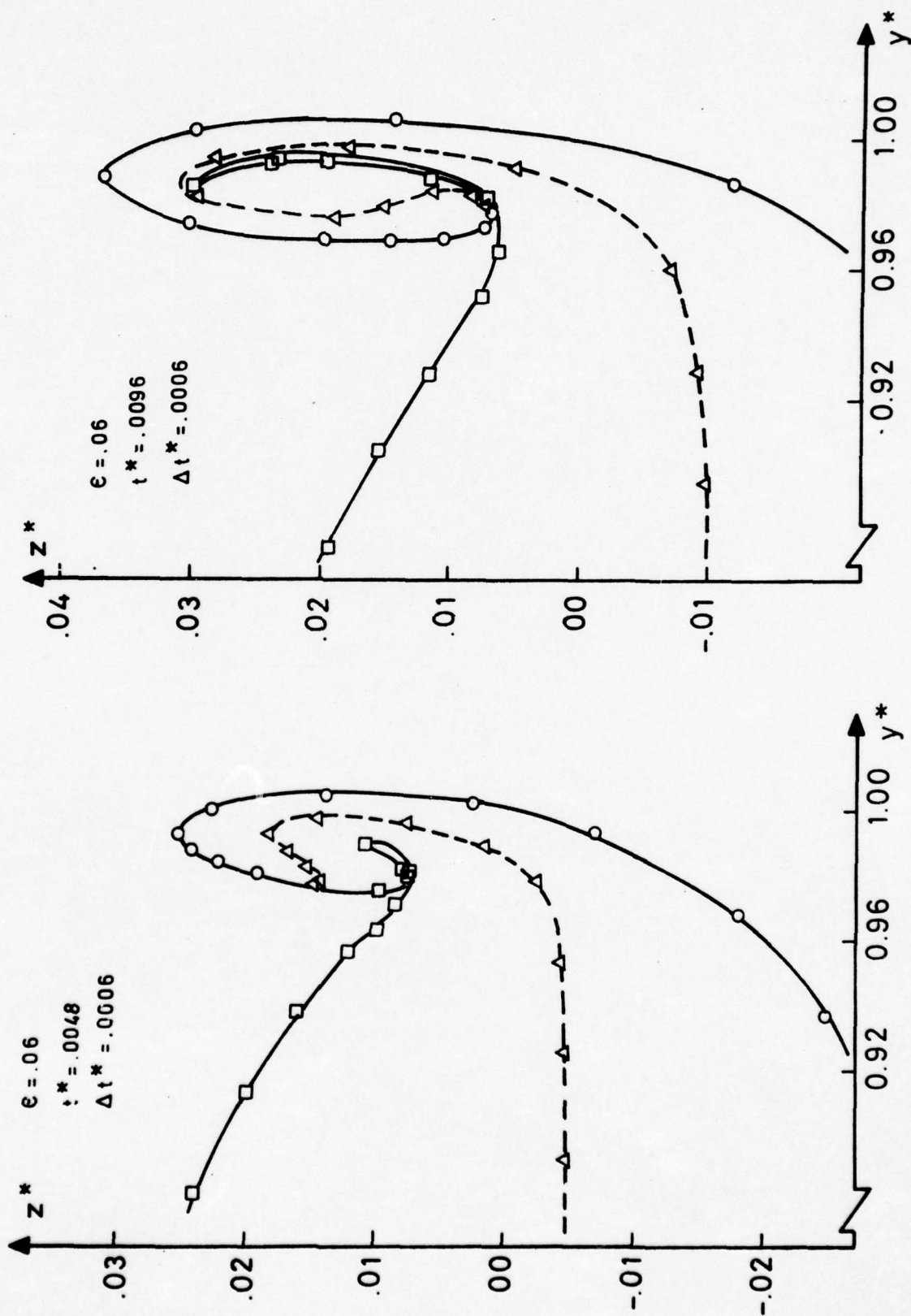


FIGURE 20 - THE INITIAL ROLL UP AT THE TIP OF A 6% THICK ELLIPTIC WAKE.

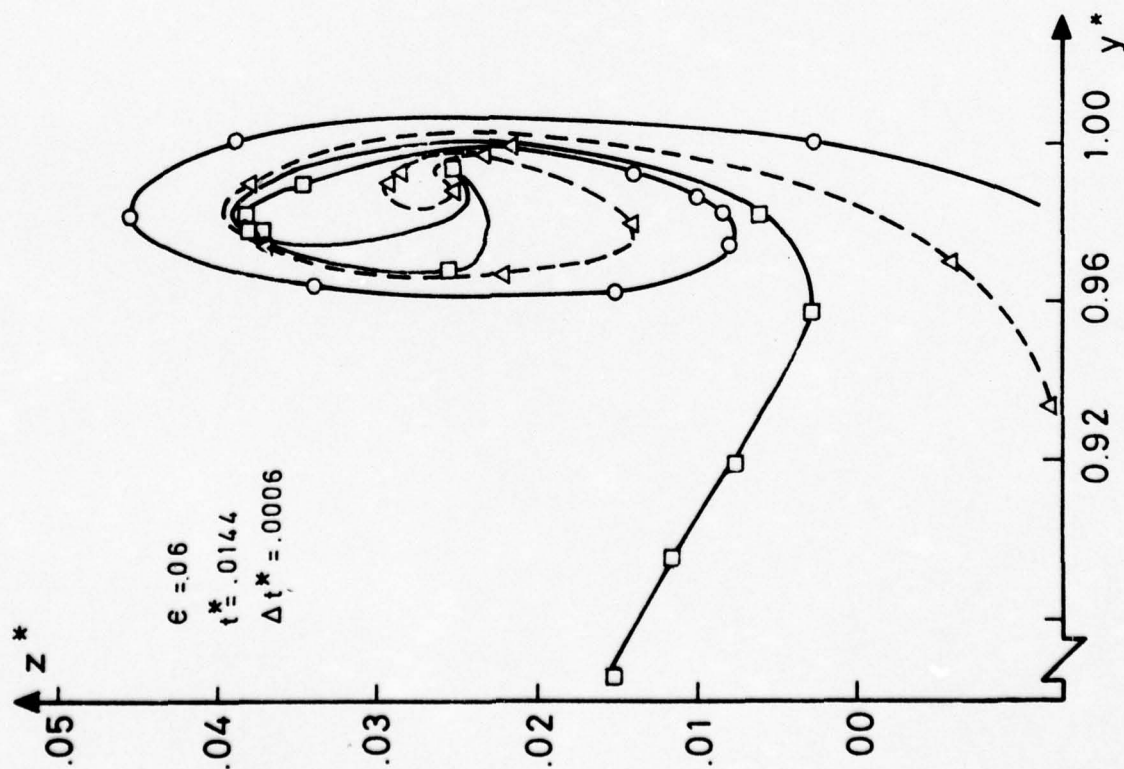
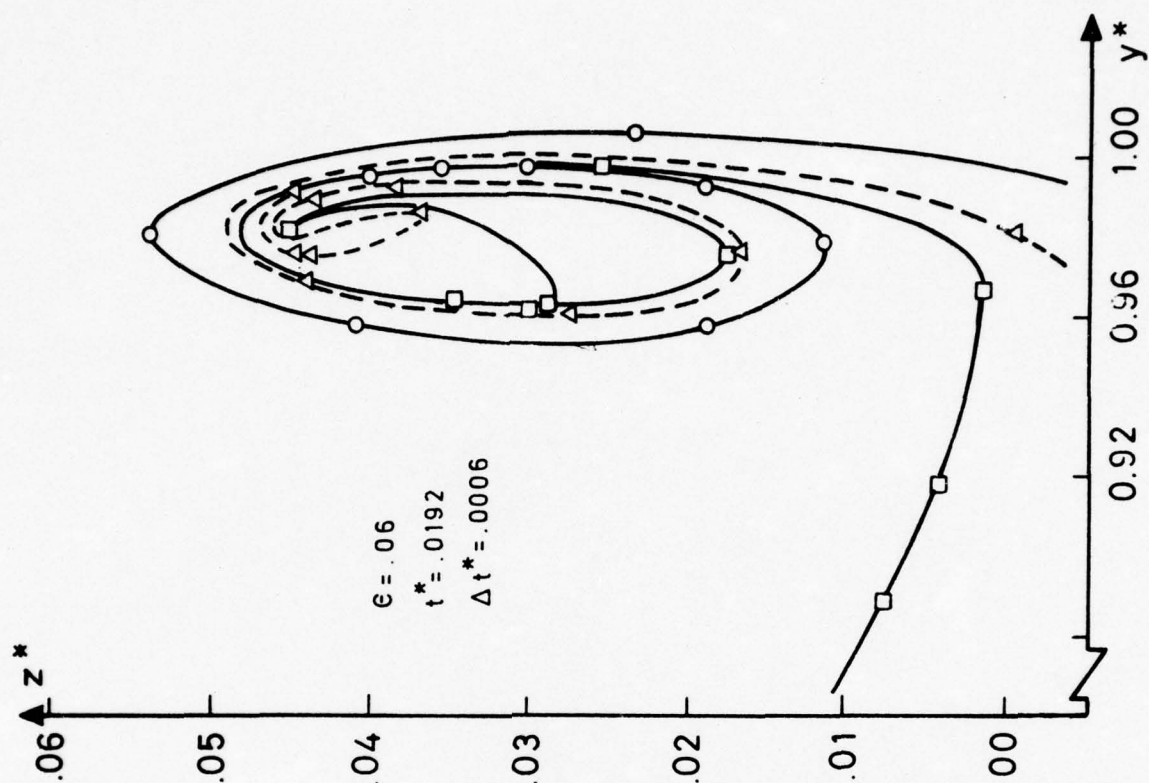


FIG.20 CONT.

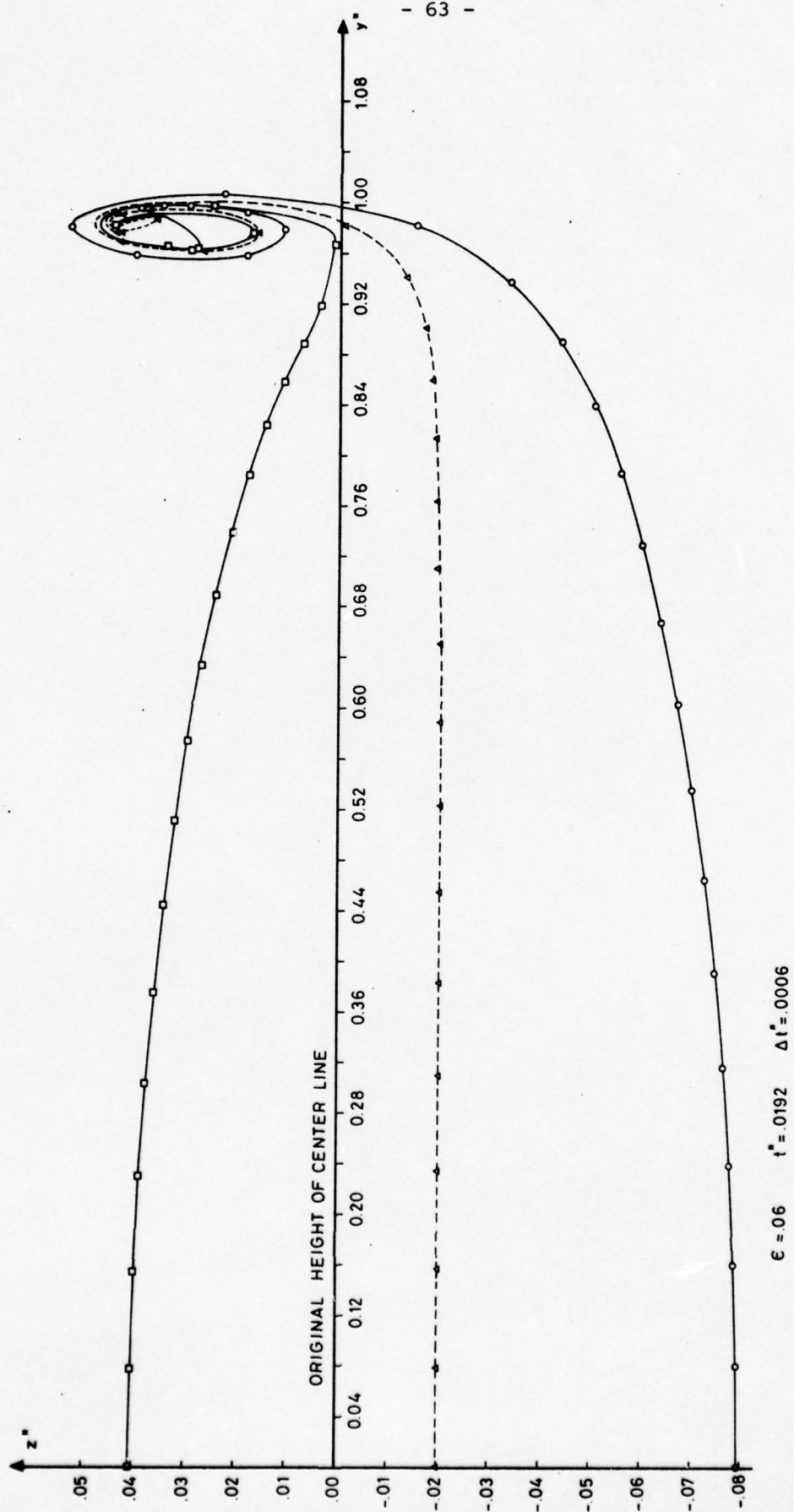


FIG.21 EXAMPLE OF A COMPLETE HALF WAKE

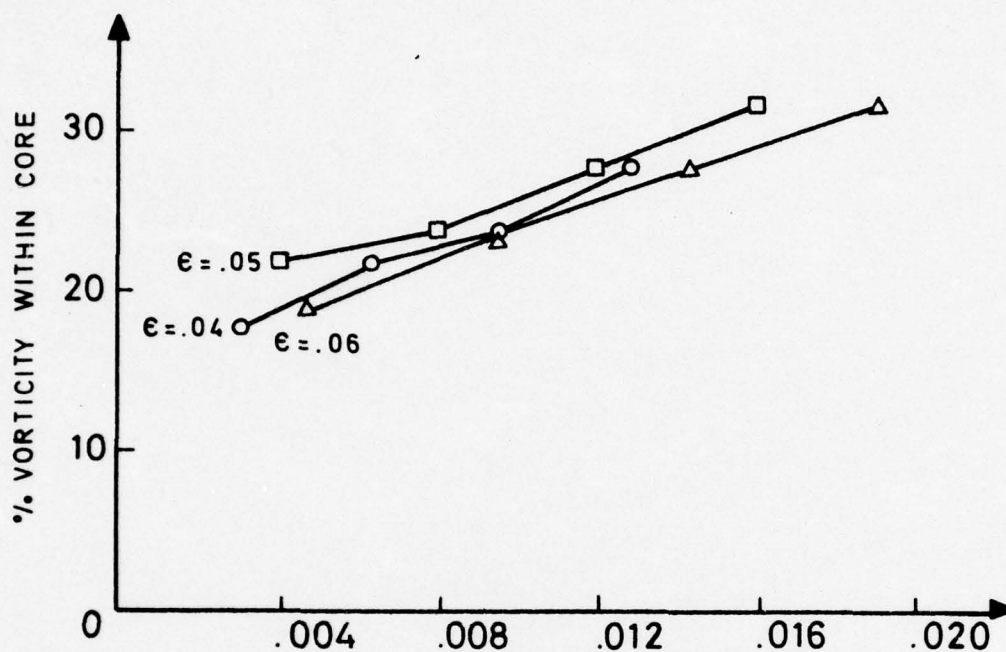


FIGURE 22 - VORTICITY WITHIN CORE AS A FUNCTION OF t^*

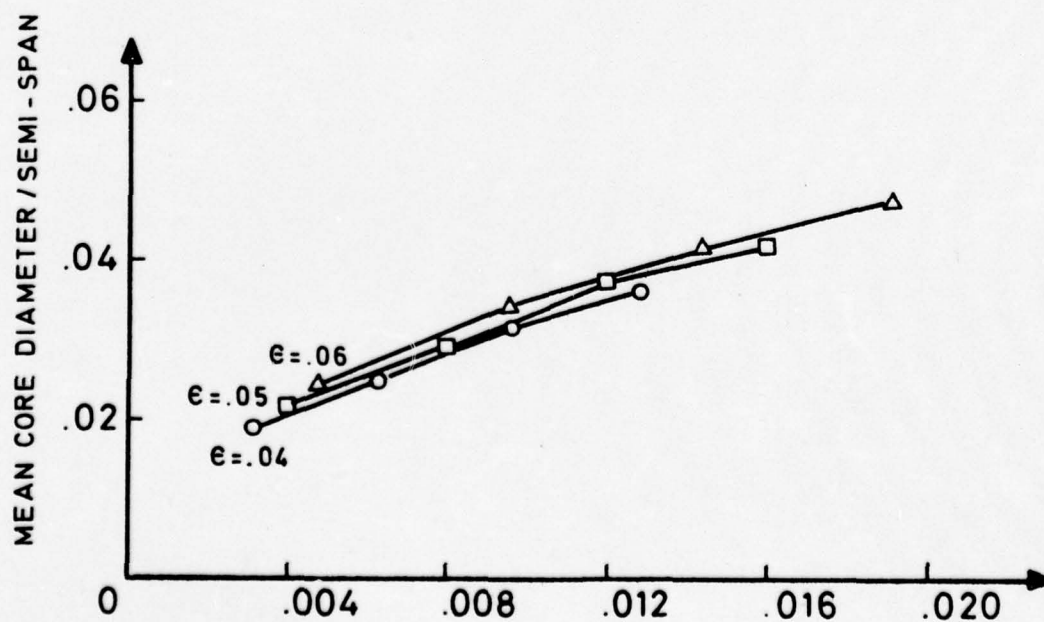


FIGURE 23 - MEAN CORE DIAMETER AS A FUNCTION OF t^*

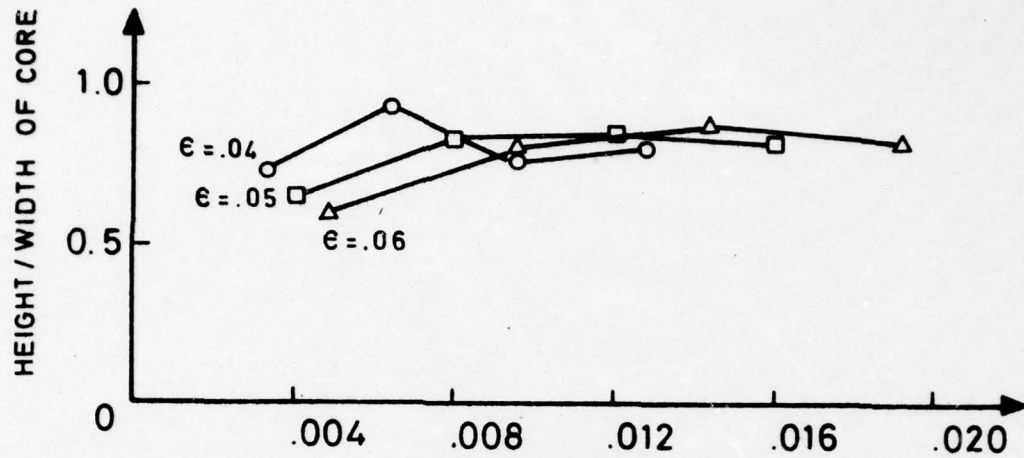


FIGURE 24 - THE HEIGHT TO WIDTH RATIO OF THE CORE AS A FUNCTION OF t^*

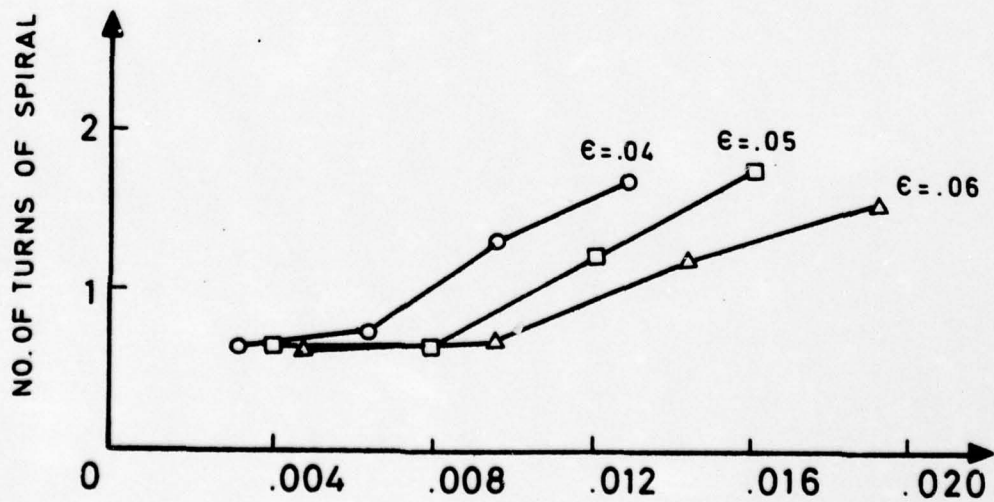


FIGURE 25 - NUMBER OF TURNS OF THE TIP SPIRAL AS A FUNCTION OF t^* .

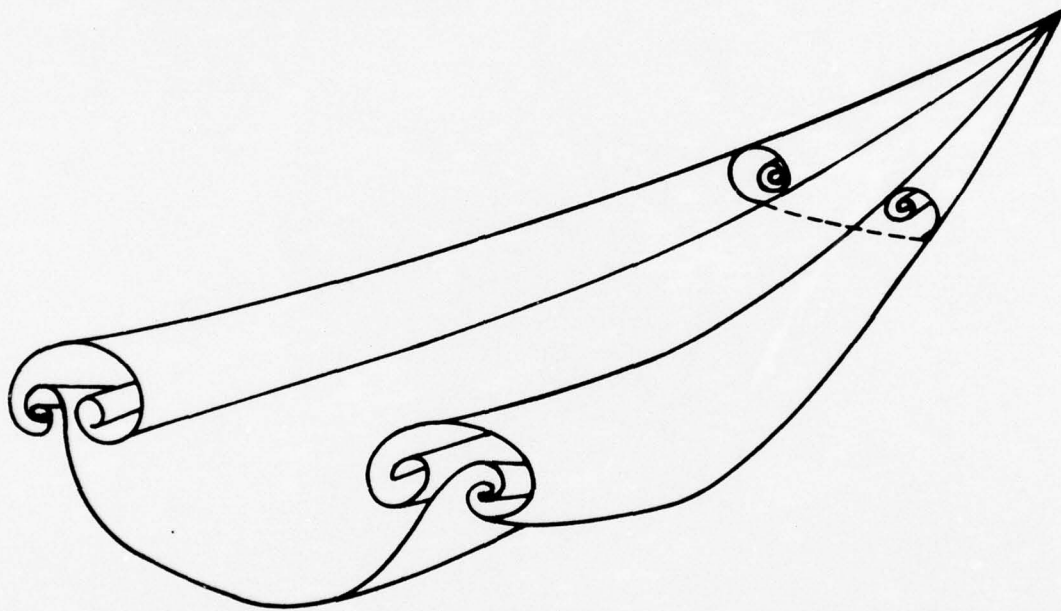


FIG. 26 - MALTBY'S MODEL [34].

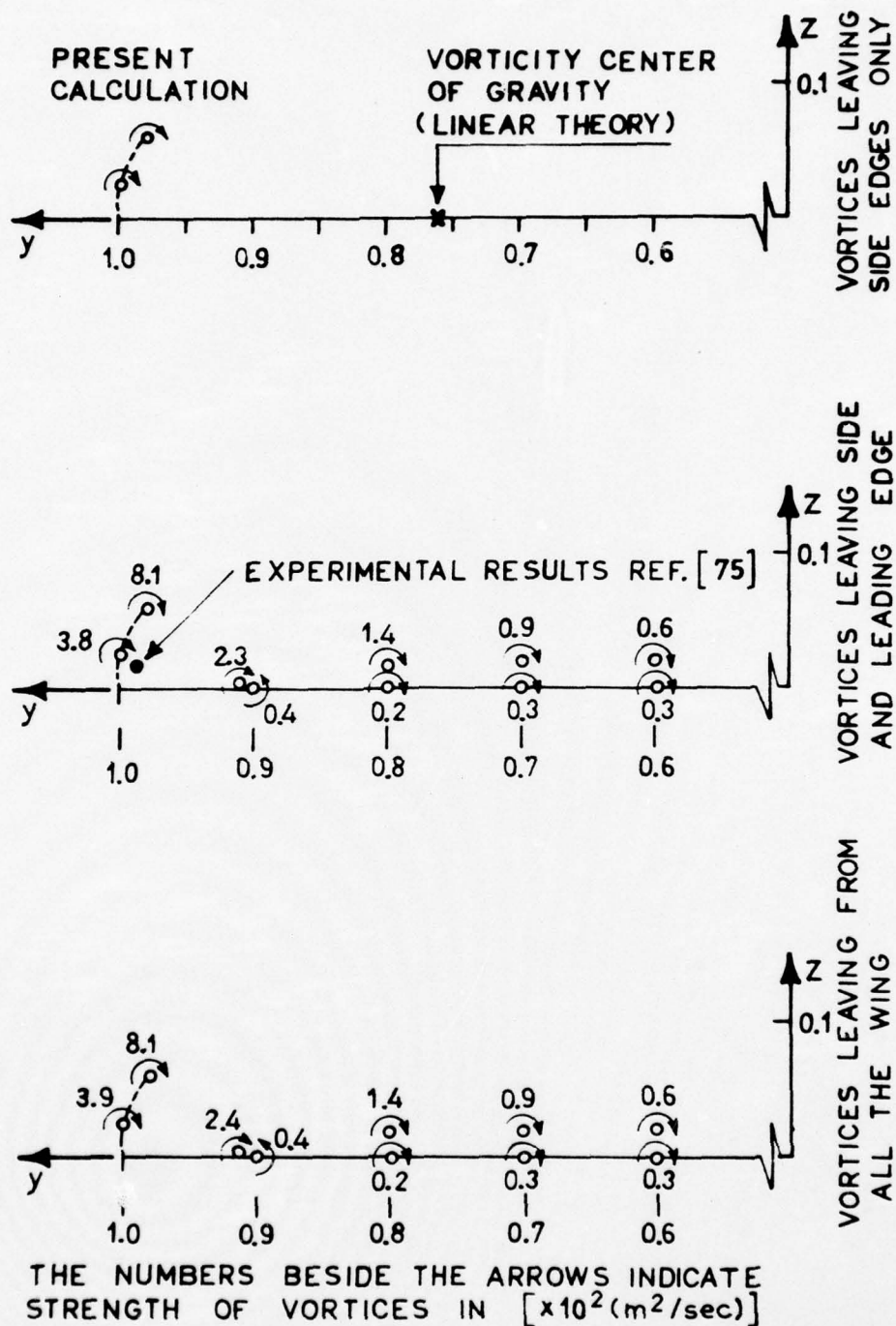


FIG. 27 - COMPARISON OF THE VORTEX SHEET AT THE TRAILING EDGE FROM A RECTANGULAR WING $AR=5.33$ OBTAINED FROM DIFFERENT MODELS. ($\alpha=12^\circ$)

- EXPERIMENTAL RESULTS [37] SPANWISE
- EXPERIMENTAL RESULTS [37] NORMAL
- PRESENT WORK

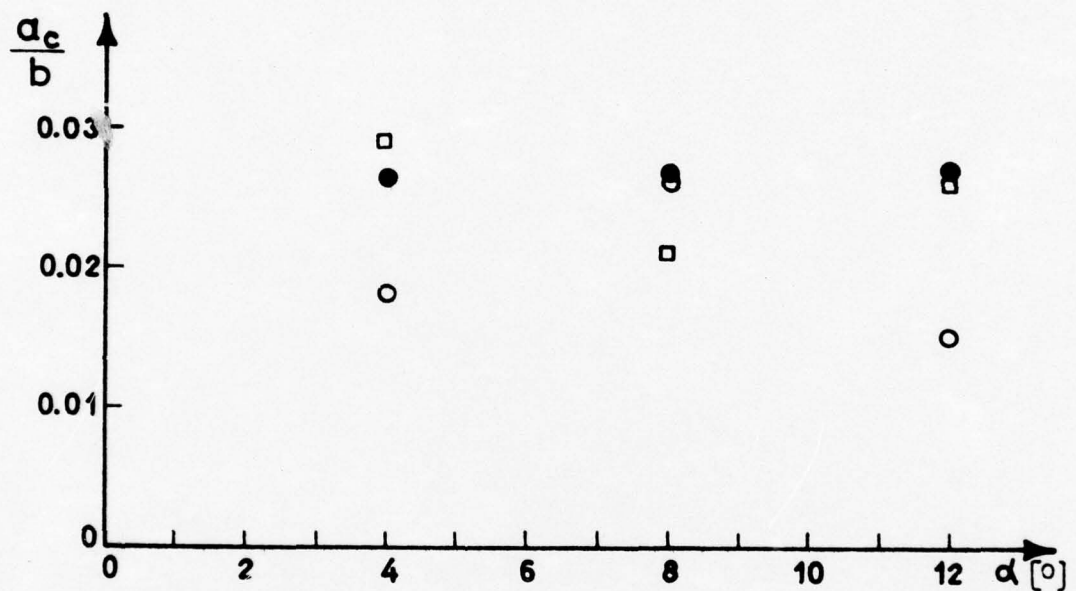


FIG.28 - COMPARISON OF THE MEASURED CORE SIZE WITH THE CALCULATED RESULTS FOR A RECTANGULAR WING OF AR=5.33 AT THE TRAILING EDGE PLANE.

- - ROUND L.E. - $1/c = 0.092$ - REF. [39]
- △ - SHARP L.E. - REF. [39]
- - SCHOLZ REF. [40]
- - WINTER REF. [41]
- + - FLACHSBART REF. [41]

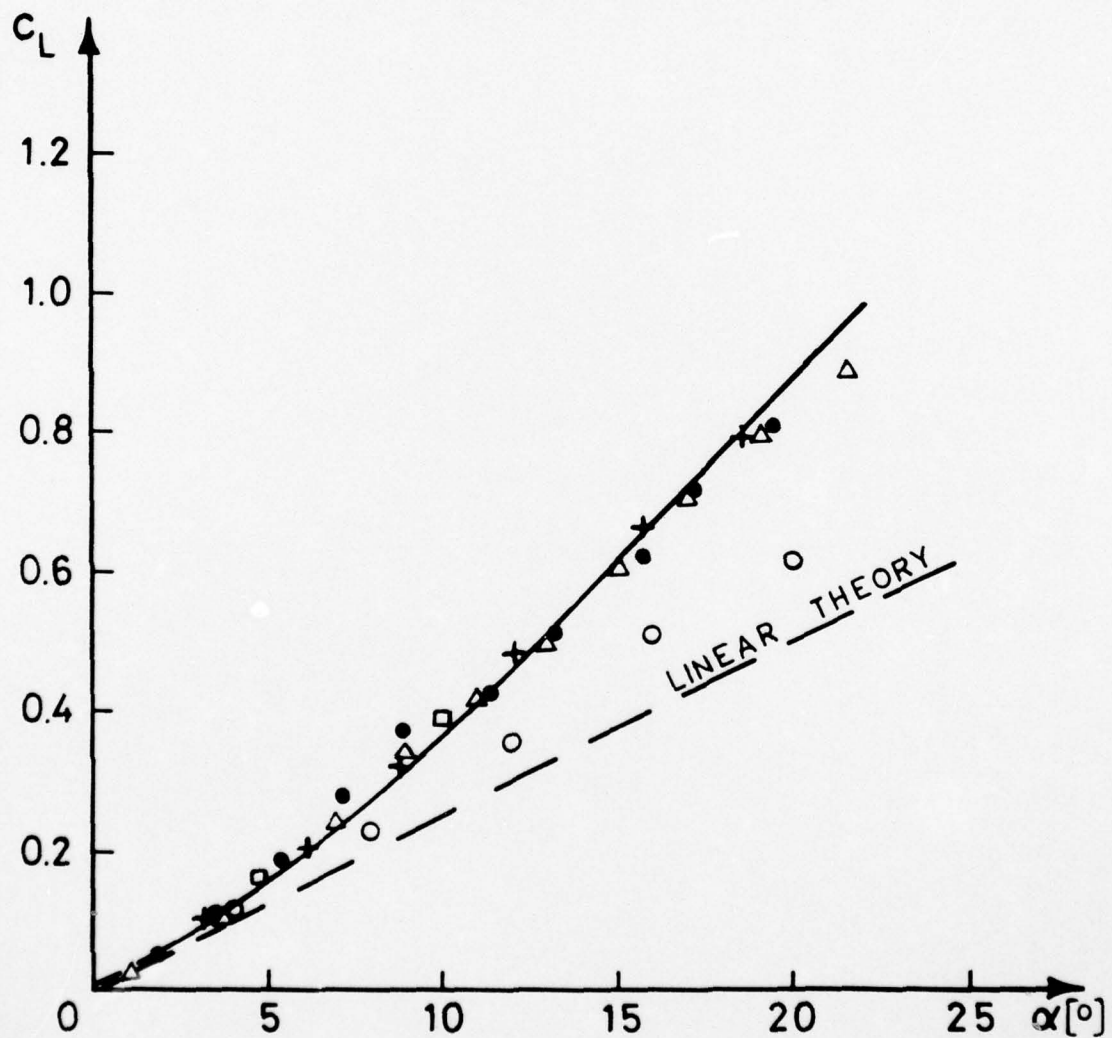


FIG. 29 - THE LIFT COEFFICIENT OF A RECTANGULAR WING OF $AR=1$

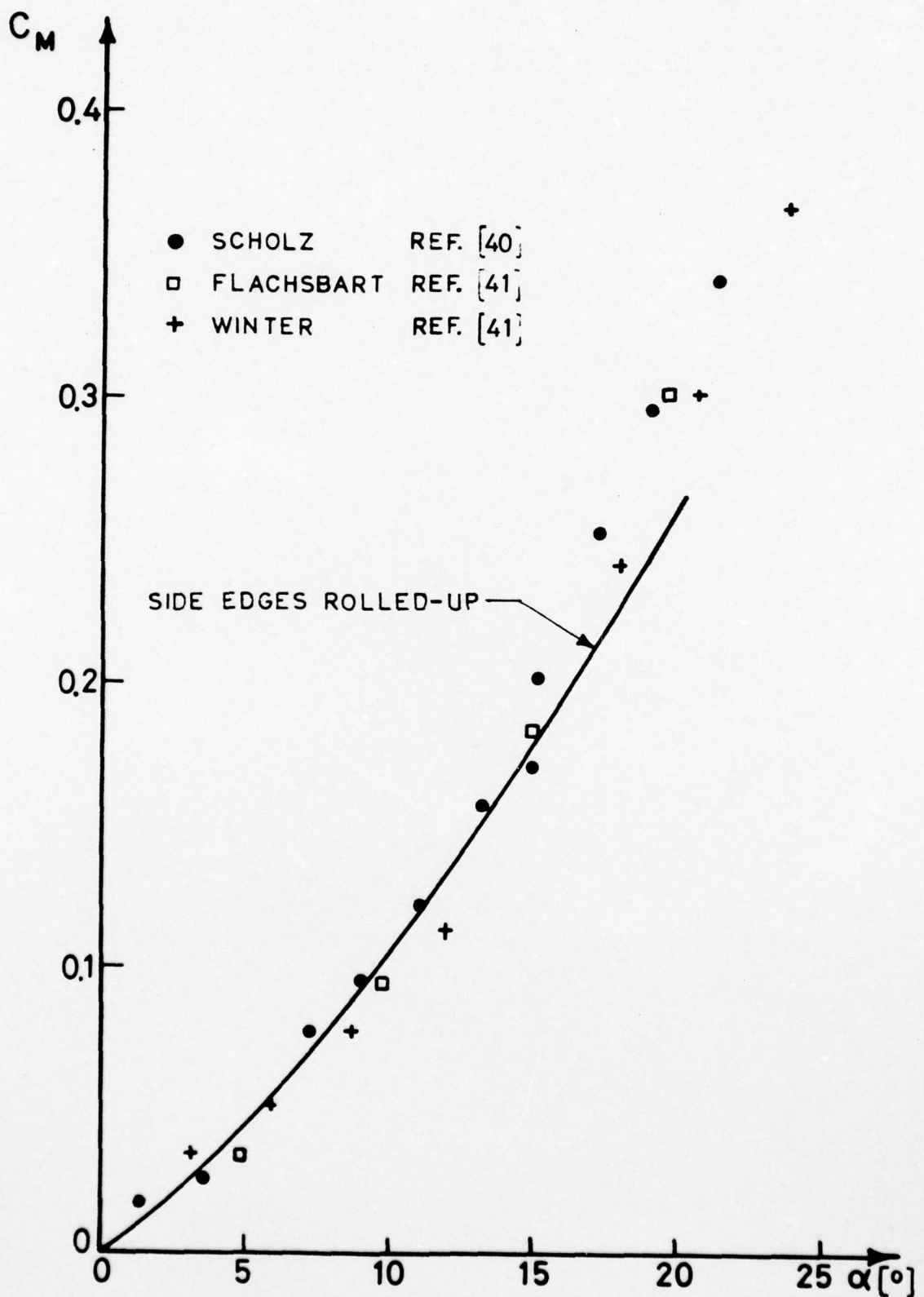


FIG.30-THE PITCHING MOMENT COEFFICIENT OF A RECTAN - GULAR WING OF $AR=1$.

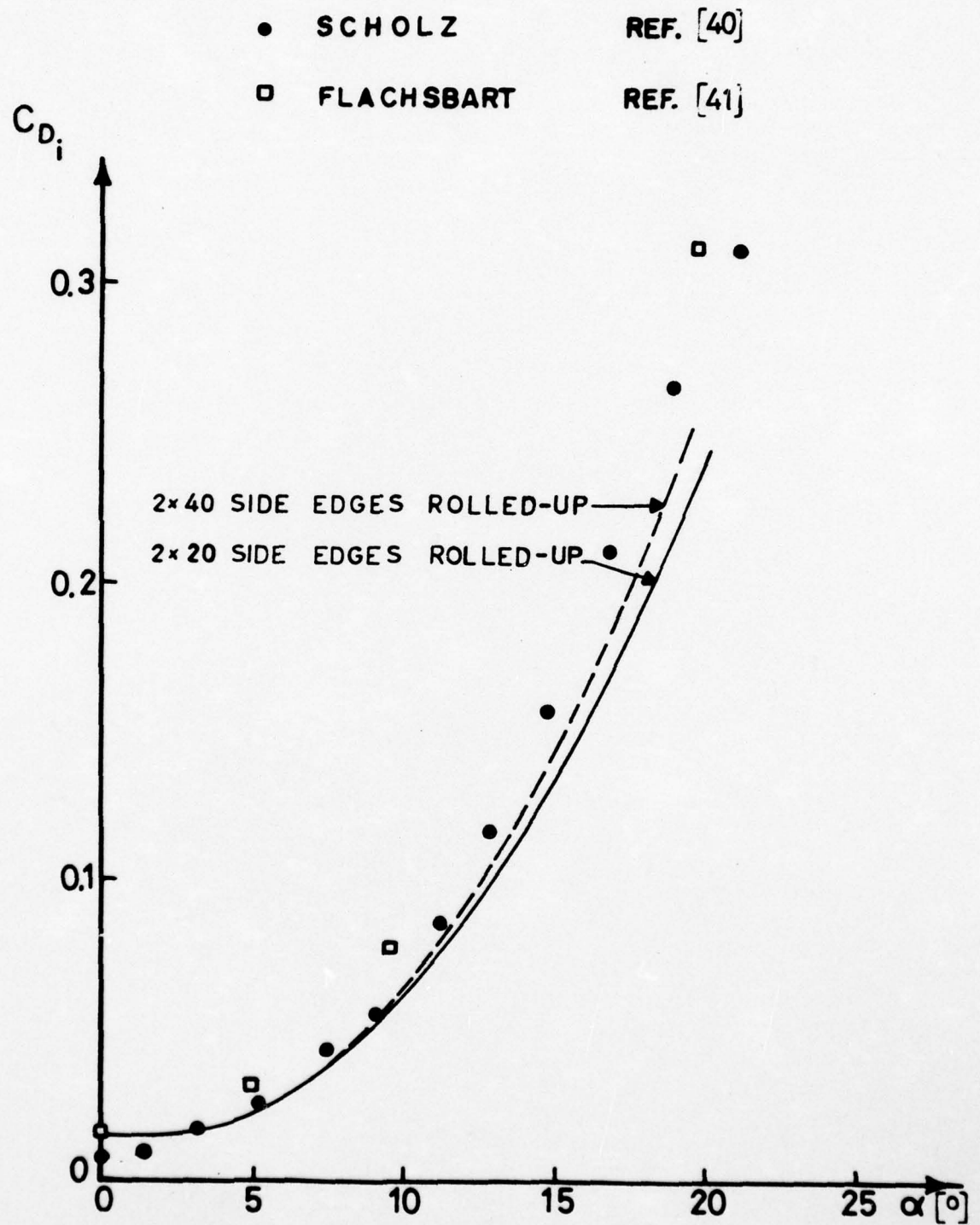


FIG.31-THE INDUCED DRAG COEFFICIENT OF A RECTANGULAR WING OF AR=1.

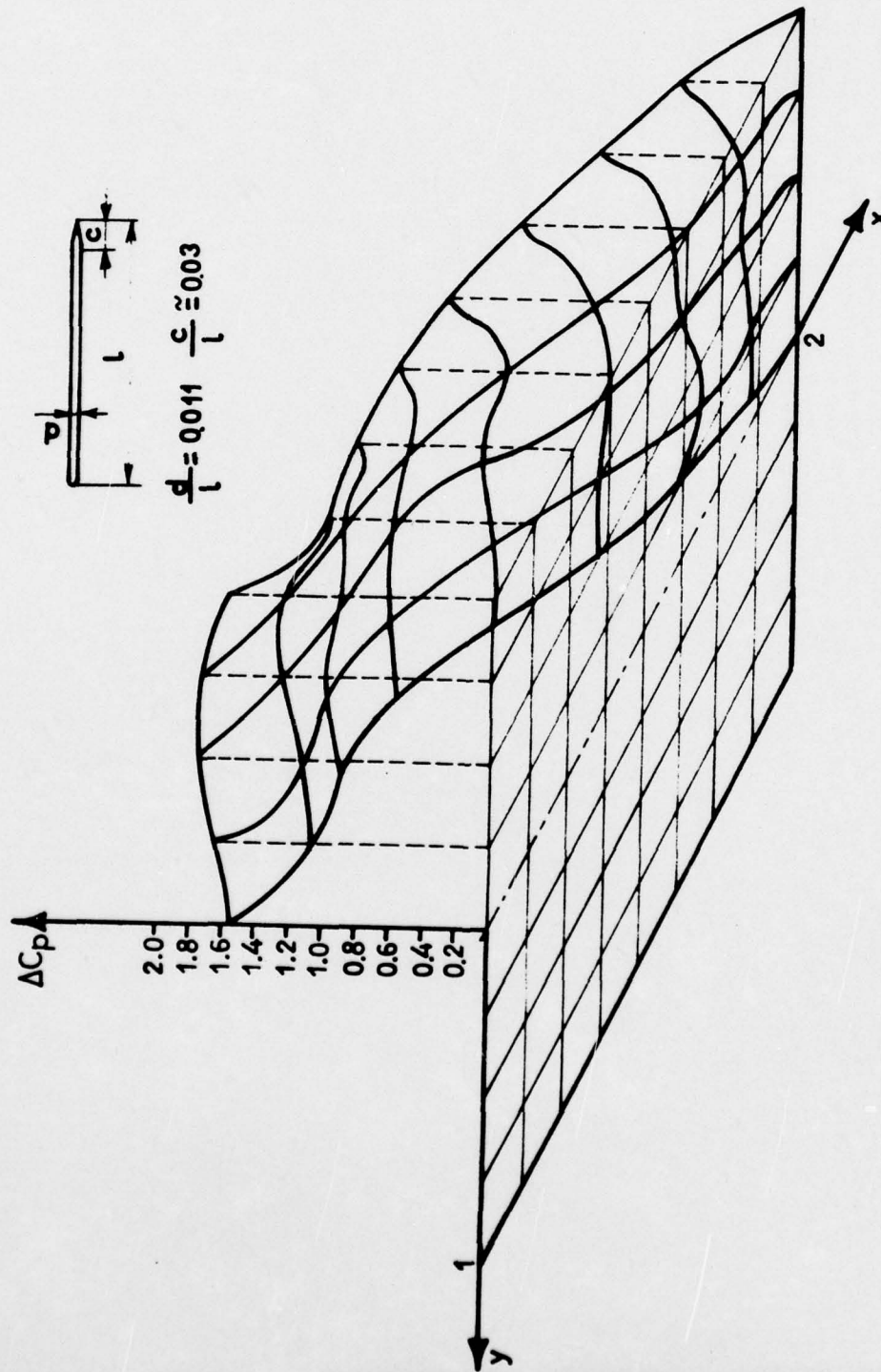


FIG. 32 - $\Delta C_p \Delta$ OF A RECTANGULAR WING OF $AR=1$ AT $\alpha = 20^\circ$; EXPERIMENTAL RESULTS OF SCHOLZ [40].

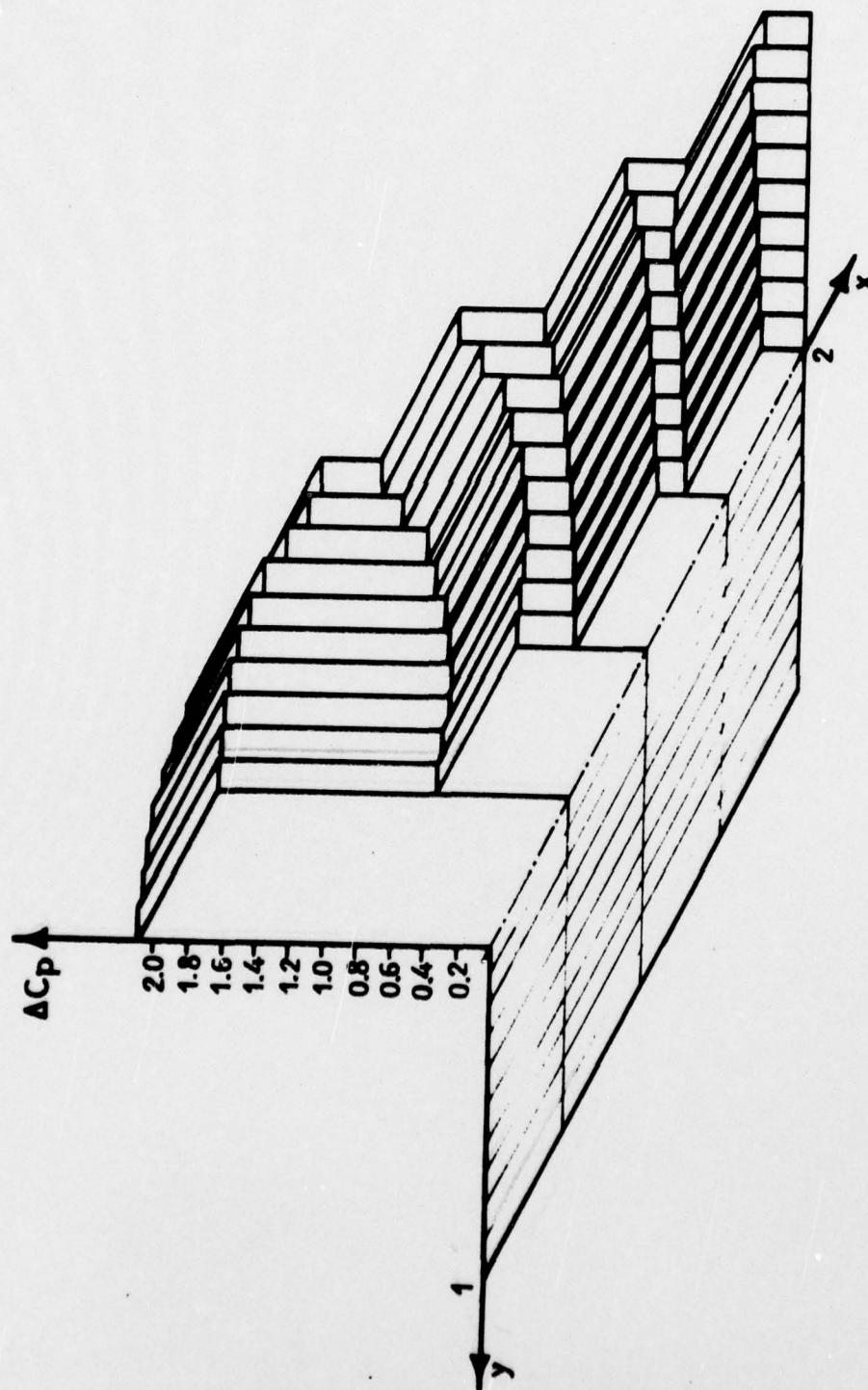


FIG. 33 - THE ΔC_p CALCULATED BY THE PROPOSED METHOD FOR A RECTANGULAR WING OF AR=1 AT $\alpha = 20^\circ$.

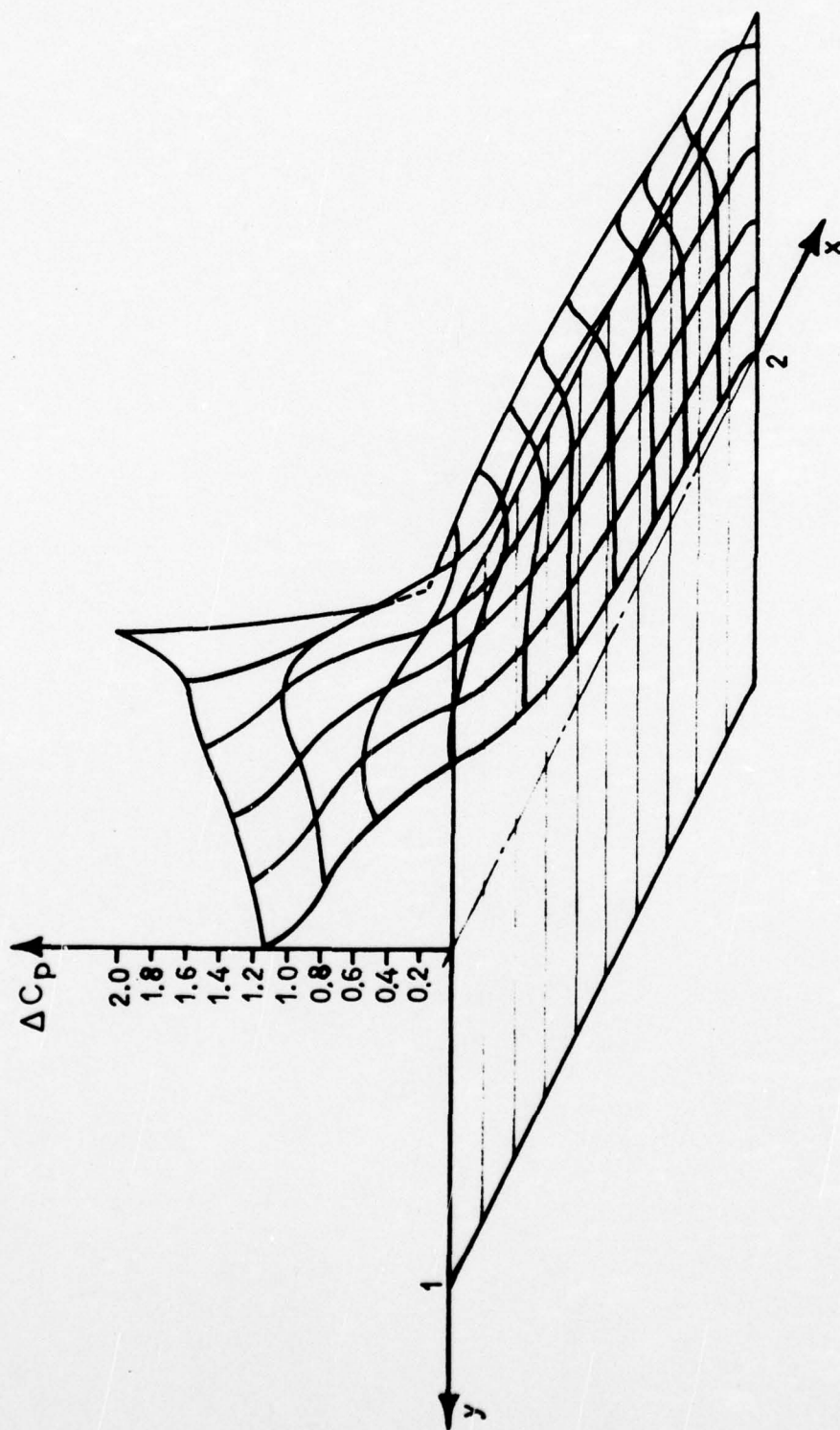


FIG. 34 - ΔC_p OF A RECTANGULAR WING OF $AR=1$ AT $\alpha=10^\circ$, EXPERIMENTAL RESULTS OF SCHOLZ [40].

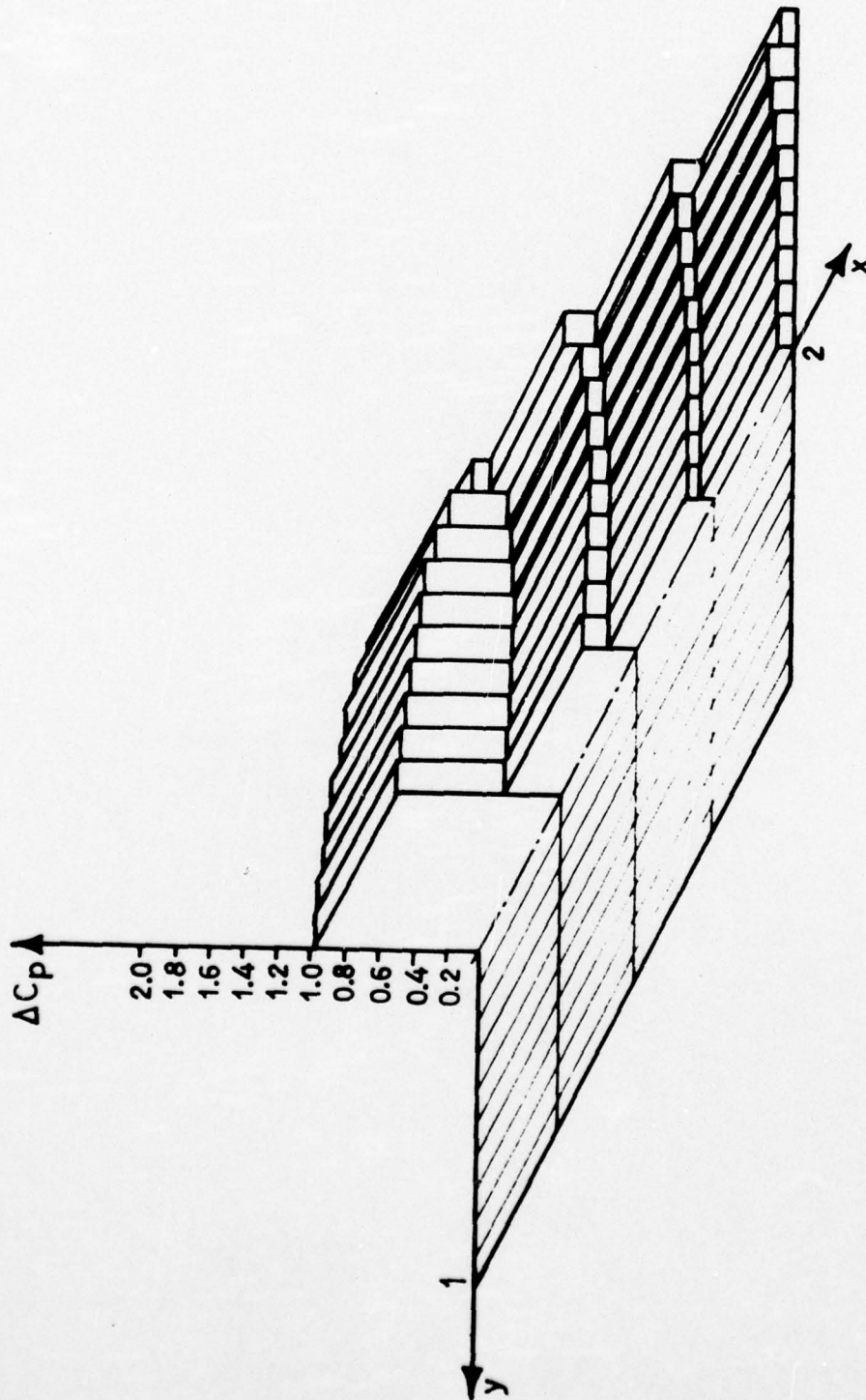


FIG.35-THE ΔC_p CALCULATED BY THE PROPOSED METHOD FOR
A RECTANGULAR WING OF $AR=1$ AT $\alpha=10^\circ$.

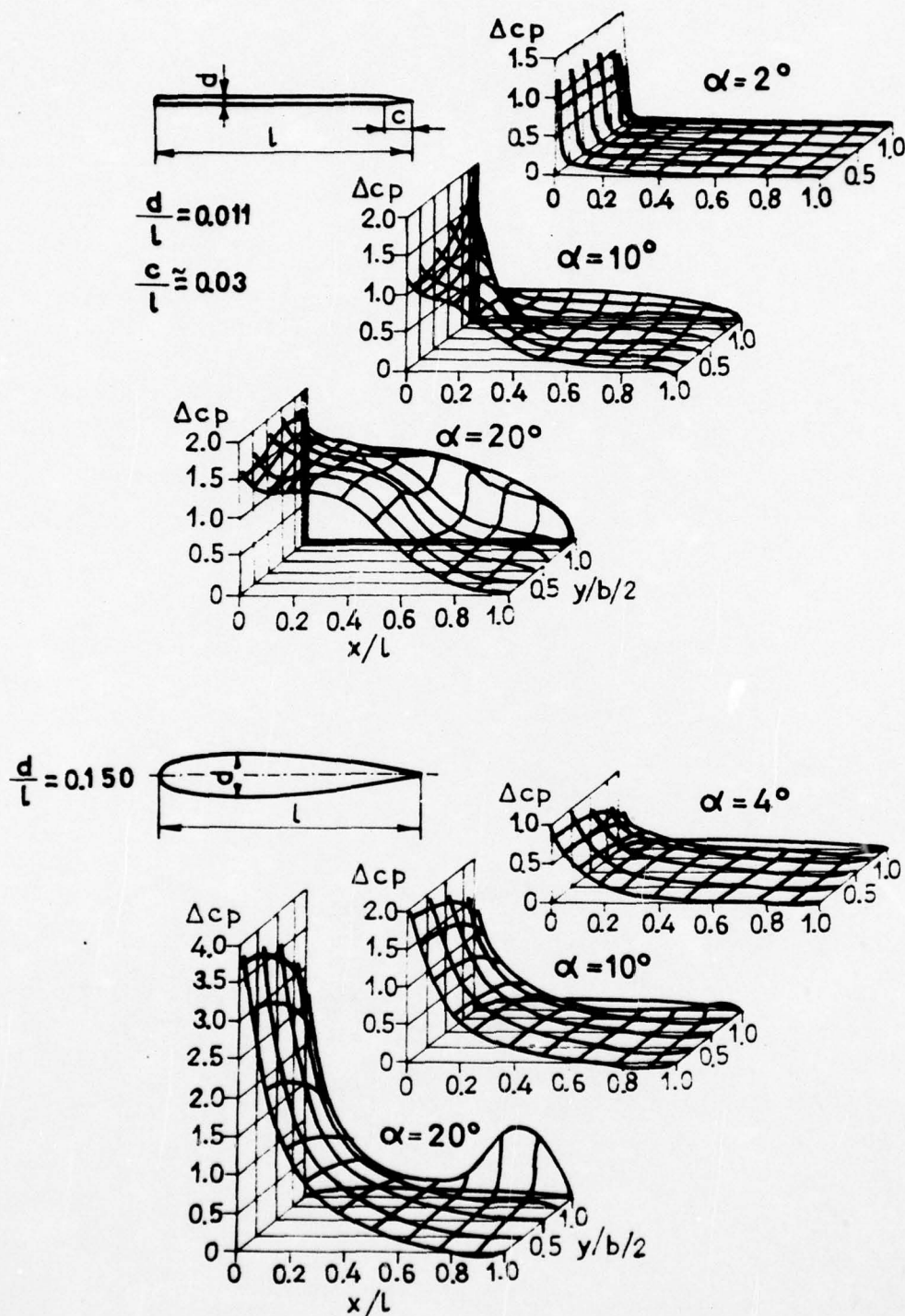


FIG. 36 - THE INFLUENCE OF THE PROFILE SHAPE ON THE PRESSURE DISTRIBUTION OF A RECTANGULAR WING OF $AR=1$. [30]

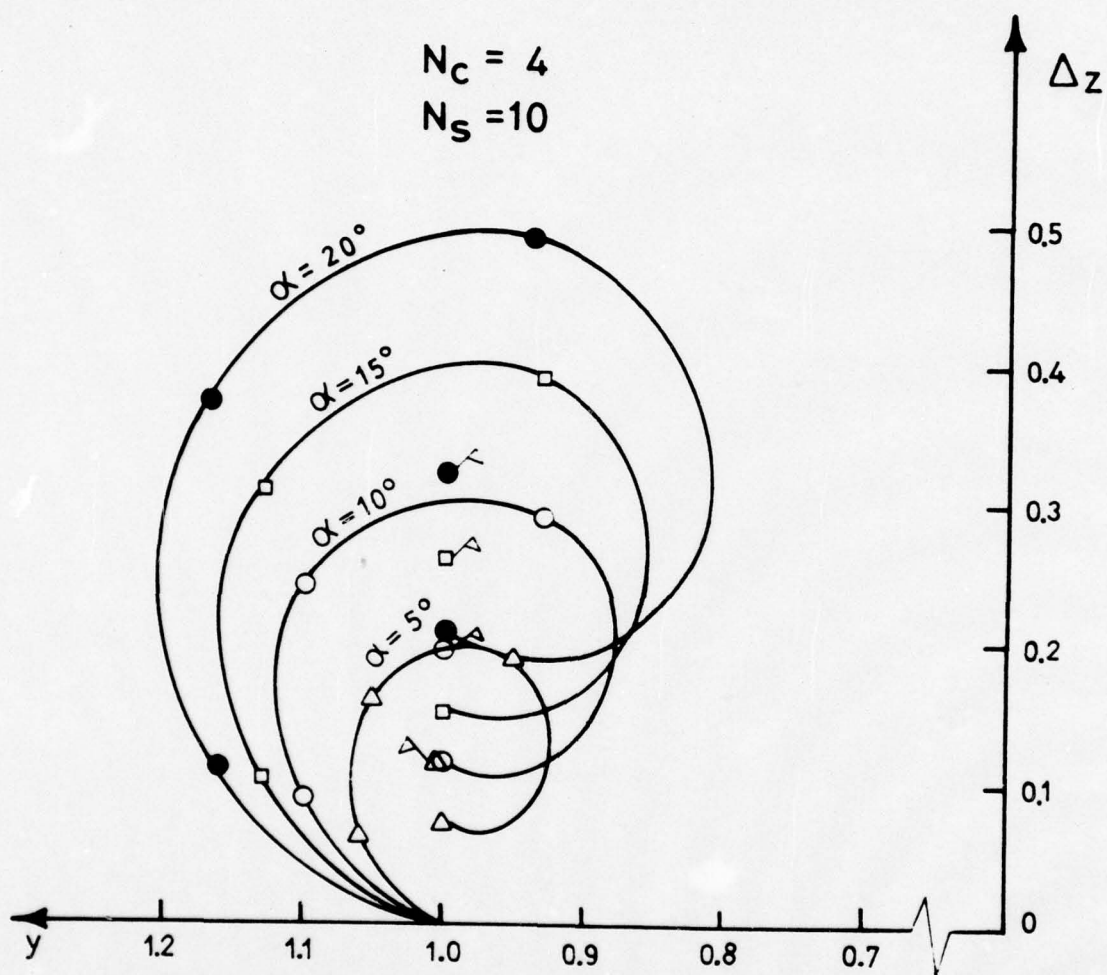


FIG.37-THE ROLLING UP OF THE VORTEX SHEET
AT THE TRAILING EDGE PLANE OF A
RECTANGULAR WING OF $AR=1$ AS A
FUNCTION OF INCIDENCE.

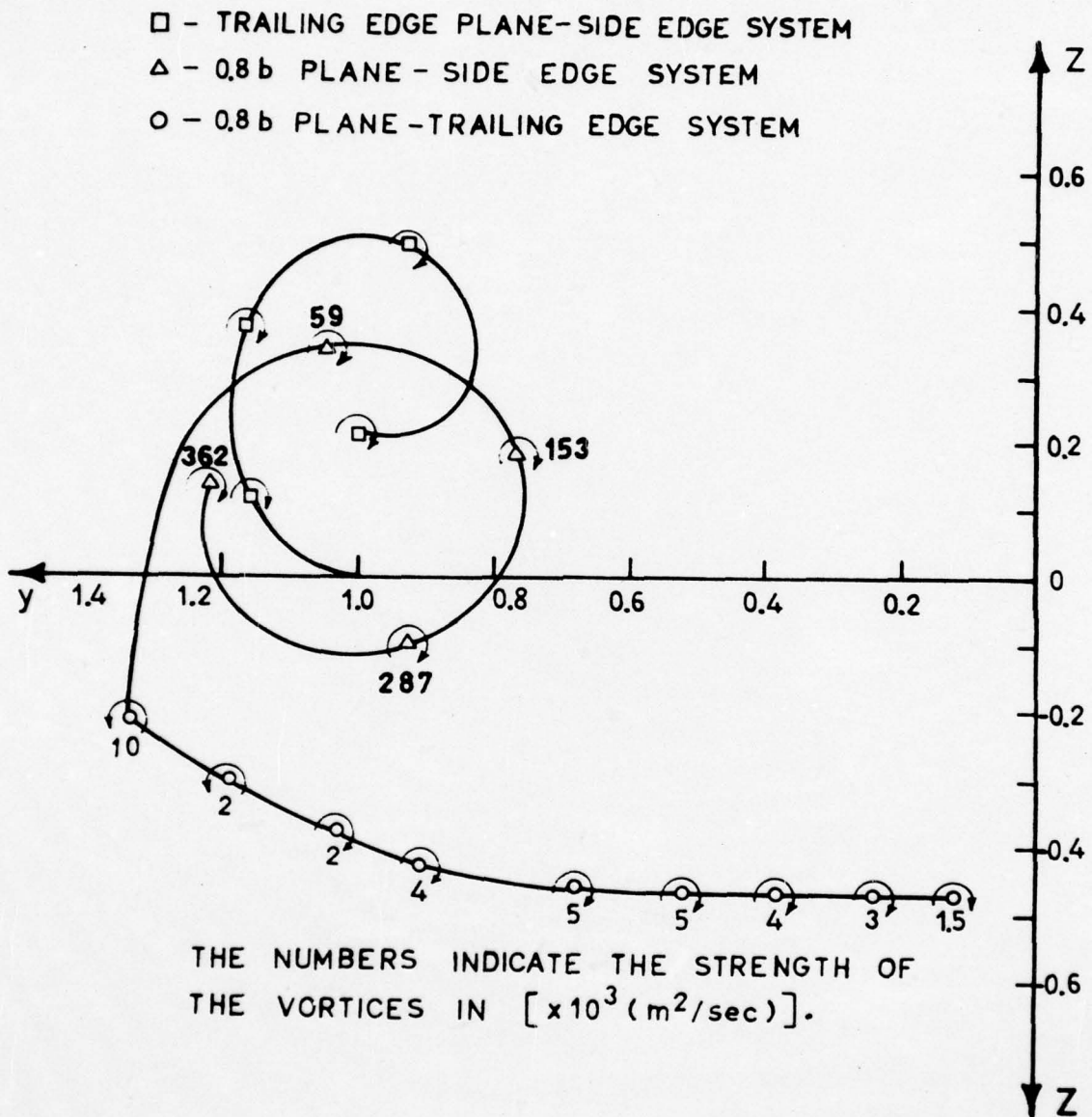


FIG.38-THE NEAR WAKE DEVELOPMENT
BEHIND A RECTANGULAR WING OF $AR=1$,
AT $\alpha=20^\circ$.



FIG. 39 - THE ROLLING UP OF THE VORTICES SHED FROM
SIDE AND TRAILING EDGE OVER A RECTANGULAR
WING OF $AR=1$ AT $\alpha=10^\circ$.

AD-A032 552

TECHNION - ISRAEL INST OF TECH HAIFA DEPT OF AERONAU--ETC F/G 20/4
INVESTIGATIONS OF THE ROLLING-UP OF THE VORTEX WAKE AND CALCULA--ETC(U)
JUN 76 J ROM, H PORTNOY, C ZOREA AF-AFOSR-2145-71

UNCLASSIFIED

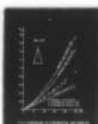
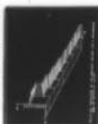
TAE-277

AFOSR-TR-76-1146

NL

2 OF 2

AD
A032552



END

DATE

FILMED

1-77

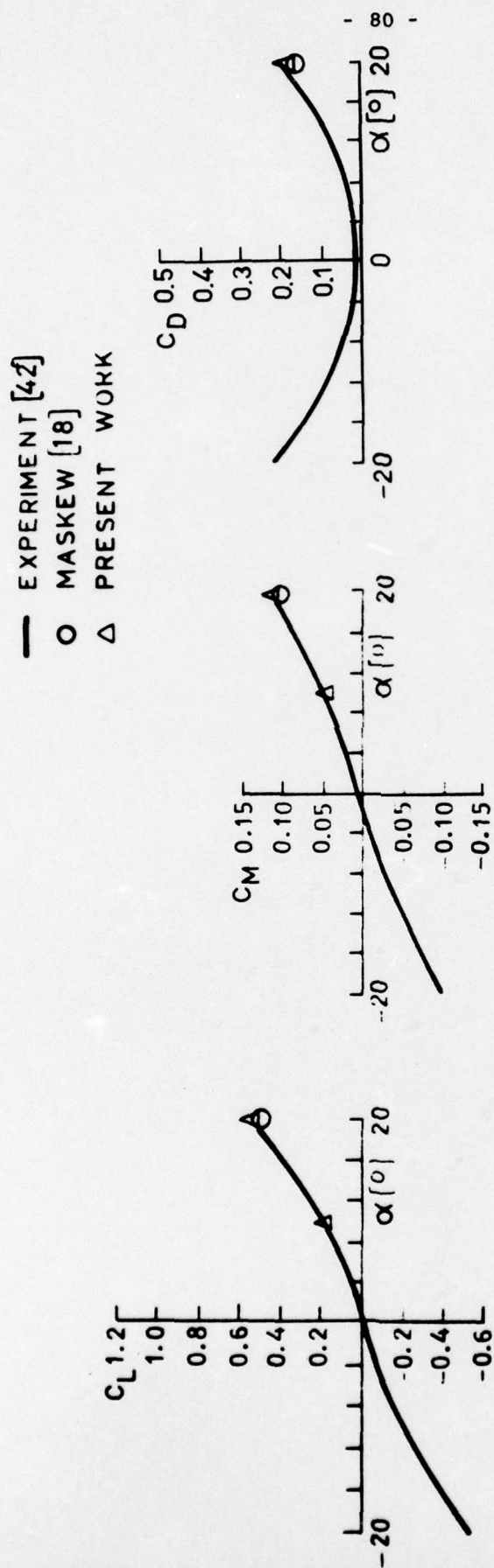


FIG.40 - COMPARISON OF THE AERODYNAMIC COEFFICIENTS C_L , C_M , C_D FOR A RECTANGULAR WING OF $AR = 0.25$.

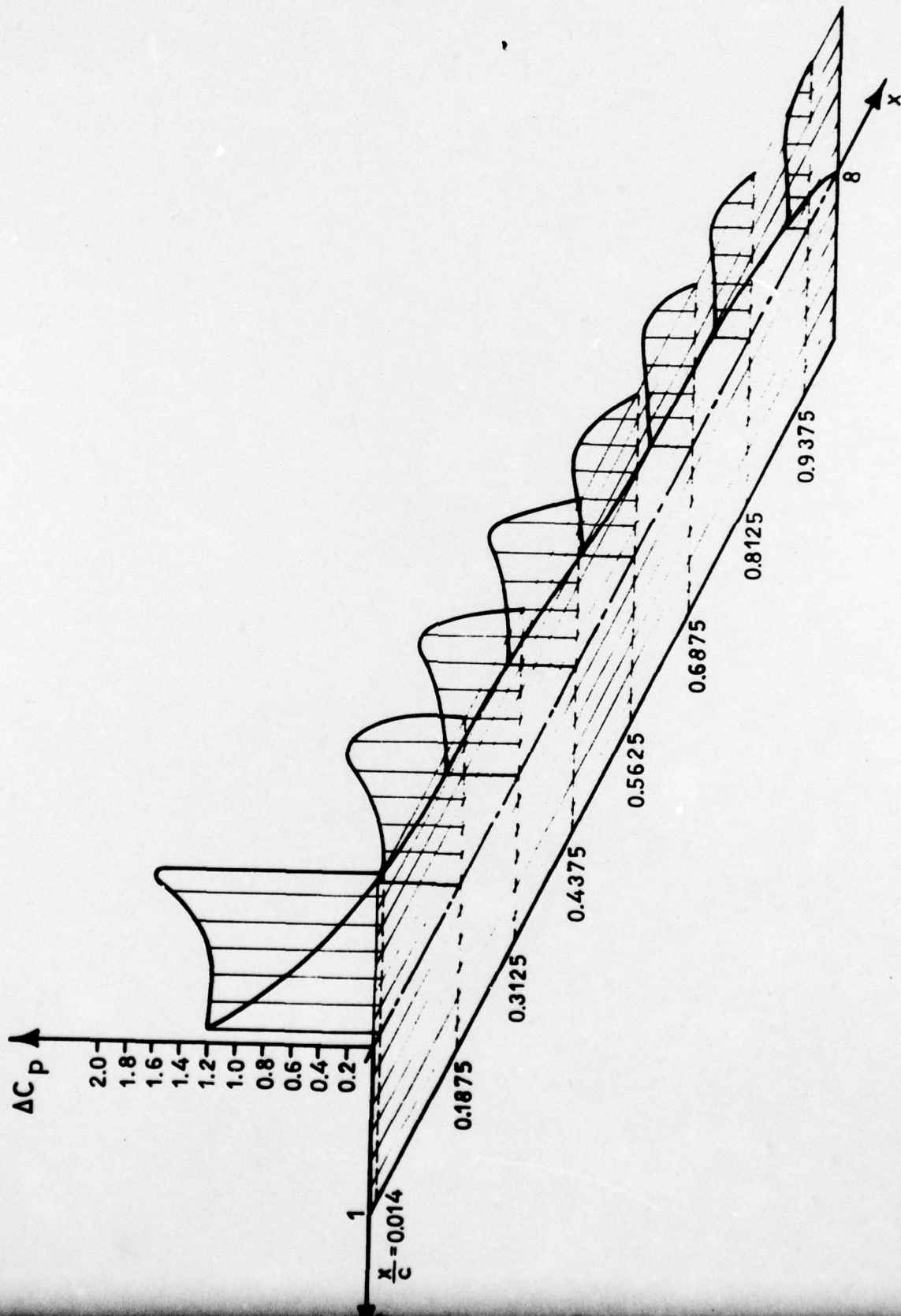


FIG. 41 - ΔC_p OF A RECTANGULAR WING OF $AR=0.25$ AT $\alpha=20^\circ$ FOLLOWING THE EXPERIMENTAL RESULTS OF WICKENS [42].

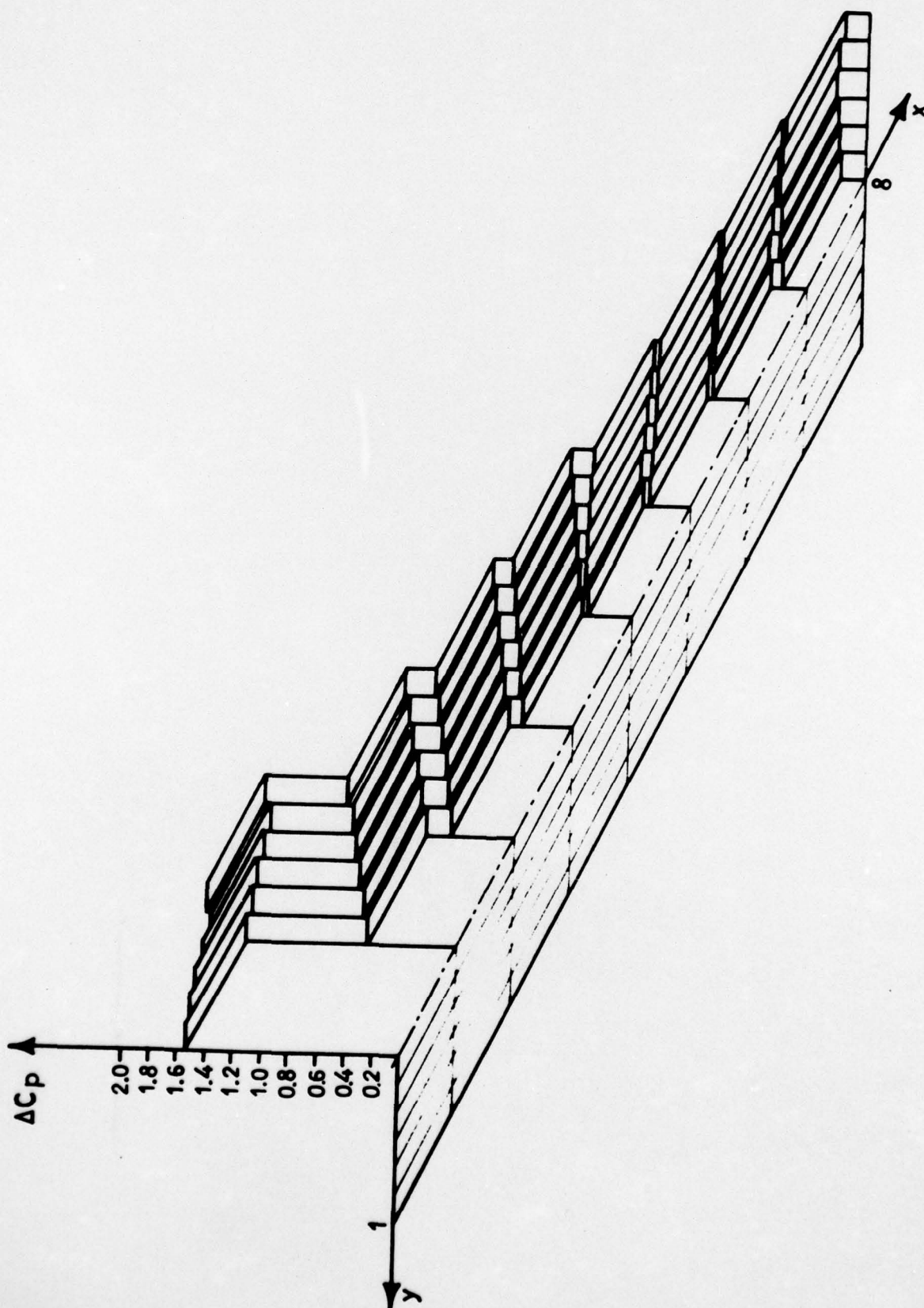


FIG. 42 - ΔC_p CALCULATED BY THE PROPOSED METHOD FOR A RECTANGULAR WING OF $AR=0.25$ AT $\alpha=20^\circ$.

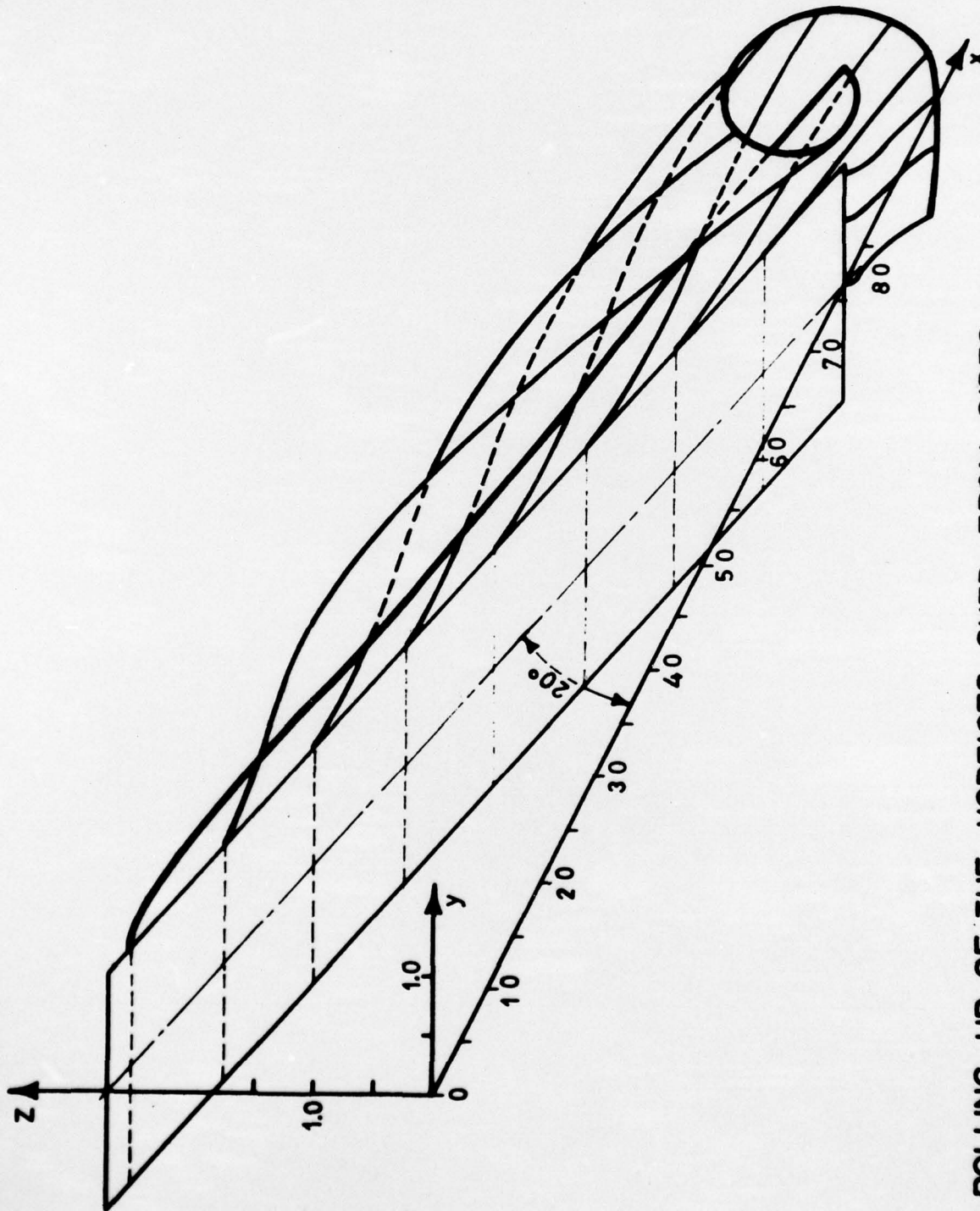


FIG.4.3 - ROLLING UP OF THE VORTICES SHED FROM SIDES AND TRAILING EDGES OF A RECTANGULAR WING OF $AR=0.25$ AT INCIDENCE $\alpha=20^\circ$.

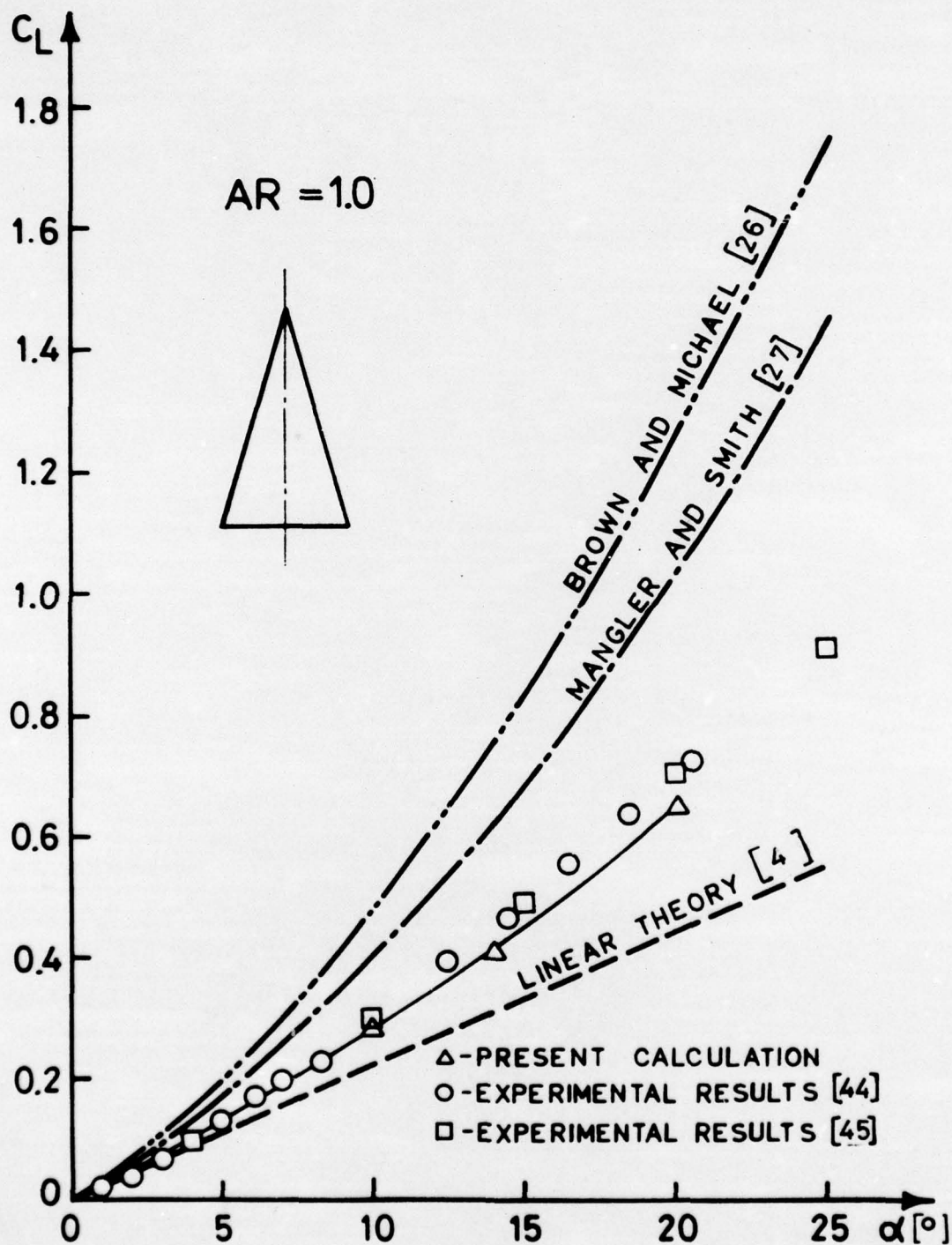


FIG.44-COMPARISON OF EXPERIMENTAL AND COMPUTED LIFT COEFFICIENT C_L AS A FUNCTION OF α FOR DELTA WING OF $AR=1$.

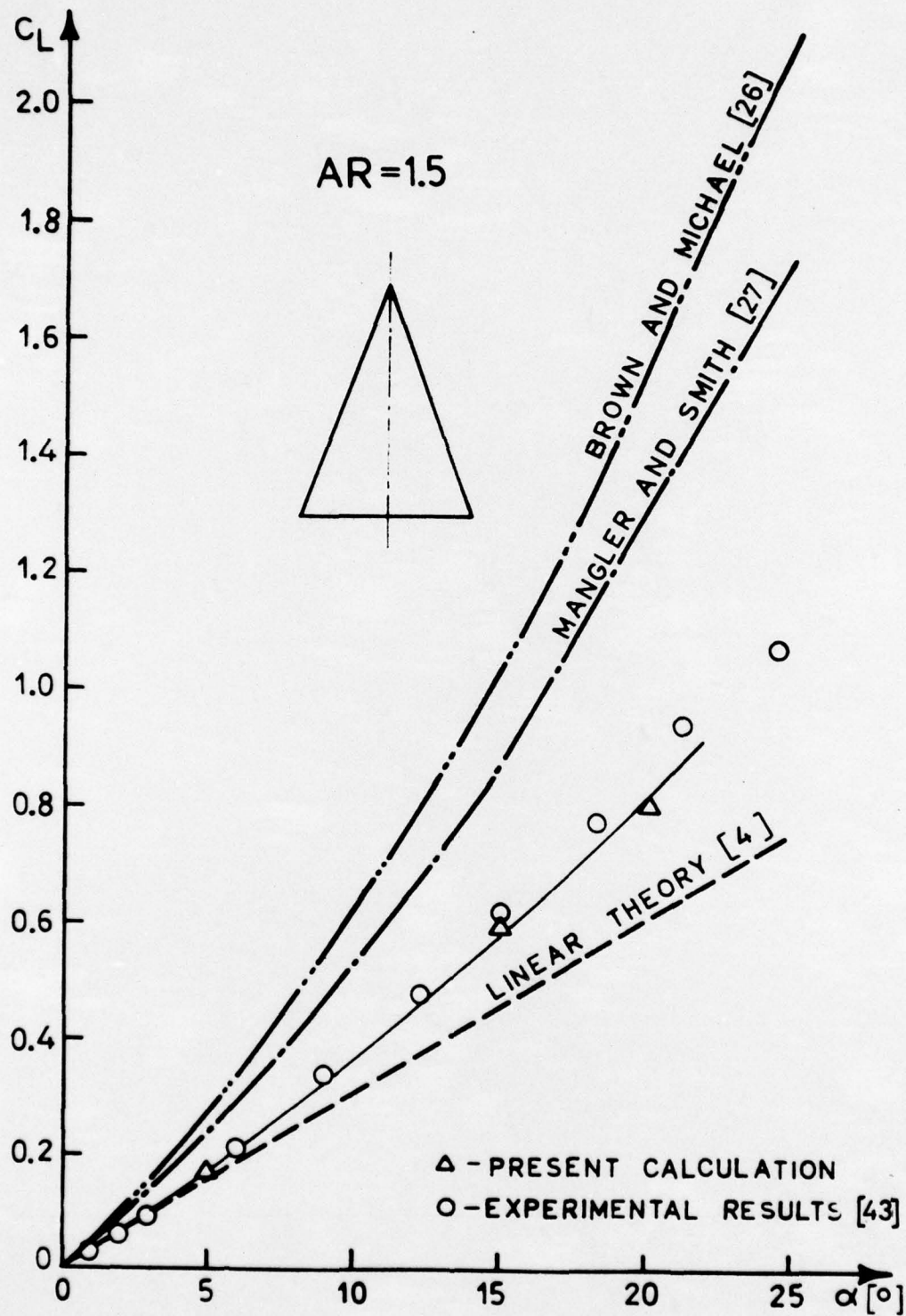


FIG.45-COMPARISON OF EXPERIMENTAL AND COMPUTED LIFT COEFFICIENT C_L AS A FUNCTION OF α FOR DELTA WING OF $AR=1.5$.

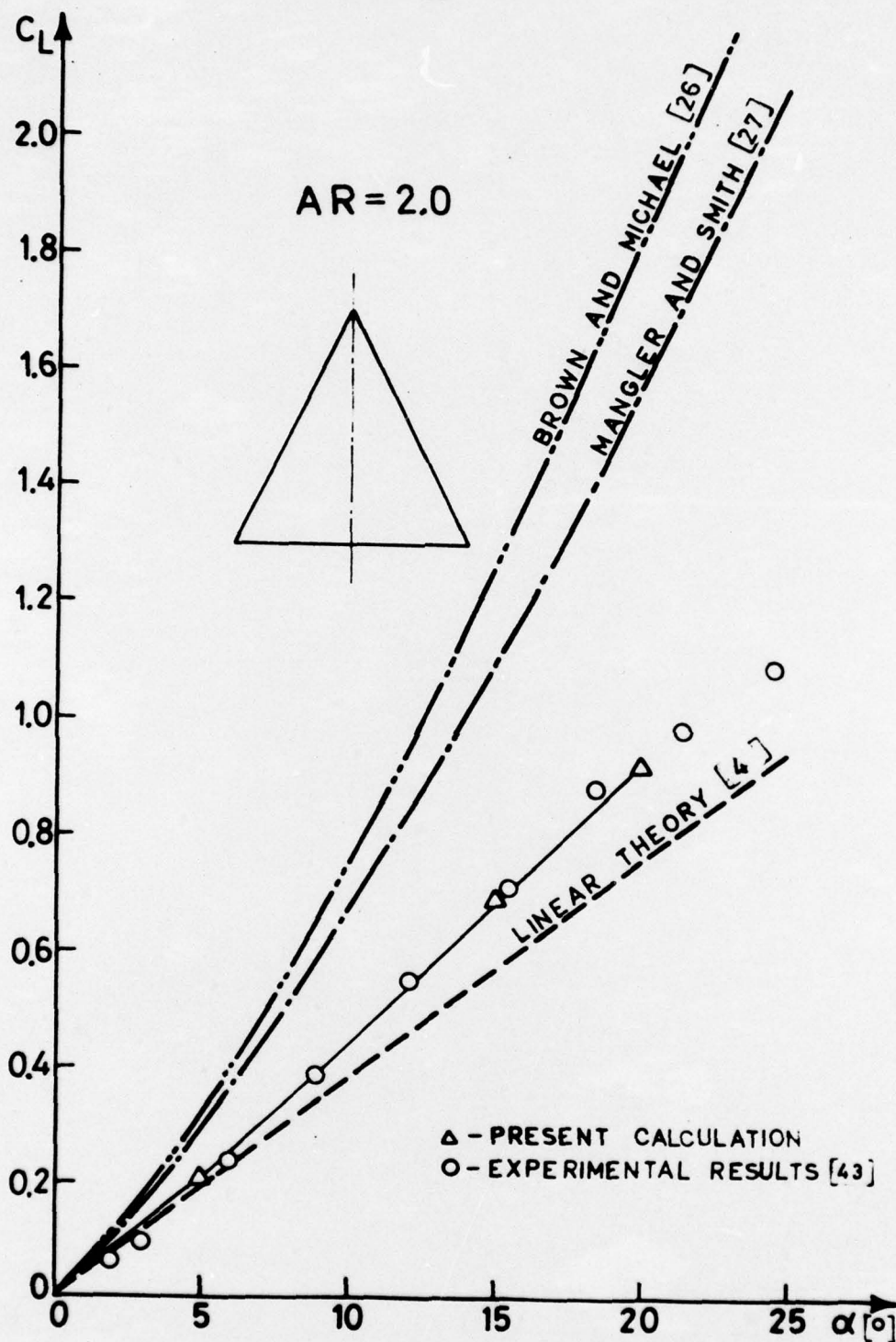


FIG.46 COMPARISON OF EXPERIMENTAL AND COMPUTED LIFT COEFFICIENT C_L AS A FUNCTION OF α FOR DELTA WING OF $AR = 2$.

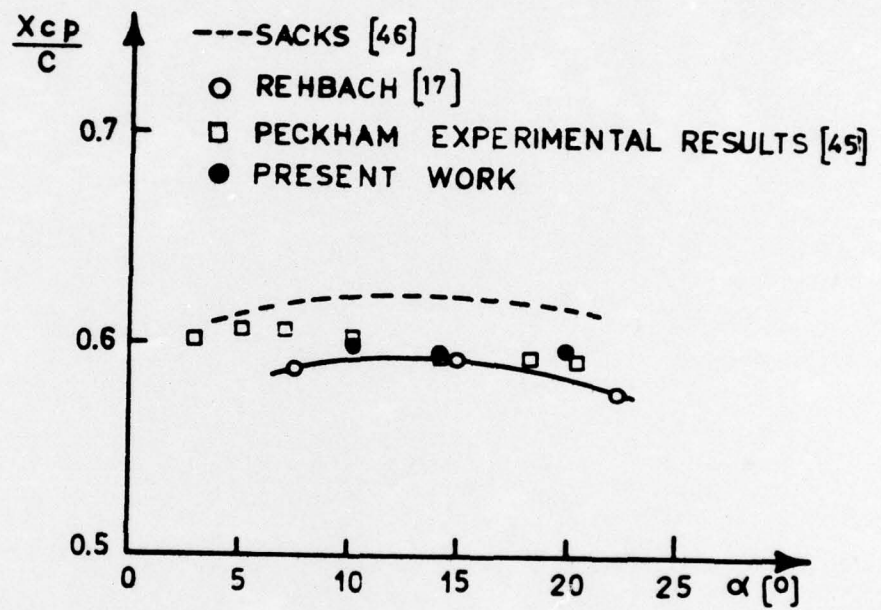


FIG.47 -CENTER OF PRESSURE OF A DELTA WING OF AR=1 AS A FUNCTION OF INCIDENCE.

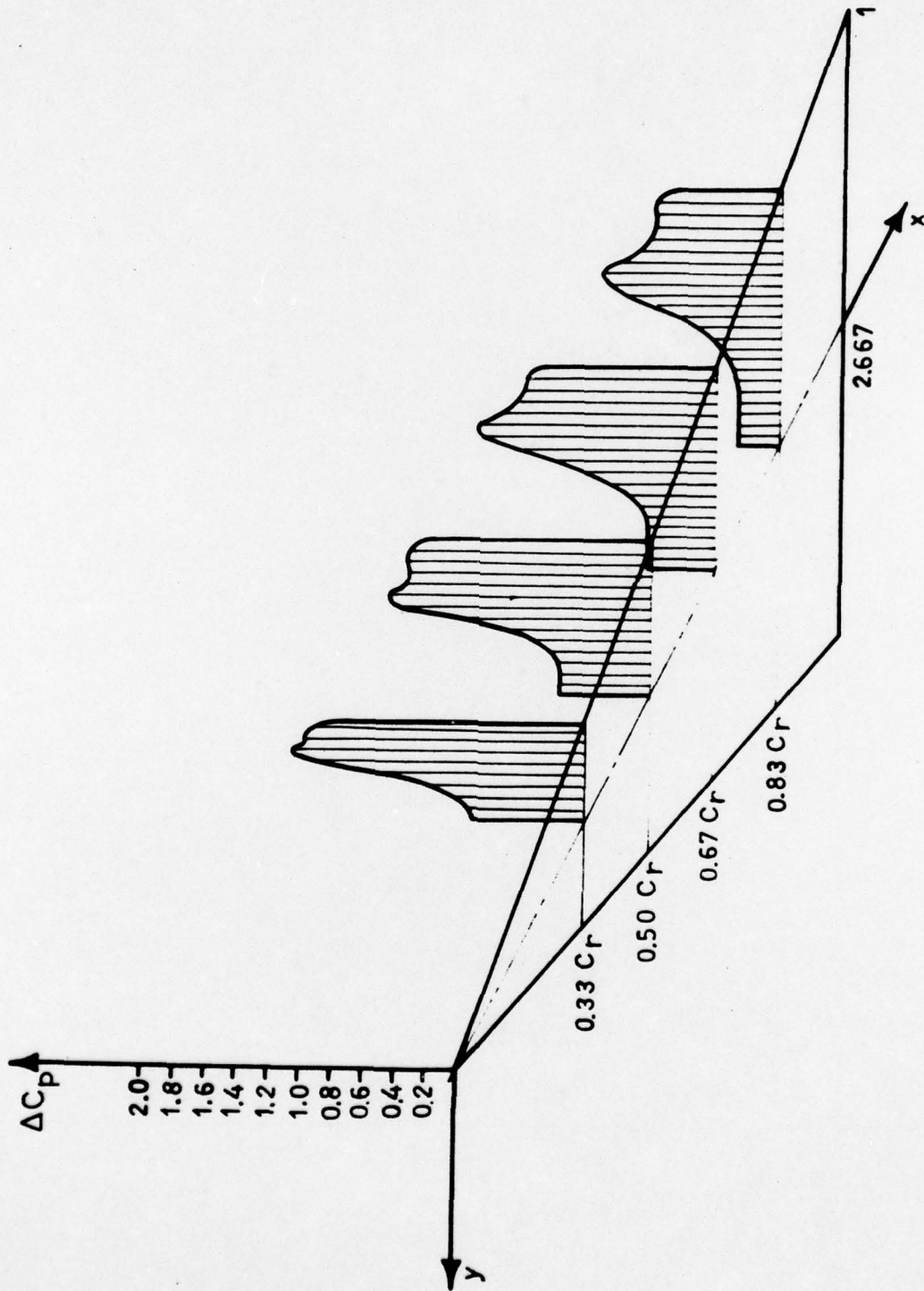


FIG.48 $-\Delta C_p$ OF A DELTA WING OF $AR=1.46$ AT $\alpha = 19.1^\circ$; EXPERIMENTAL RESULTS FROM REF. [47].

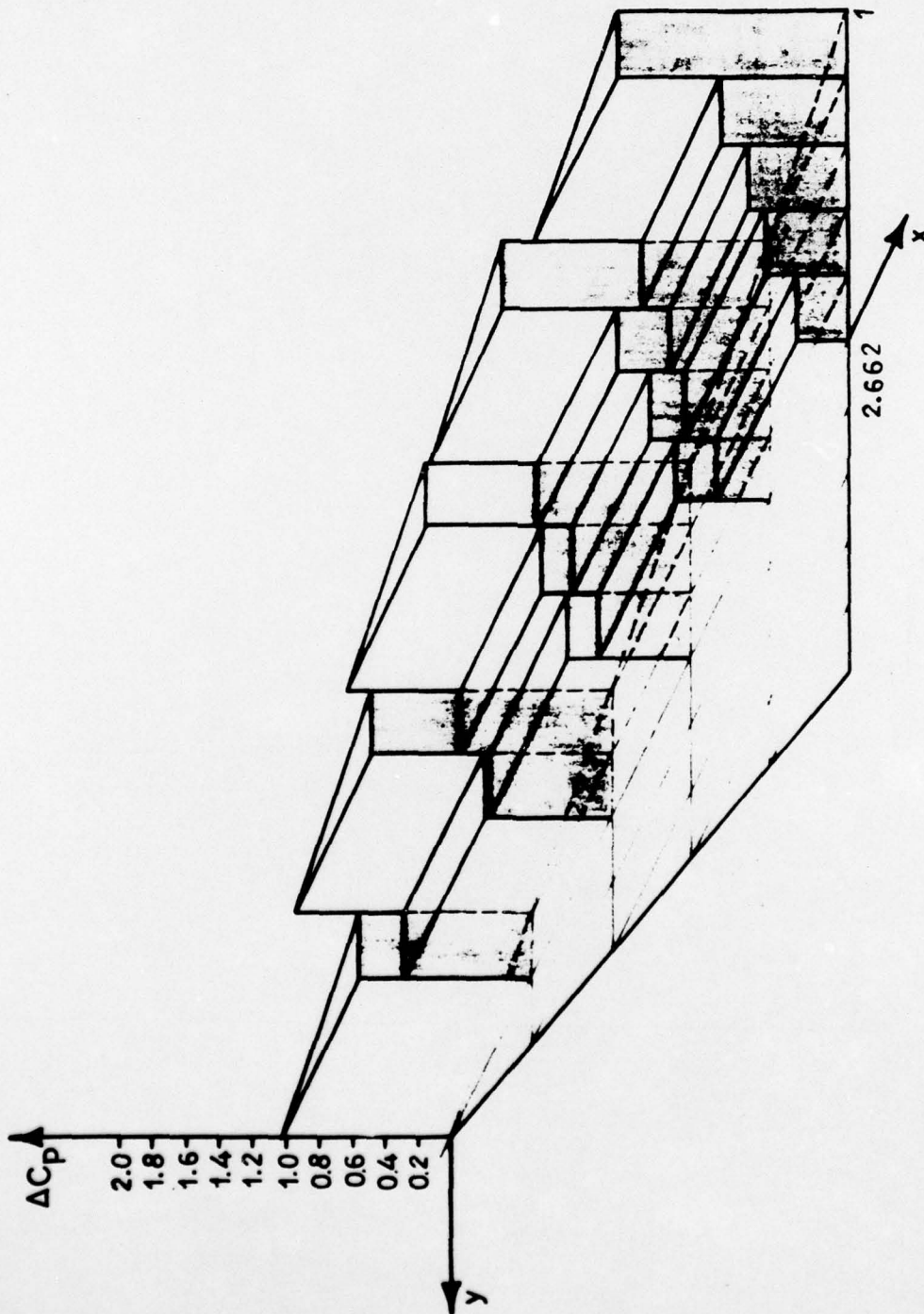


FIG.49 - THE ΔC_p CALCULATED BY THE PROPOSED METHOD
FOR A DELTA WING OF $AR=1.46$ AT $\alpha=20^\circ$.

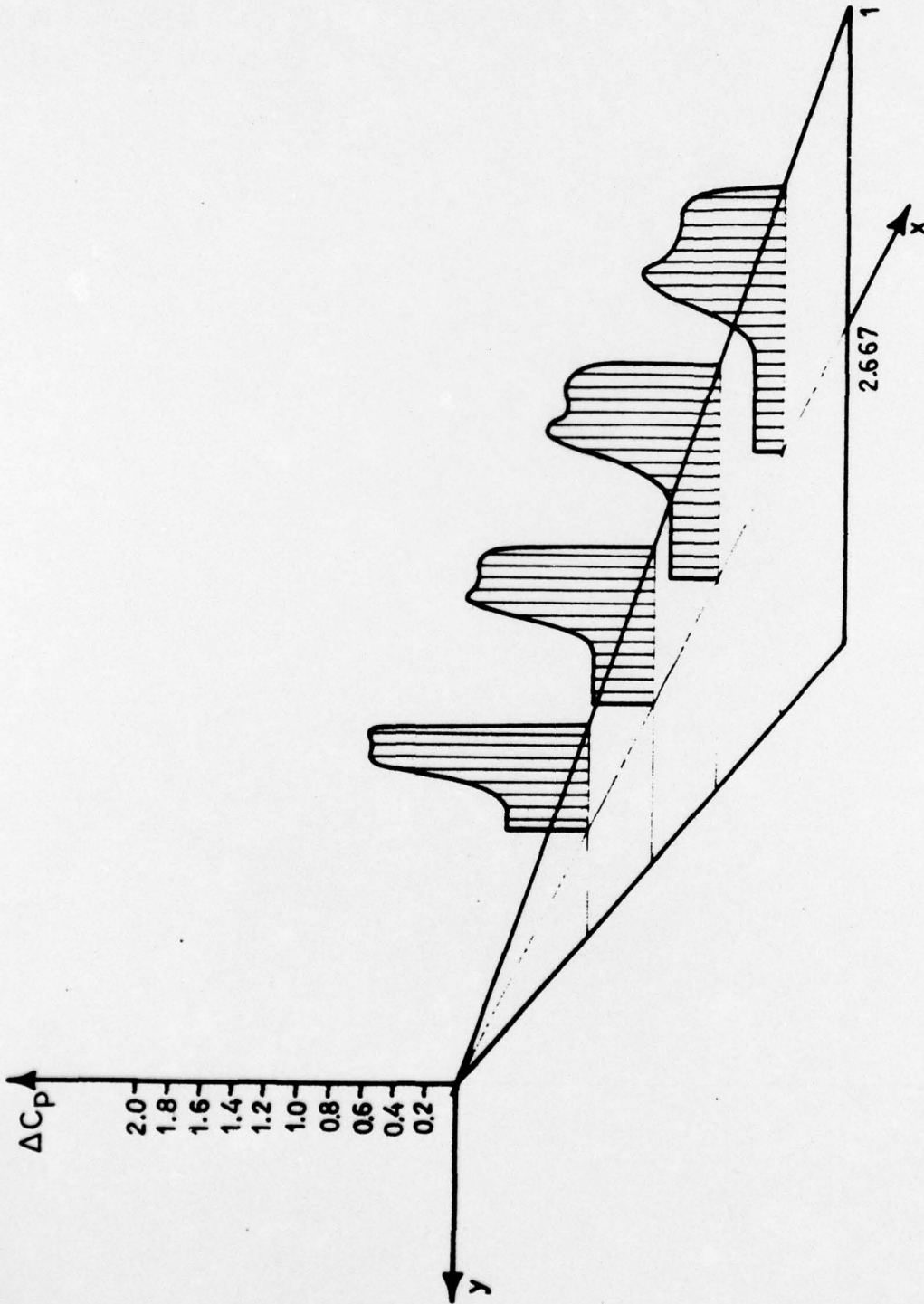


FIG. 50 - ΔC_p OF A DELTA WING OF $AR=1.46$ AT $\alpha=14^\circ$; EXPERIMENTAL RESULTS FROM REF. [47].

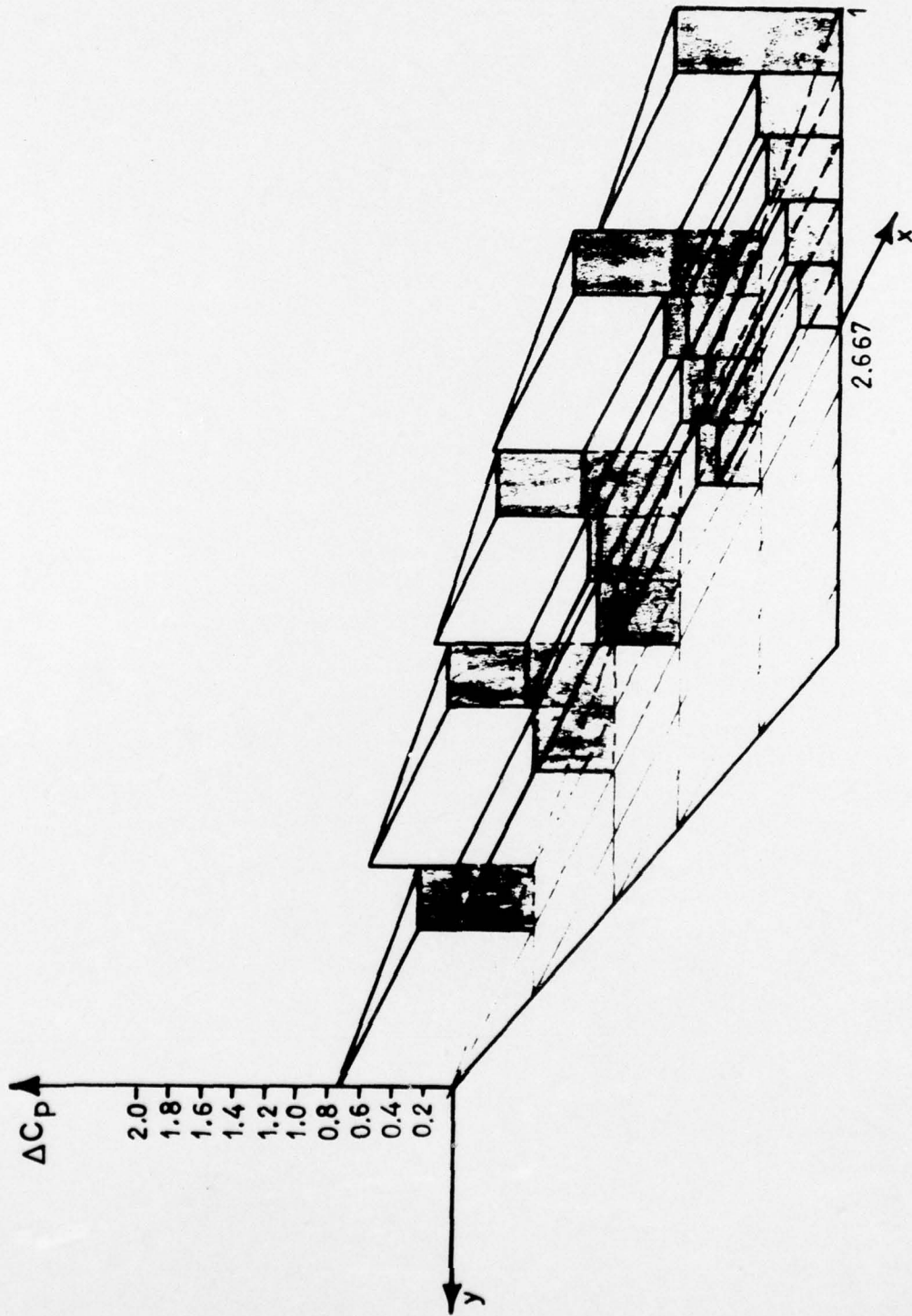


FIG.51-THE ΔC_p CALCULATED BY THE PROPOSED METHOD FOR
A DELTA WING OF $AR=1.46$ AT $\alpha=15^\circ$.

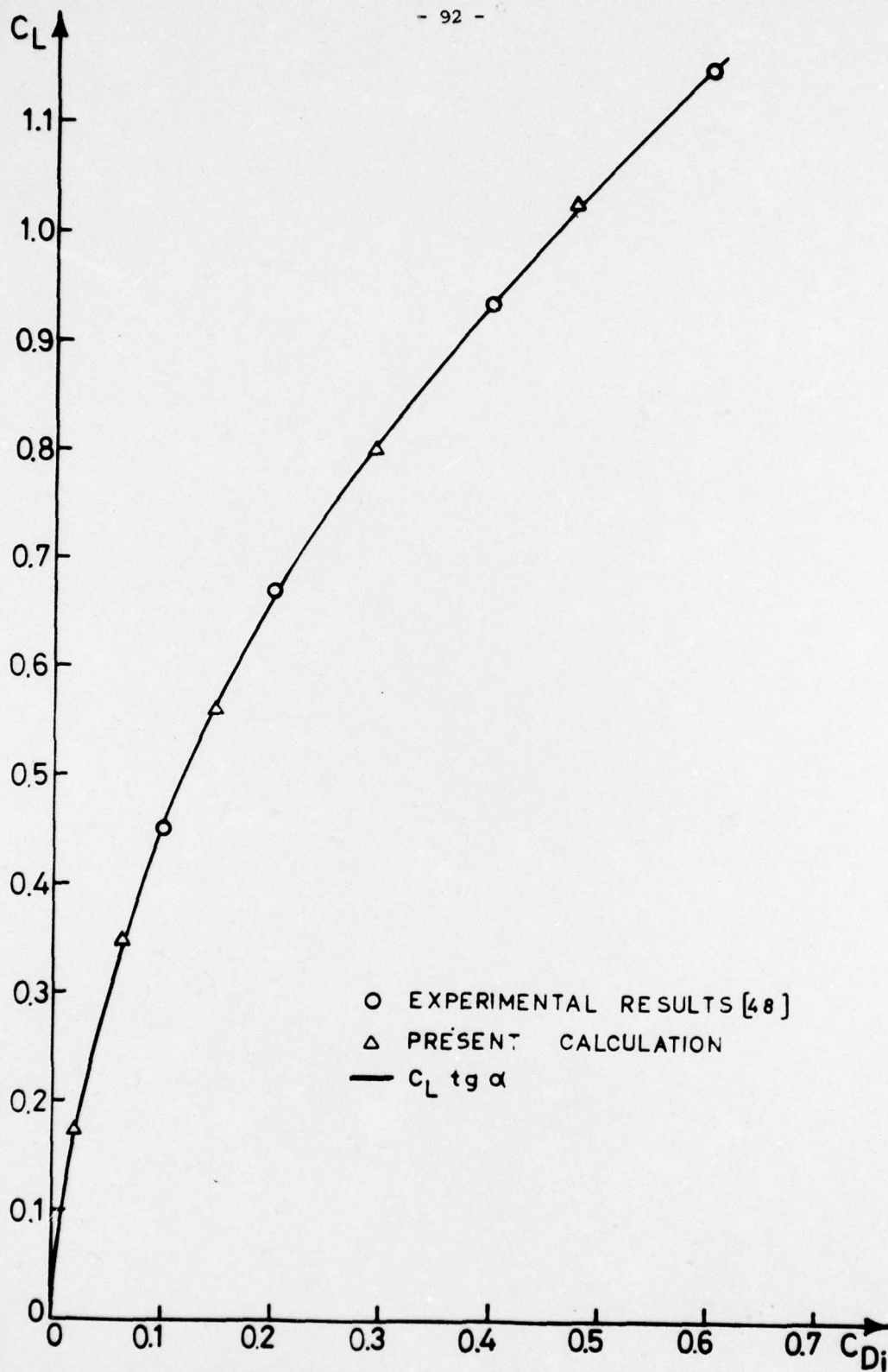


FIG.52 LIFT COEFFICIENT C_L VS INDUCED DRAG COEFFICIENT C_{Di} ($AR=1.46$).

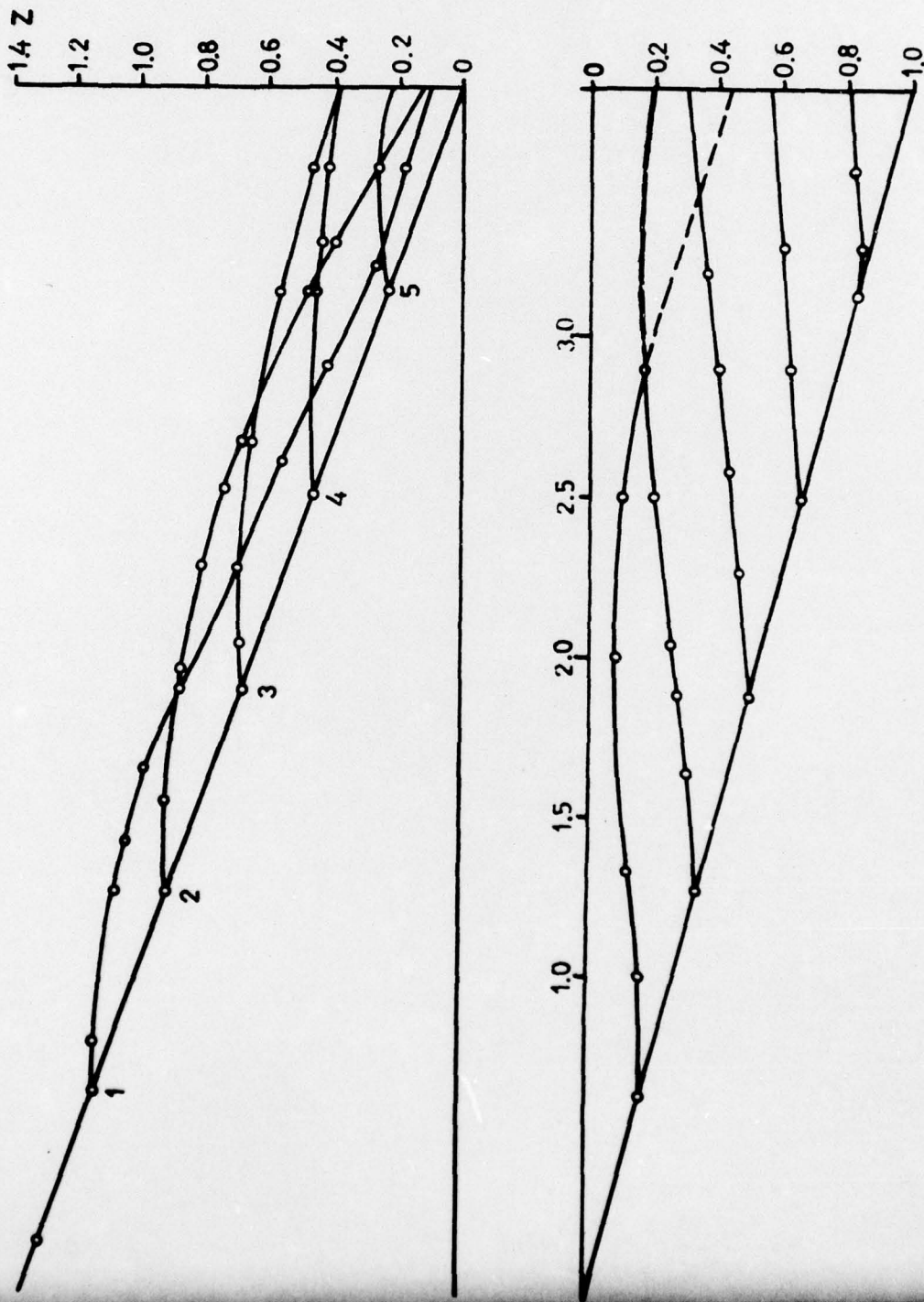


FIG.53-VORTEX LINES ON A DELTA WING OF $AR=1$ AT $\alpha=20^\circ$
(6x6 SUBDIVISIONS).